

7. SITE 1211¹

Shipboard Scientific Party²

PRINCIPAL RESULTS

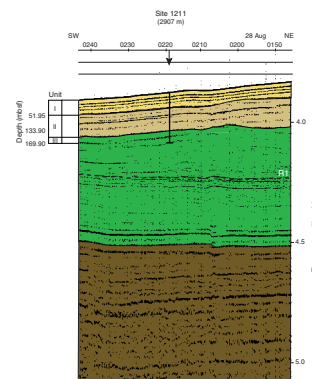
Background

Site 1211 is located in lower bathyal (2907 m) water depth on the southern flank of the Southern High of Shatsky Rise. The site is on seismic line TN037-17A (Fig. F1) at the location of Deep Sea Drilling Program (DSDP) Site 305, which was rotary core barrel (RCB) cored. The drilled section at Site 305 contains a relatively thick sequence of Lower Cretaceous chalk and chert, Upper Cretaceous ooze and chert, and Cenozoic ooze (Larson, Moberly, et al., 1975). The undisturbed part of the sequence at Site 305 was highly disturbed by rotary drilling and the record of the Eocene–Oligocene transition, the Paleocene–Eocene Thermal Maximum (PETM), and the Cretaceous/Tertiary (K/T) boundary has been lost. Thus, the triple advanced piston corer (APC) coring strategy for Site 1211 was designed to recover a complete and undisturbed record of the Site 305 sequence.

Site 1211 is the second deepest site in the Upper Cretaceous–Paleogene part of the Shatsky Rise depth transect. The site is more than 200 m deeper than Site 1212, the next shallowest site, and more than 500 m deeper than Site 1209, the shallowest site. Thus, drilling results from Site 1211 will contribute to broad, leg-based objectives that are aimed at understanding changes in Late Cretaceous and Paleogene ocean circulation at a time of global warmth.

Holes 1211A, 1211B, and 1211C were cored with the APC. Hole 1211A terminated at 158.9 meters below seafloor (mbsf) at the highest chert layer in the upper Maastrichtian. In Hole 1211B, this chert layer was penetrated with extended core barrel (XCB) center bit drilling and a total of 169.9 m was cored reaching the lower Maastrichtian. Because there is some recovery of coherent Maastrichtian and Campanian ooze from Site 305, we decided not to penetrate multiple chert layers to core

F1. Interpretation of seismic reflection profile, Site 1211, p. 32.



¹Examples of how to reference the whole or part of this volume.

²Shipboard Scientific Party addresses.

the lowermost Maastrichtian and Campanian sequence with the APC. Hole 1211C was cored to immediately below the K/T boundary at 138.3 mbsf to fill stratigraphic gaps in the composite sequence constructed from Holes 1211A and 1211B. The lack of overlap between the first two holes resulted from double coring an interval in the upper section of Hole 1211B (see “Composite Depths,” p. 20, in the “Site 1211” chapter).

Summary of Results

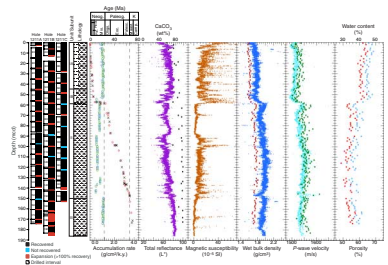
Coring at Site 1211 recovered three lithologic units that have been separated based on sediment composition (Fig. F2). Lithologic Unit I ranges from Holocene to lower Miocene (0 to ~17.3 Ma; 0–53.4 mbsf) and consists of nannofossil ooze, clayey nannofossil ooze, and nannofossil clay that are shades of gray, green, yellow, orange, and brown in color. This unit has a higher clay content than underlying units. Two subunits are distinguished. Subunit IA (Holocene to lower Pliocene; 0 to ~4.8 Ma; 0–41.4 mbsf) is olive-gray and yellowish gray in color, contains siliceous microfossils and rare ash layers, and often shows a marked decimeter-scale cyclicity. Subunit IB (lower Pliocene to lower Miocene; ~4.8 to ~17.3 Ma; 41.4–53.4 mbsf) is yellowish orange and grayish orange in color and contains centimeter to decimeter-scale cycles. An unconformity from lower Miocene to upper Oligocene separates lithologic Unit I from Unit II (see “Biostratigraphy,” p. 56, in “Specialty Syntheses” in the “Leg 198 Summary” chapter). Lithologic Unit II ranges from the upper Oligocene to lowermost Paleocene (~27 to 65 Ma; 53.38–133.80 mbsf) and consists of yellowish brown and dark yellowish brown nannofossil ooze with minor amounts of nannofossil ooze with clay, clayey nannofossil ooze, and clay with nannofossils. A number of minor diastems occur in this interval as indicated by thin, darker horizons. More significant unconformities are found in the middle Eocene (~40–45 Ma) and upper Paleocene (~56–59 Ma). The unit has a generally higher carbonate content than Unit I. Color reflectance data show decimeter-scale carbonate cyclicity. Lithologic Unit III ranges from the uppermost to lower Maastrichtian (65 to ~70 Ma; 133.8–169.9 mbsf) and consists of pale orange nannofossil ooze and chert. The unit has extremely high carbonate contents. One chert layer was penetrated in lithologic Unit III.

The Site 1211 stratigraphic section shows broad similarity to the sections recovered at Sites 1209 and 1210 suggesting, in general, common sedimentation histories. In particular, the critical boundaries, for example the Paleocene/Eocene (P/E) and K/T boundaries, show a similar sequence of lithologies. However, sedimentation rates throughout the section are generally significantly lower at Site 1211 than at the previous two sites (Fig. F3), and there are additional unconformities and condensed intervals. All of these differences appear to reflect changes in carbonate preservation coincident with the greater water depth.

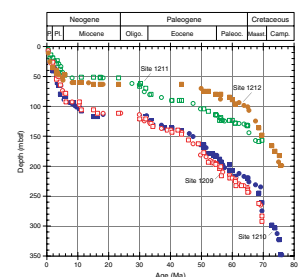
Highlights

The major highlight of coring at Site 1211 is similar to the highlights at Sites 1209 and 1210, namely the recovery of all of the critical intervals, most of which were recovered in all three holes. These include the Eocene/Oligocene (E/O) boundary, the PETM, a biotic event in the mid-Paleocene, the K/T boundary, and probably the mid-Maastrichtian deepwater event (MME). In the first part of this section we describe the

F2. Coring results, Site 1211, p. 33.



F3. Age-depth curves, p. 34.



general stratigraphy of these intervals. In the absence of detailed data and analysis, however, a discussion of the significance of these events would be broadly similar to Sites 1209 and 1210. More detail on the critical events is presented in “Principal Results,” p. 1, in the “Site 1209” chapter.

The stratigraphic record at Site 1211 reveals differences from that at Sites 1209 and 1210 that appear to be related to increased water depth. In the second part of this section, we integrate results from the three sites and explore the significance of these differences in the framework of the Shatsky Rise depth transect.

Recovery of Critical Events

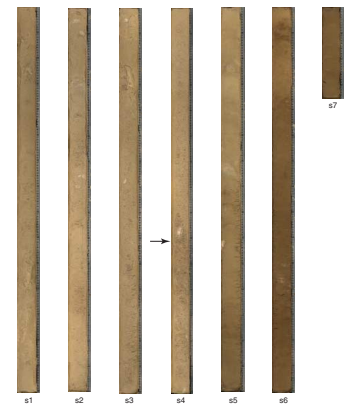
Sediment recovered at Site 1211 contains the record of the Eocene–Oligocene transition, the PETM, an event in the mid-Paleocene, the K/T boundary, and possibly the MME. The lithologic record of each of these intervals at Site 1211 appears to be similar to those of Sites 1209 and 1210, but it also shows significant differences.

The Eocene–Oligocene transition has been recovered in Holes 1211A, 1211B, and 1211C. Cores and reflectance data from the boundary transition show a subtle gradual upward lightening in color, likely as a result of an increase in carbonate content (Fig. F4). This change is evidence for a deepening of the lysocline and calcite compensation depth (CCD). Prominent color cycles in the transition interval suggest an orbital control on dissolution. The amplitude of the reflectance variations is higher than at previously drilled Southern High sites, suggesting greater variation in dissolution intensity at the deeper Site 1211.

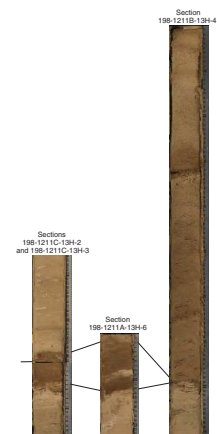
The PETM was recovered in Holes 1211A, 1211B, and 1211C; however, the lithologic record in the three holes is different (Fig. F5), and magnetic susceptibility records are hard to correlate (see “Composite Depths,” p. 20, in the “Site 1211” chapter). Part of this problem arises from the fact that the event in Holes 1211A and 1211C was cut by section breaks. In these two holes, the PETM was recovered in a yellowish brown clayey nannofossil ooze. The contact of this layer with the underlying grayish orange nannofossil ooze is affected by bioturbation (Fig. F5). The lower part of the clayey nannofossil ooze in Hole 1211A also appears to have been cut by a burrow that contains grayish orange ooze. The clayey nannofossil ooze layer is ~11 cm thick in Hole 1211A and 8 cm thick in Hole 1211C and is overlain abruptly by grayish orange nannofossil ooze. In Hole 1211B, the base of the PETM corresponds to a sharp change from a pale orange nannofossil ooze to a yellowish brown clayey nannofossil ooze. This color is uniform for 16 cm then grades to a grayish orange over the next ~30 cm. All sediment in the section above the base of the PETM is darker than it is below the PETM base.

Based on lithology and color, it is impossible to correlate the PETM in Holes 1211A and 1211C with the event in Hole 1211B. However, biostratigraphy suggests that there is a diastem right above the base of the event in Hole 1211B. Samples from the lower 6–7 cm of the clay-rich unit in Holes 1211A and 1211C contain the nannolith *Fasciculithus* in similar abundance to the lower part of the PETM at Sites 1209 and 1210. Nannofossils in the lower part of the event are also poorly preserved, and abundant calcite blades are seen in samples as at the previous sites. The planktonic foraminifer *Morozovella velascoensis*, the last occurrence (LO) of which defines the top of Zone P5, occurs 33 cm above the base of the event in Hole 1211A and ~24 cm above the base

F4. Lithology of the E/O boundary interval, p. 35.



F5. Correlation of PETM sections, p. 36.



of the event in Hole 1211C. In Hole 1211B, however, *Fasciculithus* disappears 1–2 cm above the base of the event and *M. velascoensis* is absent in a sample 6 cm above the base. The nannolith *Discoaster diastypus*, the first occurrence (FO) of which defines the base of nannofossil Zone CP9, is found 2–3 cm above the base of the event in Hole 1211B, 34 cm above the base of the event in Hole 1211C, and 10 cm above the base in Hole 1211A, which may have a slight gap at this level (this event is found 2 to 4 m above the base of the event at Sites 1209 and 1210). These preliminary data show that the PETM interval in Holes 1211A and 1211C is correlative with the lowermost 1 cm of the event in Hole 1211B. All three sections are highly condensed compared to records from Sites 1209, 1210, and 1212. The condensed nature of the PETM at Site 1211 suggests that it was in a depth range that was sensitive to carbonate solubility changes across the PETM.

The mid-Paleocene biological event was recognized in Holes 1211A, 1211B, and 1211C by a 5- to 10-cm-thick nannofossil ooze that has a slightly darker color than surrounding sediment. The base of the unit is gradational with the underlying sediment, except in Hole 1211C, where a void lies directly under the event. The interval shows a sharp magnetic susceptibility peak and a density decrease. Preliminary nannofossil biostratigraphy suggests significant differences between Sites 1209 and 1210 and Site 1211. At the former sites, this event corresponds to the evolutionary FO of the nannolith *Heliolithus kleinpellii*, an important component of late Paleocene assemblages and a marker for the base of Zone CP5 (58.4 Ma in the timescale of Berggren et al., 1995). Assemblages in the lower part of this interval are highly dissolved. At Site 1211, a sharp increase in *H. kleinpellii* occurs within the darker sediment interval; however, this coincides with the FO of younger taxa *Discoasteroides bramlettei* and *Discoaster mohleri*. In continuous sections, the FO of *D. bramlettei* lies in the upper part of Zone CP5 (e.g., Perch-Nielsen, 1985), whereas the FO of *D. mohleri* at 57.5 Ma defines the base of Zone CP6. The co-occurrence of these FOs suggests that the dark claystone represents a condensed interval of close to 1 m.y.

The K/T boundary stratigraphy at Site 1211 is very similar to that at Sites 1209, 1210, and 1212. The boundary succession includes pale orange nannofossil ooze of latest Maastrichtian age (nannofossil Zone CC26) overlain by lowermost Paleocene (foraminiferal Zone P α) yellowish orange foraminiferal ooze. This lithology grades upward into a white foraminiferal nannofossil ooze then back into a grayish orange nannofossil ooze. The boundary between the uppermost Maastrichtian and the lowermost Paleocene is clearly bioturbated, and careful sampling of burrows yields planktonic foraminifers dominated by *Guembelitra* with rare *Hedbergella holmdelensis* that suggest a possible Zone P0 age. Light brown to amber, spherical particles ~100 μ m in diameter found in a sample from these burrows may be altered tektites.

The MME is likely to have been recovered at Site 1211. Although *Inoceramus* prisms are not visible in the sediments, they are present in washed residues from Sample 198-1211B-17H-CC.

Carbonate Record at Site 1211

The Shatsky Rise depth transect was designed to reconstruct the effect of short-term and long-term variations in the lysocline and CCD on the Upper Cretaceous and Paleogene sedimentary record. The total depth range of sites included in this transect is almost 1000 m, from Site 1209 (2387 m) to Site 1208 (3346 m). Site 1208 was clearly below

the CCD for a significant part of the early Paleogene and the Maastrichtian, as much of this stratigraphic interval corresponds to an unconformity (see **“Principal Results,”** p. 1, in the “Site 1208” chapter). Site 1211 (2907 m) is the deepest site in the Shatsky Rise transect with a nearly complete Maastrichtian to Eocene section.

The Site 1211 section shows broad similarities to its shallower neighbors, Sites 1209 and 1210 (2573 m) but is considerably more condensed (Figs. F3). Lower sedimentation rates in the major, continuous parts of the Site 1211 section as well as the longer duration of several hiatuses have reduced the thickness of the stratigraphic column. The major Miocene–Oligocene hiatus is similar in duration at all of the sites, however. This hiatus is thought to represent regionally increased erosion coincident with intensified deepwater flow during the latest Oligocene and early Miocene (see **“Site 1207,”** p. 16, and **“Site 1208,”** p. 22, in **“Principal Results”** in the “Leg 198 Summary” chapter). Preliminary biostratigraphy suggests unconformities in the Site 1211 section in the middle Eocene (~40–45 Ma) and upper Paleocene (~56–59 Ma) that are unique among the Southern High sites or at least much longer in duration than gaps in these intervals at the other sites.

Throughout the Paleogene section at Site 1211 are a number of 5- to 20-cm-thick yellow-brown clay-rich nannofossil ooze levels that have abundant phillipsite-, pyrite-, and manganese-coated foraminifers. Carbonate content of these layers are as low as ~50 wt%. There are ~26 such intervals >5 cm in thickness. These levels are thought to result from lengthy seafloor exposure during intervals of intense dissolution when the site was located close to the lysocline/CCD. The late Paleocene to middle Eocene is an interval with a steadily falling but generally shallow CCD in the North Pacific (Rea et al., 1995). The paleodepth of Site 1211 is thought to be comparable to the present day (see **“Biostratigraphy,”** p. 56, in **“Specialty Syntheses”** in the “Leg 198 Summary” chapter); thus, the unconformities at Site 1211 may be intervals when the CCD shoaled to depths around 2900 m. A few clay-rich intervals in the upper Maastrichtian may also represent short-term lysocline/CCD shoaling events.

Superimposed on this long-term record for CCD variation are short-term (<1 m.y.) events that led to abrupt shoaling of the lysocline/CCD. The two most prominent events are in the mid-Paleocene at the time of a prominent biological event (see **“Principal Results,”** p. 1, in the “Site 1209” chapter). The second is at the PETM. Both of these events are highly condensed at Site 1211 compared to Sites 1209, 1210, and 1212 as a result of dissolution. For the mid-Paleocene event, dissolution lasted up to 1 m.y. beyond the end of the event.

Color reflectance data from Site 1211 show low-amplitude cyclic variation throughout the Paleogene (see **“Lithostratigraphy,”** p. 8, in the “Site 1211” chapter). The percent total reflectance is usually closely correlated with carbonate content. For much of this interval, carbonate likely reflects the amount of dissolution. This suggests that the intensity of dissolution was controlled by a mechanism that varied in intensity on orbital timescales. Two possible mechanisms are changing deep-water circulation and surface water productivity. The cycle record at Site 1211 should allow development of an orbital chronology for the Paleogene section.

BACKGROUND AND OBJECTIVES

Site 1211 is located in lower bathyal (2907 m) water depth on the southern flank of the Southern High of Shatsky Rise. The site is at the location of DSDP Site 305. Thus, the stratigraphic sequence is known, although significant disturbance in Cenozoic and Upper Cretaceous sediments resulting from RCB drilling at Site 305 has blurred the signal of short-term events such as the PETM and the Eocene–Oligocene transition.

According to the reconstruction of Nakanishi et al. (1989), basement underlying the site was formed in the latest Jurassic within Magneto-chron M20 (~145 Ma). The drilled sequence at Site 305 had a total depth of 640.5 m and reached the Hauterivian. The site contains a relatively thick sequence of Lower Cretaceous chalk and chert, overlain by Upper Cretaceous ooze and chert and Cenozoic ooze (Larson, Moberly, et al., 1975). A major unconformity was found between the middle Miocene and the upper Oligocene. Minor unconformities are thought to exist in the middle Eocene. Otherwise, biostratigraphic results (e.g., Bukry, 1975; Caron, 1975; Luterbacher, 1975) suggest a reasonably continuous sequence. Sites 305 and 1211 are located on seismic line TN037-17A (Fig. F1). Observation of the seismic profile shows a significant unconformity beneath the upper part of the Upper Cretaceous, probably the Campanian. Thus, it is likely that at least part of the Santonian–Cenomanian interval is missing at this site as proposed by Sliter (1992) based on a reevaluation of planktonic foraminiferal biostratigraphy.

Site 1211 is the second deepest site in the Shatsky Rise depth transect. The shallowest site, Site 1209 at 2387 m, is ~500 m shallower than Site 1211; the deepest site, Site 1208 at 3346 m, is ~400 m deeper. The goal of coring at Site 1211 is to recover with triple APC coring a complete and undisturbed record of the Site 305 sequence. As part of this depth transect, drilling at Site 1211 addresses a number of leg-related objectives. The sediments recovered at this site will be used to

1. Determine the evolution of surface and deepwater properties through the Late Cretaceous and Paleogene using shore-based stable isotope studies and microfossil assemblage investigations. In particular, we are interested in the onset and demise of the Cretaceous “greenhouse” and the onset of Antarctic glaciation in the Eocene.
2. Determine the nature of chemical (i.e., CCD, nutrients, and oxygenation) and physical oceanographic changes (temperature gradients) during transient climatic events, such as the E/O boundary, the PETM, late Paleocene and early Eocene hyperthermals, and the MME.
3. Compare fluctuations in the CCD through time with other records from Shatsky Rise and interpret them in a paleoceanographic framework.
4. Shed light on the nature and origin of orbital cycles using geochemical and biotic data.
5. Refine Cretaceous and Paleogene timescales by improving correlations between the geomagnetic polarity timescale and low-latitude biostratigraphies and generating high-resolution orbital stratigraphies in intervals with prominent cyclicity.

OPERATIONS

Transit from Site 1210 to Site 1211

The 24-nmi transit to Site 1211 was completed without incident in 2.5 hr at an average speed of 9.6 kt. After arriving at the site coordinates, the thrusters and hydrophones were lowered and the ship was switched over to dynamic positioning (DP) mode at 0225 hr on 27 September 2001, initiating operations at Site 1211.

Hole 1211A

An APC/XCB bottom hole assembly (BHA) was assembled and run to near the seafloor. The bit was positioned at 2912.0 meters below rig floor (mbrf), and Hole 1211A was spudded with the APC at 0915 hr on 27 September. The mudline core contained 2.85 m of sediment, establishing a seafloor depth of 2918.7 mbrf, or 2907.5 meters below sea level (mbsl) (Table T1). APC coring continued through Core 11H to 97.8 mbsf. While deploying Core 12H, the barrel dropped off the overshoot and fell to the bottom. Two unsuccessful retrieval attempts and wireline trips were made before the core barrel was returned during the third run. The cause of the problem was identified as the safety tube located in the overshoot, which had dislodged and resulted in the core barrel becoming jammed in the pipe. We resumed APC coring through Core 18H, which did not achieve full stroke, impeded by a chert layer. Coring was terminated at 158.9 mbsf, with an average recovery of 102.4%. The drill string was tripped up, clearing the seafloor at 0610 hr on 28 September and ending drilling at Hole 1211A.

Hole 1211B

The ship was offset 15 m to the north and the bit was positioned 2 m higher than at Hole 1211A to achieve stratigraphic overlap and position critical intervals away from core breaks. Hole 1211B was spudded at 0700 hr on 28 September, recovering 6.15 m of sediment in Core 1H, indicating a seafloor depth of 2917.4 mbrf, or 2906.2 mbsl. Coring with the APC continued through Core 17H at 151.6 mbsf. An incomplete stroke on Core 17H resulted in deployment of the XCB center bit to drill 1.6 m through a chert layer. The APC was redeployed for Cores 18H and 19H. When Core 19H did not stroke completely, coring operations were suspended at 169.9 mbsf. The drill string was retrieved, with the bit clearing the seafloor at 0625 hr on 29 September, ending drilling at Hole 1211B.

After leaving Site 1211, it was found that one of the critical intervals, the PETM, was condensed in Hole 1211B (see “[Biostratigraphy](#),” p. 13), and the stratigraphic overlap between Holes 1211A and 1211B was poor (see “[Composite Depths](#),” p. 20). As a result, the drillship returned to Site 1211 later in the leg.

Transit from Site 1213 to Site 1211

After departing Site 1213, we proceeded due south to distance ourselves from the forecast center of severe tropical depression Krosa. During the night, the storm accelerated to 40 kt and moved rapidly to the northeast, passing north of the operational location. After passage of the storm, we reversed course and proceeded back to Site 1211. A total

T1. Coring summary, p. 64.

of 116 nmi were covered during the 22.7-hr transit at an average speed of 5.1 kt. At 1742 hr on 10 October, the ship was switched over to DP mode, recommencing operations at Site 1211.

Return to Site 1211

Hole 1211C

An APC/XCB BHA was assembled and run to 2916.0 mbrf, near the seafloor. Hole 1211C was spudded with the APC at 0545 hr on 11 October. The mudline recovered 7.30 m of sediment, indicating a seafloor depth of 2918.2 mbrf, or 2906.9 mbsl. APC coring continued to a depth of 138.3 mbsf, and coring was terminated when the objective was achieved. Cores 4H through 15H were oriented, and APC coring averaged 101.9% recovery. The drill string was retrieved, clearing the rig floor at 0125 hr on 12 October and concluding operations at Site 1211.

LITHOSTRATIGRAPHY

Description of Lithologic Units

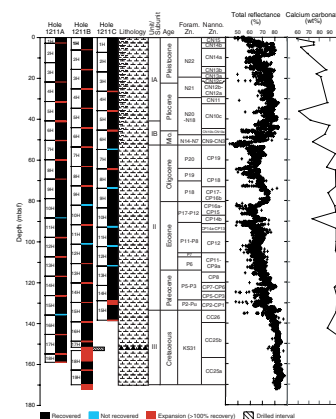
Advanced piston coring at Site 1211 recovered 158.9 m of sediment in Hole 1211A, 169.9 m in Hole 1211B, and 138.6 m in Hole 1211C. Excellent recovery of Holocene through lower Maastrichtian sediments provides a useful corollary to Site 305 that was RCB cored during DSDP Leg 32 at the same location.

The sediment from Holes 1211A, 1211B, and 1211C is divided into three lithologic units (Fig. F6). Unit I, extending from 0.0 to 51.95 mbsf in Hole 1211A, 53.38 mbsf in Hole 1211B, and 53.67 mbsf in Hole 1211C, ranges from the Holocene to lower Miocene. This unit consists of cyclically bedded lighter-colored nannofossil ooze and darker-colored nannofossil ooze with clay or clayey nannofossil ooze. The average carbonate content is ~77 wt% (Fig. F6). Typical biogenic silica contents are ~1% but range up to 15% in a few darker-colored intervals. Rare layers of volcanic ash are present. An unconformity at the base of Unit I separates lower Miocene clay from upper Oligocene nannofossil ooze (Fig. F7). Unit II extends from the upper Oligocene (51.95 mbsf in Hole 1211A, 53.38 mbsf in Hole 1211B, and 53.67 mbsf in Hole 1211C) to the basal, clay-rich layer at the K/T boundary (133.87 mbsf in Hole 1211A, 133.80 mbsf in Hole 1211B, and 133.02 mbsf in Hole 1211C). The general lithology of Unit II is soft, nearly homogeneous nannofossil ooze punctuated by intervals of more clay-rich sediment. Unit III extends from the upper to the lower Maastrichtian at 158.9 mbsf in Hole 1211A, 169.9 mbsf in Hole 1211B, and 138.64 mbsf in Hole 1211C (Unit III only spans upper Maastrichtian sediment in Hole 1211C) and consists predominantly of pale orange homogeneous nannofossil ooze.

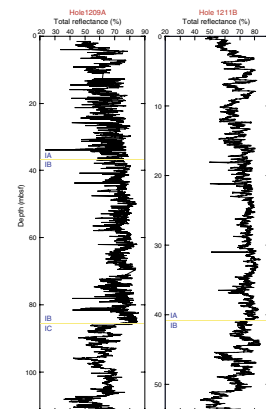
Lithologic Unit I

Intervals: 198-1211A-1H-1, 0 cm, through 7H-2, 15 cm; 198-1211B-1H-1, 0 cm, through 6H-7, 28 cm; and 198-1211C-1H-1, 0 cm, through 6H-6, 87 cm
 Depths: 0.0 to 51.95 mbsf in Hole 1211A; 0.0 to 53.38 mbsf in Hole 1211B; and 0.0 to 53.67 mbsf in Hole 1211C
 Age: Holocene to early Miocene

F6. Core recovery, lithology, lithologic units, age with corresponding biostratigraphic zonations, color reflectance, and percent carbonate, Hole 1211B, p. 37.



F7. Comparison of color reflectance data of Unit I sediments, Holes 1209A and 1211B, p. 38.



Unit I at Site 1211 consists of alternating intervals of nannofossil clay and nannofossil ooze. Somewhat subtle lithologic changes support the division of Unit I into two subunits. Subunit IA is predominantly greenish gray in color and characterized by a higher clay content, the presence of siliceous microfossils, rare diagenetic color banding, pyrite, pumice, and ash layers. The division between Subunits IA and IB is placed at a color change from greenish gray sediment to yellowish brown and orange sediment. The Subunit IA/IB contact is placed at the top of the first pale yellowish brown (10YR 6/2) nannofossil ooze in Sections 198-1211A-5H-6, 70 cm, 198-1211B-5H-5, 28 cm, and 198-1211C-5H-2, 125 cm. The Subunit IA/IB color change also marks the downhole disappearance of ash beds and biogenic silica, and a decrease in pyrite.

Subunit IA

Subunit IA extends from 0.0 to 39.51 mbsf in Hole 1211A (interval 198-1211A-1H to 5H-6, 70 cm), from 0.0 to 40.88 mbsf in Hole 1211B (interval 198-1211B-1H to 5H-5, 28 cm), and from 0.0 to 38.55 mbsf in Hole 1211C (interval 198-1211C-1H to 5H-2, 125 cm), spanning the Holocene to lower Pliocene. Below the uppermost 20-cm layer of moderate yellowish brown (10YR 5/4) clay with nannofossils lies an interval of alternating darker (light olive gray; 5Y 6/1) and lighter (yellowish gray; 5Y 8/1) nannofossil clay to clayey nannofossil ooze. The average carbonate content for Subunit IA sediment is ~75 wt%. Diatoms, and to a lesser extent radiolarians, are present in Subunit IA sediments, although they seldom exceed a few percent of the sedimentary constituents. The nature of the contacts between the Subunit IA lithologies varies from relatively distinct and horizontal to gradational and bioturbated. The cyclic alternation of light and dark lithologies tends to occur in decimeter-scale intervals of varying thicknesses with no apparent downcore trend. The sediment in Subunit IA is rarely to moderately bioturbated, although the apparent intensity of bioturbation is usually directly related to the degree of color contrast—burrows are more visible across lithologic contacts with color changes. Postdepositional Subunit IA sedimentary constituents that were observed commonly at other Leg 198 sites, such as green authigenic clay laminae (saponite) and pyrite (discrete blebs, burrow fill, and streaks), are sparse at Site 1211.

Subunit IB

Subunit IB extends from 39.51 to 51.95 mbsf in Hole 1211A (interval 198-1211A-5H-6, 70 cm, to 7H-2, 15 cm), from 40.88 to 53.38 mbsf in Hole 1211B (interval 198-1211B-5H-5, 28 cm, to 6H-7, 28 cm), and from 38.55 to 53.67 mbsf in Hole 1211C (5H-2, 125 cm, to 6H-6, 87 cm), spanning the lower Pliocene to lower Miocene. Similar to Subunit IA, Subunit IB consists of nannofossil ooze with varying amounts of clay. The major distinction between the subunits lies in the color change from variations of greenish gray in Subunit IA to hues of yellowish brown and grayish orange in Subunit IB. Subunit IB red/blue reflectance ratios are nearly twice as high as in Subunit IA, corresponding to the overall higher carbonate contents (average Subunit IB values = ~80 wt%). Color transitions are gradational, and apparent dark–light cyclicity occurs variably as centimeter- to decimeter-scale alternations throughout this subunit. Total color reflectance percentages (L^*), which generally correlate to carbonate content, exhibit a slight downcore decrease followed by an increase, locally peaking near the boundary between Units I and II (Figs. F6, F7). Pyrite is very rare in Subunit IB, and

volcanic ash and green authigenic clay laminae are absent. Pumice fragments are found in Cores 198-1211B-5H and 6H. Bioturbation is rare to moderate with identifiable *Zoophycos* trace fossils found in Core 198-1211A-6H.

Lithologic Unit II

Intervals: 198-1211A-7H-2, 15 cm, through 15H-6, 20 cm; 198-1211B-6H-7, 28 cm, through 15H-3, 120 cm; and 198-1211C-6H-6, 87 cm, through 15H-3, 122 cm

Depths: 51.95 to 133.87 mbsf in Hole 1211A; 53.38 to 133.80 mbsf in Hole 1211B; and 53.67 to 133.02 in Hole 1211C

Age: late Oligocene to early Paleocene

Unit II consists of nearly homogeneous very pale orange (10YR 8/2) to grayish orange (10YR 7/4) nannofossil ooze with intervals of moderate yellowish brown (10YR 5/4) and dark yellowish brown (10YR 4/4) nannofossil ooze with clay, clayey nannofossil ooze, and clay with nannofossils. Similar to the other Shatsky Rise sites, the Unit II ooze is much softer than that of Unit I, often rendered soupy during the drilling and splitting process. Carbonate content of the Unit II nannofossil ooze averages ~94 wt% (Fig. F6). Visible bioturbation is typically rare, primarily as a result of the minimal color contrast. Within the grayish orange (10YR 7/4) and very pale orange (10YR 8/2) ooze, apparent bioturbation is characterized by whitish centimeter-scale burrow fills. Color and lithologic changes in Unit II are primarily gradational and mottled; however, some light/dark contacts are relatively sharp.

The base of Unit II lies at the K/T boundary. The boundary is overlain by a basal, grayish orange (10YR 7/4) clay-enriched layer, which, in turn, is overlain by a white (N9) foraminifer-nannofossil ooze with millimeter-scale pyritized burrows.

Lithologic Unit III

Intervals: 198-1211A-15H-6, 20 cm, through 18H-CC; 198-1211B-15H-3, 120 cm, through 19H-CC; and 198-1211C-15H-3, 122 cm, through 15H-CC

Depths: 133.87 to 158.9 mbsf in Hole 1211A; 133.80 to 169.9 mbsf in Hole 1211B; and 133.02 to 138.64 mbsf in Hole 1211C

Age: late to early Maastrichtian

Unit III consists of generally soft, very pale orange (10YR 8/2) nannofossil ooze, with several centimeter-scale intervals of moderate yellowish brown (10YR 4/2) clayey nannofossil ooze in the uppermost Maastrichtian (Core 198-1211B-16H). This unit is distinguished from Unit II by its relatively high abundance of foraminifers (up to 15%) and the presence of *Inoceramus* fragments in Cores 198-1211B-17H and 18H. Overall carbonate contents are ~95 wt%, similar to the Unit II oozes. Bioturbation is rarely apparent, characterized by discrete whitish burrow fill and slight mottling. The final core in Hole 1211B (198-1211B-19H) contains chert fragments, which may have contributed to the soupy texture and flow-in (drilling disturbance) encountered toward the base of the core.

Interpretation

Sedimentation

Unit I

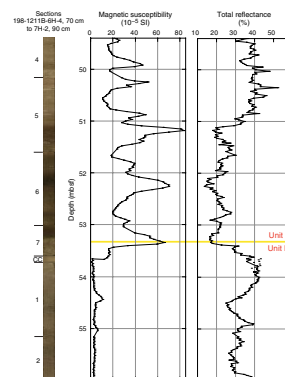
Cyclic sedimentation during the Pleistocene and Pliocene at Site 1211 is similar to that at Site 1210, characterized by relatively low-amplitude cyclicity compared to the cyclic sedimentation recorded in the sediment farther north (e.g., Site 1209; **F8**). This may be attributable to overall lower surface water productivity on the southern flank of the Southern High, as indicated by the diminished abundance of siliceous microfossils compared to sites further north on the Southern, Central, and Northern Highs. In addition, the average sedimentation rate for the Pleistocene and Pliocene (8.6 m/m.y.) is significantly lower than those recorded at the Central and Northern Highs (up to 42 m/m.y.), also suggesting lower surface water productivity (Fig. **F16**). However, despite the lower rates of primary productivity, the cyclicity was most likely dictated by small-scale changes in the intensity of surface water productivity. Relative biogenic silica enrichment occurs within the darker, more olive-green lithologies (up to 15% diatoms), with the lighter gray intervals remaining depleted in opal (~1%). It is unlikely that the light-dark sediment cycles resulted from glacial-interglacial fluctuations in deep-water corrosiveness given the relatively shallow water depth of ~2900 m, which lies above the subtropical northern Pacific CCD (Rea et al., 1995).

The relatively low Pleistocene and Pliocene sedimentation rates may have contributed to the more yellowish sediment hue than the corresponding Subunit IA sediment cored on the Central and Northern Highs and northern part of the Southern High. The more yellowish sediment color suggests greater oxidation of the Site 1211 Subunit IA sediment than the darker, more greenish gray Subunit IA sediments found at the sites with higher sedimentation rates. As a result, the transition from the light olive-gray and yellowish gray Subunit IA sediment to the grayish orange (10YR 7/4) and very pale orange (10YR 8/2) Subunit IB sediment is more subtle than it is at the Central and Northern Highs (Sites 1207 and 1208) and at the northern portion of the Southern High (Site 1209). At every site cored on Shatsky Rise, Subunit IB is characterized by distinctly lower sedimentation rates, perhaps enabling more oxidation of Fe-bearing constituents and imparting the more reddish brown color that defines the subunit. The difference between sedimentation rates in Subunits IA and IB is less pronounced at Site 1211 than at the other sites. However, changes in the sedimentation rate (as determined by shipboard biostratigraphy; **F20**) do not coincide with the Subunit IA/IB boundary, suggesting that other factors contributed to the fundamental change in the redox state of Unit I sediments (e.g., bottom-water composition and age, and/or organic matter accumulation).

Unit II

The upper boundary of Unit II is placed at the base of the clayey interval marking an unconformity spanning the lower Miocene to the upper Oligocene. The Unit I/II boundary is clearly seen in the magnetic susceptibility and color reflectance data (Fig. **F8**). The nearly homogeneous, pale orange nannofossil ooze of Unit II is punctuated by numerous darker brown clayey intervals. In contrast to the productivity-controlled sedimentation within Unit I, Unit II sedimentary variations seem to be dictated by fluctuations in the depth of the lysocline during

F8. Composite digital photograph, magnetic susceptibility, and color reflectance for the Unit I/II boundary interval, Hole 1211B, p. 39.



the Paleogene. Smear slide estimates and coulometric analyses indicate that carbonate levels dropped to as low as ~50 wt%, and these clay-rich intervals are interpreted as having resulted from periodic lysoclinical and CCD shoaling. At ~2900 m water depth, Site 1211 lay only a few hundred meters above the CCD during portions of the Paleogene, as constrained by lithologic examination of similar-aged carbonate-depauperate sediment from Site 1208 (~3300 m). Thus, subtle fluctuations in either the depth of the CCD or the vertical extent of carbonate corrosivity (resulting from lysoclinical shoaling) may have caused the periodic carbonate dissolution evident at Site 1211 (e.g., Oxburgh and Broecker, 1993).

Numerous (~26) clayey intervals are present throughout Unit II. Below the Eocene–Oligocene transition, low-amplitude fluctuations in the magnetic susceptibility and color reflectance records (Fig. F9) indicate cyclic changes in the sedimentary carbonate content. Such cyclicity suggests the possibility of orbitally controlled lysocline depth changes, potentially related to variation in productivity or deepwater mass composition. Shore-based investigations hopefully will shed light on the nature and causes of Paleogene cyclicity.

Among the lysocline “events” recorded at Site 1211, Unit II sediments represent the PETM and a newly recognized, prominent level in the mid-Paleocene. Although it is widely accepted that the PETM carbonate dissolution resulted from the oxidation of methane released from sedimentary methane hydrate reservoirs (Dickens et al., 1995, 1997), the cause(s) of the mid-Paleocene event is unknown as yet.

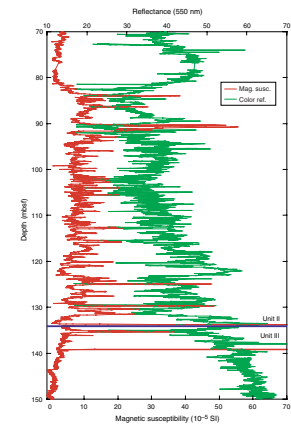
Unit III

Below the K/T boundary sequence lies Maastrichtian pale orange nannofossil ooze, very similar to Unit II ooze. Unit III oozes are distinguished by the higher abundance of foraminifers and the presence of *Inoceramus* fragments (prior to their mid-Maastrichtian extinction). Cyclicity, if present, is not easily observed in these somewhat soupy, very light colored, high-CaCO₃ oozes.

Comparison to DSDP Site 305

Coring at Site 1211 represents the return to DSDP Site 305; thus, it is instructive to compare the new APC-recovered sediment to that previously recovered with RCB coring. The primary distinction lies in the quality of cores recovered within Unit I and the overall depth of coring, which determined the placement of unit boundaries. Unit I at Site 305 (Holocene to upper Miocene) consisted of the pale orange and yellowish brown sediment that is similar to Subunit IB at Site 1211. Rotary coring at that site precluded recovery of a separate and distinct interval of soft, uppermost light olive-gray sediment of Subunit IA found at Site 1211. Below Unit I, the pale orange oozes of the Paleogene and Maastrichtian were grouped together as Unit II at Site 305, whereas we place the Unit I/II boundary at the base of the unconformity spanning the upper Miocene through the upper Oligocene (Sections 198-1211A-7H-2, 15 cm [51.95 mbsf]; 198-1211B-6H-7, 28 cm [53.38 mbsf]; and 198-1211C-6H-6, 87 cm [53.67 mbsf]). Upper to lower Maastrichtian sediments at Site 1211 are classified as lithologic Unit III, based on the break in sedimentation associated with the K/T boundary coupled with the increased abundance of foraminifers and the presence of *Inoceramus* remains. Coring at Site 1211 terminated in the lower Maastrichtian because of the presence of chert. Rotary coring at Site 305 continued through the Maastrichtian chert intervals and terminated in the

F9. Hole 1211B color reflectance and magnetic susceptibility data for the majority of the interval spanning Unit II and the upper portion of Unit III, p. 40.



Aptian–Barremian. Basal lithologies at Site 305 consisted of porcellanite, chert, pelagic shale, and limestone (Larson, Moberly, et al., 1975).

Diagenesis

All of the sediment recovered from the two holes at Site 1211 is ooze or clay. The lack of indurated sediment in any of the holes, with the exception of the basal chert layer, implies that the burial depths were never significantly greater than they are at present (158.9, 169.9, and 138.6 mbsf in Holes 1211A, 1211B, and 1211C, respectively).

The lack of other diagenetic features that had been relatively common in other Leg 198 Unit I sediment, such as green authigenic clay banding and pyrite, bears discussion. Several factors may have contributed to this difference. Lower overall sedimentation rates and the generally more yellow-brown hues of Subunit IA at Site 1211 suggest greater oxidation. The lower pyrite content implies that the majority of redox reactions occurred under oxic conditions, with less sulfate reduction (see “**Inorganic Geochemistry**,” p. 23) and hence less hydrogen sulfide available for pyrite formation. In addition, a lower supply of biogenic silica and the presence of fewer volcanic ash layers resulted in diminished pore water silica available for authigenic clay formation (see “**Inorganic Geochemistry**,” p. 23).

BIOSTRATIGRAPHY

Holes 1211A, 1211B, and 1211C comprise apparently complete upper Pleistocene to upper Miocene and upper Oligocene to lower Maastriichtian sequences separated by a condensed interval and at least two unconformities (upper to middle Miocene and lower Miocene to uppermost Oligocene) representing ~20 m.y. of condensed or missing record. High-resolution sampling for both calcareous nannofossil and planktonic foraminiferal biostratigraphy suggests that several key intervals were recovered, including the E/O boundary, the P/E boundary transition, the PETM, and the K/T boundary. The main calcareous nannofossil and foraminiferal datums are summarized in Tables T2 and T3.

Calcareous nannofossils are generally abundant and moderately to well preserved throughout the Cenozoic and Cretaceous sediments of Holes 1211A, 1211B, and 1211C. Planktonic foraminifers exhibit variable preservation and diversity. In particular, preservation is generally poor in samples from the Miocene, Oligocene, and upper Eocene.

Studies of benthic foraminifers were conducted on selected core catcher samples from Holes 1211A and 1211B, and stratigraphic ranges are summarized in Tables T4 and T5. Neogene benthic foraminifers are well preserved and rare to few in abundance; Paleogene and Cretaceous forms are moderately well preserved and rare to few in abundance.

Calcareous Nannofossils

Neogene

The Neogene section ranges from the upper Pleistocene (Subzone CN14b) to the lower–middle Miocene (Zones CN3 and CN4). The Pleistocene to upper Miocene interval appears to be relatively complete. Although a number of zones and subzones have not been recognized, they probably lie within cores. The base of this interval is in Subzone CN9a (upper Miocene), constrained by the FO of *Discoaster berggrenii*

T2. Calcareous nannofossil datums, ages, and depths, p. 66.

T3. Planktonic foraminifer datums, ages, and depths, p. 67.

T4. Cenozoic and Cretaceous benthic foraminifers, Hole 1211A, p. 68.

T5. Cenozoic and Cretaceous benthic foraminifers, Hole 1211B, p. 70.

and the FO of *Amaurolithus*. A lower to middle Miocene interval is present in Core 198-1211A-7H (Samples 198-1211A-7H-2, 10 cm, and 7H-2, 20 cm) based on the presence of *Sphenolithus heteromorphus* (Zones CN3 and CN4); this interval may be bounded by unconformities. The underlying Oligocene sediment (identified in Sample 198-1211A-17R-2, 86 cm) is assigned to Subzone CP19b.

Paleogene

The Paleogene section ranges in age from late Oligocene (Subzone CN19b) to the K/T boundary and includes the E/O and P/E boundary transitions. The Oligocene is relatively complete, although the Miocene/Oligocene boundary interval is absent, and Zone CP17 (lower Oligocene) was not identified. The uppermost Oligocene sediment analyzed (Sample 198-1211A-17R-2, 86 cm) contains *Sphenolithus ciproensis*, which has an LO in Subzone CP19b (25.5 Ma).

The E/O boundary is identified at the LO of *Discoaster barbadiensis* in Samples 198-1211A-10H-1, 140 cm, and 198-1211B-9H-7, 45 cm. The Eocene is relatively complete with all the CP zones identified. The P/E boundary and PETM interval are rather condensed and may be incomplete. In Hole 1211A, the FO of *Discoaster diastypus* (Subzone CP9a), LO of *Fasciculithus*, and FO of *Tribrachiatus orthostylus* (Subzone CP9b) are all recorded in Sample 198-1211A-13H-6, 1 cm, indicating a condensed or absent Subzone CP9a interval. In Hole 1211B, the FO of *Discoaster diastypus* (Sample 198-1211B-13H-4, 77 cm) and FO of *Tribrachiatus orthostylus* (Sample 13H-4, 56 cm) are separated by 21 cm, again suggesting a condensed interval. In Hole 1211C, the interval separating these datums is 100 cm (FO of *D. diastypus* in Sample 198-1211C-13H-2, 120 cm, and FO of *T. orthostylus* in Sample 13H-2, 20 cm), indicating a more complete record. The remainder of the Paleocene appears to be relatively complete in all three holes, although sedimentation rates are low (0.5–2.5 m/m.y.) (see “Sedimentation and Accumulation Rates,” p. 21).

The K/T boundary is present in Sections 198-1211A-15H-4, 198-1211B-15H-3, and 198-1211C-15H-3. The nannofossil succession is similar to that observed at Site 1210. Sediments bearing common *Micula prinsii* (Zone CC26; Sample 198-1211B-15H-3, 125 cm) are overlain by a white carbonate interval that has a mixed assemblage at the base, incorporating Cretaceous nannofloras together with common calcisphere fragments (interval 198-1211B-15H-3, 115–120 cm). Above this, smear slides are dominated by fine micrite, minute foraminifers, and abundant calcispheres, with few reworked Cretaceous nannofossil taxa (interval 198-1211B-15H-3, 108 cm, through 15H-2, 90 cm). These samples consistently contain survivor taxa (e.g., species of *Lapideacassis*, *Cyclagelosphaera*, and *Markalius*). The first new Paleocene coccolith taxa include the genus *Neobiscutum*, recorded in Sample 198-1211B-15H-3, 102 cm, and *Cruciplacolithus primus* in Sample 198-1211B-15H-3, 62 cm.

Cretaceous

An apparently continuous section of rapidly deposited upper to lower Maastrichtian sediments was recovered at Site 1211. The calcareous nannofossils from this interval are well preserved and the assemblages are diverse. Zones CC26 to CC24 were identified, but the zonal boundaries are somewhat uncertain, due to problems concerning the identification and stratigraphic range of a number of the marker taxa,

particularly *Micula murus* and *Reinhardtites levis*. The nature of these difficulties will be a focus of postcruise investigations.

Planktonic Foraminifers

Neogene

The Neogene section ranges from upper Pleistocene to upper Miocene, with a major unconformity separating the upper Miocene and upper Oligocene. Planktonic foraminifers at Site 1211 are generally moderately preserved. They are abundant to common in the Pleistocene and Pliocene but decline in abundance and preservation through the Miocene.

The youngest sediments recovered in Hole 1211A are assigned to the upper part of Zone N22 based on the presence of *Truncorotalia truncatulinoides* in Sample 198-1211A-1H-CC and on the absence of *Truncorotalia tosaensis*. The remainder of the Pleistocene sequence (Samples 198-1211A-2H-CC, 198-1211B-1H-CC through 2H-CC, and 198-1211C-1H-CC through 2H-CC) also belongs to Zone N22 and contains common *Globigerina bulloides*, *Globorotalia inflata*, *Truncorotalia crassaformis*, *Orbulina universa*, *Neogloboquadrina dutertrei*, *Neogloboquadrina pachyderma* (dextral), rare to few *T. truncatulinoides*, and *T. tosaensis*. They are supplemented by few *Globorotalia menardii*, *Globorotalia tumida*, and pulleniatinids. In the Pliocene sediments, the FOs of *T. tosaensis*, *T. crassaformis* (Samples 198-1211A-3H-CC, 198-1211B-2H-CC, and 198-1211C-3H-CC), and *Sphaeroidinella dehiscens* (Samples 198-1211A-5H-CC, 198-1211B-3H-CC, and 198-1211C-4H-CC) permit the differentiation of Zones N21 and N20–N19, respectively. Other useful events are the LOs of *Dentoglobigerina altispira* (Samples 198-1211A-4H-CC and 198-1211B-4H-CC), *Sphaeroidinellopsis seminulina* (Samples 198-1211A-5H-CC and 198-1211B-4H-CC), and *Globoturborotalita nepenthes* (Samples 198-1211A-5H-CC and 198-1211B-5H-CC).

The uppermost Miocene is present in Sample 198-1211B-6H-CC, which contains common *G. tumida*, *Globoconella conoidea*, *Globoturborotalita nepenthes*, and *Sphaeroidinellopsis seminulina*. This section is assigned to Zone N18 based on the presence of *G. tumida* and the absence of *Sphaeroidinella dehiscens*. Although the planktonic assemblage is poorly preserved in Sample 198-1211A-6H-CC, the presence of rare to few taxa such as *Dentoglobigerina altispira*, "*Globigerina*" *venezuelana*, *Globoquadrina dehiscens*, *G. nepenthes*, and *Globigerinoides extremus* and the absence of *G. tumida*, *Globigerinoides conglobatus*, and *Globorotalia conomiozea* are indicative of Subzone N17a.

Paleogene

A major unconformity separates the upper Miocene from the Oligocene sequence drilled in Holes 1211A (interval 198-1211A-7H-CC through 9H-CC), 1211B (interval 198-1211B-6H-CC through 8H-CC), and 1211C (interval 198-1211C-6H-CC through 8H-CC). In general, the Oligocene assemblage shows low diversity and poor preservation. Subdivision of the Oligocene section is difficult, due to the paucity of zonal marker species. The planktonic foraminiferal assemblages are represented mainly by dissolution-resistant taxa such as *Catapsydrax dissimilis*, *Catapsydrax unicavus*, "*Globigerina*" *euapertura*, *Globigerina pseudovenezuelana*, *Globoquadrina tripartita*, *Globigerina sellii*, and few globorotaloidids. Sample 198-1211A-7H-CC and interval 198-1211B-

6H-CC to 7H-CC are tentatively assigned to the upper Oligocene Subzone P21b based on the presence of very rare *Paragloborotalia opima* and on the absence of chiloguembelinids. The presence of *Subbotina angiporoides* and the absence of "*Globigerina*" *ampliapertura* allow us to assign Sample 198-1211A-8H-CC to lower Oligocene Zone P20–P21a. The underlying Sample 198-1211B-8H-CC yields few "*G.*" *ampliapertura*, *Subbotina angiporoides*, *S. gortanii*, *S. praeturritilina*, and *Globoquadrina tapuriensis* and indicates lower Oligocene Zones P19 to P18.

Dissolution and generally poor preservation also characterize the upper Eocene. Sample 198-1211A-9H-6, 118–119 cm, is assigned to Zones P16 to P17 based on the presence of "spines" of *Hantkenina*, poorly preserved specimens of *Hantkenina alabamensis*, *Pseudohastigerina micra*, and *Pseudohastigerina naguwichiensis*. The assemblage is dominated by dissolution-resistant taxa, including *Turborotalia pseudoampliapertura*, *Globorotaloides suteri*, *Subbotina eocaena*, *C. unicavus*, and "*Globigerina*" *euapertura*. A similar assemblage is present in Sample 198-1211B-9H-CC. Sample 198-1211A-10H-CC, which contains few *Globigerinatheka tropicalis*, *Globigerinatheka index*, *Globigerinatheka subconglobata*, *G. senni*, subbotinids, common fragments of *Globigerinatheka* spp., hantkeninids, and turborotalids, is assigned to Zone P14 based on the absence of *Globigerinatheka semiinvoluta* and "*Orbulinoides*" *beckmanni*.

Preservation improves lower in the middle Eocene. Samples 198-1211B-10H-CC and 198-1211C-10H-CC contain a moderately well-preserved assemblage, which includes *G. subconglobata*, *G. senni*, *Morozovella aragonensis*, *Acarinina bullbrooki*, *Igorina broedermanni*, *Subbotina eocaenica*, *Subbotina cryptomphala*, and *Guembelitrioides lozanoi*. This assemblage is indicative of the upper part of Zone P10 based on the absence of *Morozovella lehneri* and *Morozovella caucasica*.

Samples 198-1211A-11H-CC, 198-1211B-11H-CC, and 198-1211C-11H-CC are characterized by the presence of *Morozovella aragonensis*, *M. caucasica*, *Igorina broedermanni*, *Acarinina pentacamerata*, *Acarinina soldadoensis*, *Subbotina cryptomphala*, *Guembelitrioides lozanoi*, and *Globigerinatheka senni*. The absence of *Hantkenina*, together with the presence of *M. caucasica* and *Acarinina pentacamerata*, allows us to assign this assemblage to the lower Eocene Zones P9 to P8. Zone P7 is distinguished from the overlying sediments by the co-occurrence of *M. aragonensis*, *M. formosa*, and *Subbotina inaequispira* and by the absence of *Acarinina pentacamerata* in Samples 198-1211A-12H-CC and 198-1211B-12H-CC.

Lower Eocene Zone P6 has been recognized in Sample 198-1211B-13H-4, 16–17 cm. Characteristic taxa of Zone P6 include *Morozovella subbotinae*, *Morozovella formosa*, *Morozovella gracilis*, *Subbotina velascoensis*, and *A. soldadoensis* in the absence of both *M. aragonensis* and *M. velascoensis*.

The LO of *Morozovella velascoensis* is used to define the P5/P6 zonal boundary, as well as the P/E boundary and lies between Samples 198-1211B-13H-4, 73–74 cm, and 13H-4, 89–90 cm, and between Samples 198-1211A-13H-5, 86–87 cm, and 13H-5, 128–129 cm. The PETM (Zachos et al., 1993) occurs within Zone P5, and the interval is well identified in Sections 198-1211A-13H-6, 198-1211B-13H-4, 198-1211C-13H-2, and 13H-3.

The underlying samples (198-1211A-13H-CC and 198-1211B-13H-CC) contain a diverse and well-preserved assemblage of *M. velascoensis*, *Morozovella occlusa*, *Morozovella acuta*, *M. subbotinae*, *Morozovella aequa*, *Morozovella pasionensis*, *Acarinina soldadoensis*, *Acarinina mckannai*, and *Acarinina nitida*, indicative of Zone P5. *Morozovella angulata*, *Morozovella*

conicotruncana, *Subbotina triloculinoides*, *Igorina albeari*, and *Parasubbotina pseudobulloides* mark Zone P3 in Sample 198-1211B-14H-CC.

Sample 198-1211B-14H-CC contains *Praemurica uncinata*, *Praemurica inconstans*, *Parasubbotina varianta*, *Morozovella praeangulata*, *Globoanomalina compressa*, and *Parasubbotina pseudobulloides*. This interval is assigned to lower Paleocene Zone P2 based on the absence of *M. angulata* and *M. conicotruncata*.

The interval containing Zone P1 at Site 1211 was not observed in core catcher samples. However, several samples taken across the K/T boundary permit the recognition of the *Parvularugoglobigerina eugubina* Zone (Zone P α) in the interval between Samples 198-1211A-15H-4, 88–89 cm, and 15H-5, 0–1 cm. The boundary between the lowermost Paleocene and the uppermost Maastrichtian is clearly bioturbated, and careful sampling of burrows yields an identifiable biostratigraphy. Few well-preserved Paleocene taxa indicative of the P α Zone, including *P. eugubina*, *Parvularugoglobigerina extensa*, and woodringinids, are underlain by a rich assemblage dominated by minute *Guembelitra* indicative of Zone P0. The Paleocene components are clearly confined to burrows. The highest Cretaceous assemblages are present in Samples 198-1211A-15H-4, 147–148 cm, and 198-1211B-15H-3, 119–120 cm.

Cretaceous

In general, Cretaceous planktonic foraminifers recovered at Site 1211 are abundant and well preserved. However, the uppermost Cretaceous assemblages are significantly affected by dissolution with few whole specimens. Nevertheless, the presence of large-sized Cretaceous taxa such as *Abathomphalus mayaroensis*, *Globotruncana stuarti*, *Globotruncana linneiana*, *Contusotruncana contusa*, *Pseudoguembelina costulata*, *Pseudoguembelina excolata*, and *Pseudoguembelina hariaensis*, as well as the small taxa, including *Schackoina cenomana*, *Schackoina multispinata*, *Globigerinelloides subcarinatus*, *Globotruncanella havanensis*, and *Globotruncanella petaloidea*, indicate that these assemblages belong to the upper Maastrichtian *Abathomphalus mayaroensis* Zone (Zone KS31).

The underlying Upper Cretaceous interval (Samples 198-1211A-16H-6 and 16H-CC, and 198-1211B-16H-CC through 17H-CC) is characterized by moderately to well-preserved planktonic foraminiferal assemblages yielding *Abathomphalus mayaroensis*, *Abathomphalus intermedius*, *Contusotruncana contusa*, *Racemiguembelina fructicosa*, *Pseudotextularia elegans*, *P. excolata*, *P. hariaensis*, *Globotruncanita stuarti*, *Globotruncana stuartiformis*, *Globotruncana orientalis*, *G. linneiana*, *Heterohelix rajagopalani*, and rugoglobigerinids, as well as rare *Globotruncanita angulata* and *Gublerina cuvillieri*. Based on the presence of *Abathomphalus mayaroensis*, this interval is also assigned to the upper Maastrichtian *A. mayaroensis* Zone (KS31).

Samples 198-1211A-17H-CC through 18H-CC yield common *Contusotruncana contusa* and *Racemiguembelina fructicosa* in the absence of *Abathomphalus mayaroensis*, indicating that this interval belongs to the mid-Maastrichtian *C. contusa*–*R. fructicosa* Zone (upper KS30). Other species occurring in this interval are *Contusotruncana patelliformis*, *Globotruncana bulloides*, *G. linneiana*, *G. stuarti*, *G. stuartiformis*, *Rugotruncana subcircumnodifer*, associated with rare *Gansserina gansseri* and *Gansserina wiedenmayeri*, and common pseudoguembelinids and rugoglobigerinids. The lowest part of Hole 1211B (Sections 198-1211B-18H-CC through 19H-CC) is assigned to the lower Maastrichtian–upper Campanian *Gansserina gansseri* Zone (lower KS30) based on the absence of *C. contusa*

and *R. fructicosa* and the presence of few *G. gansseri* together with *Conusotruncana fornicata*, *Globotruncana bulloides*, and globigerinelloids.

Benthic Foraminifers

Benthic foraminifers were examined in selected core catcher samples of Holes 1211A and 1211B. They are well preserved and rare to few in abundance in the Neogene. The Paleogene through Cretaceous section contains moderately preserved benthic foraminifers that are generally rare to few in abundance. Benthic foraminifers are relatively abundant in the upper Miocene, in the E/O boundary interval, and near the K/T boundary, due to dissolution of planktonic foraminifers.

Neogene

In Samples 198-1211A-1H-CC through 5H-CC and 198-1211B-1H-CC through 5H-CC, the Pleistocene to Pliocene benthic assemblages are represented by diverse taxa including *Anomalinoidea globulosus*, *Oridorsalis tener*, cibicidoidids, gyroidinoidids, *Pyrgo lucernula*, *Pyrgo murrhina*, uvigerinids, and agglutinated species (*Eggerella bradyi* and *Martinottiella* sp.). *Uvigerina* is one of the characteristic genera of the Neogene but is poorly preserved and very rare in Hole 1211B. The upper Miocene interval represented in Sample 198-1211A-6H-CC is characterized by the benthic foraminifers *A. globulosus*, *Gyroidinoides girardanus*, *O. tener*, *P. lucernula*, *P. murrhina*, and abundant *Stilostomella subspinosa*.

Neogene benthic foraminifer assemblages indicate paleowater depths in the upper abyssal zone (2000–3000 m) based on the presence of *A. globulosus*, cibicidoidids (*Cibicidoides mundulus* and *Cibicidoides wuellerstorfi*), *Pyrgo murrhina*, *P. lucernula*, and uvigerinids (*Uvigerina hispida*, *Uvigerina hispidocostata*, and *Uvigerina senticososa*) (Pflum et al., 1976; Woodruff, 1985; van Morkhoven et al., 1986).

Paleogene

The Oligocene interval (Samples 198-1211A-7H-CC, 9H-CC, and 198-1211B-6H-CC through 8H-CC) yields benthic assemblages that are generally dominated by large and abundant stilostomellids (*Orthomorphina* spp., *Stilostomella abyssorum*, *Stilostomella gracillima*, *Stilostomella subspinosa*, and *Stilostomella* spp.). Other components include *Bolivina huneri*, *Globocassidulina subglobosa*, and *Vulvulina spinosa*. Near the E/O boundary (Samples 198-1211A-9H-CC and 198-1211B-8H-CC), buliminids (*Bulimina elongata*, *Bulimina impendens*, *Bulimina jarvisi*, and *Bulimina semicostata*) also characterize the benthic assemblages.

B. jarvisi, *B. semicostata*, *Clinapertina complanata*, *Nuttallides truempyi*, *Oridorsalis umbonatus*, and stilostomellids represent the Eocene benthic assemblages (Samples 198-1211A-10H-CC through 12H-CC and 198-1211B-11H-CC and 12H-CC). In Samples 198-1211A-11H-CC and 198-1211B-11H-CC and 12H-CC, benthic foraminifers are rare and small. Sample 198-1211A-12H-CC contains abundant *Aragonia aragonensis* and *Chrysalogonium* spp.

Samples 198-1211A-13H-CC and 198-1211B-13H-CC and 14H-CC contain benthic assemblages characterized by the species *Conorbinoides hillebrandti*, *Nuttallides truempyi*, *Oridorsalis umbonatus*, *Aragonia ouezzaensis*, *Aragonia velascoensis*, *Buliminella grata*, *Dentalina* spp., *Lenticulina* spp., and agglutinated taxa (*Marssonella trochoides* and *Spiroplectammia*

jarvisi). Paleogene benthic assemblages are indicative of upper abyssal depths (2000–3000 m).

Cretaceous

Sections 198-1211A-15H-CC through 18H-CC and 198-1211B-15H-CC through 19H-CC contain benthic assemblages that are generally dominated by trochospiral calcareous taxa (*Nuttallides truempyi*, *Oridorsalis umbonatus*, *Osangularia plummerae*, and *Sliterella lobulata*), *Aragonia ouezzanensis*, *A. velascoensis*, *Dentalina* spp., *Lenticulina* spp., and *Pyramidina szajnochae*. Although rare, the agglutinated species including *Gaudryina pyramidata*, *Marssonella trochoides*, and *Spiroplectammina jarvisi* also characterize the benthic assemblages of this interval.

Upper Cretaceous trochospiral calcareous benthic foraminifers indicate abyssal paleowater depths (>2500 m; after Nyong and Olsson, 1984) in nannofossil Zones CC25 and CC26. The presence of *A. velascoensis* in nannofossil Zone CC24 is indicative of lower bathyal to uppermost abyssal paleowater depth (1500–2500 m depth, according to Nyong and Olsson, 1984), suggesting a general deepening trend through the Maastrichtian.

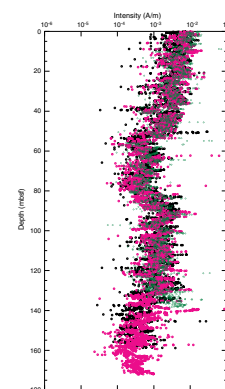
PALEOMAGNETISM

Archive halves of core sections from Holes 1211A and 1211B were measured on the shipboard pass-through magnetometer unless they displayed obvious and pervasive coring disturbance. Measurements were made on 18 APC cores from Hole 1211A, 19 APC cores from Hole 1211B, and 15 APC cores from Hole 1211C. As at previous sites, most of the data from cores older than Pliocene age are uninterpretable. This is largely attributed to deformation of these soft sediments during drilling, core recovery, or core splitting.

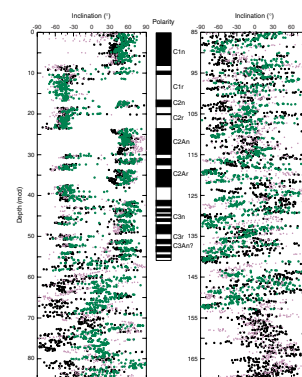
As for other Leg 198 sites, the natural remanent magnetization (NRM) of core sections was measured at 5-cm intervals, followed by measurement after two alternating-field (AF) demagnetization steps (10- and 20-mT peak fields). When time was available, additional AF demagnetization steps (usually at peak fields of 15 mT) were carried out. NRM intensity values typically stayed within a narrow range, from $\sim 10^{-2}$ to 10^{-1} A/m. After AF demagnetization at 20 mT (to remove the drill string overprint), intensity values were generally from $\sim 2 \times 10^{-4}$ to 2×10^{-2} A/m (Fig. F10). A decline of magnetization intensity of about one order of magnitude was observed with depth from the surface to 160 mbsf. An interval of lower magnetization intensities ($\sim 5 \times 10^{-4}$ A/m) is observed in the 50–90 mbsf interval, corresponding to a large part of the Oligocene–Eocene sedimentary sequence. Similar low intensity values are also found at the base of the section in the 140–160 mbsf (Upper Cretaceous) interval (Fig. F10).

Paleomagnetic data acquired from the shipboard pass-through magnetometer from Site 1211 produced an interpretable magnetic polarity stratigraphy only in the upper ~ 55 meters composite depth (mcd). In this uppermost Miocene, Pliocene, and Pleistocene section, it was possible to recognize polarity zones corresponding to the Brunhes Chron (C1n) to the base of the Gilbert Chron (C3r) in Holes 1211A and 1211B (Fig. F11). The polarity zone correlative to C3r is thinned relative to C3n, indicating increased mean sedimentation rates from the onset of C3n. Directly below C3r, several polarity chrons were evident in both

F10. Archive-half magnetization intensities after AF demagnetization at peak fields of 20 mT, p. 41.



F11. Inclination after AF demagnetization at peak fields of 20 mT, p. 42.



holes, but the polarity zone pattern is ambiguous. The next two normal polarity zones below C3r were tentatively interpreted as correlative to C3An (Fig. F11).

Measurements on cores deeper than 50 mcd showed erratic inclination values and poor correlation between holes (Fig. F11), making it impossible to interpret polarities for the upper Miocene–Cretaceous section. As at previous sites, the problem is attributed to the soft and easily deformed nature of the sediments that compromises the pass-through measurements. We are optimistic that the sediments below 55 mcd carry a primary magnetization, and it is possible that discrete samples measured postcruise will resolve the polarity stratigraphy in much of the Cenozoic section. Magnetization intensities in the Cretaceous white ooze below 130 mbsf are very low and may not be useful for shore-based resolution of a magnetic stratigraphy.

Polarity chrons recognized in the upper 50 mbsf of the section yield an age-depth curve for the upper Miocene–Pleistocene sediments (Fig. F12). Interval mean sedimentation rates were in the range 9–13 m/m.y. for the last ~4 m.y. In the 4- to 7-Ma interval, the sedimentation rates were lower, with a mean value of ~4 m/m.y. (Fig. F12). The age-depth curves for Holes 1211A and 1211B diverge in the upper 20 mbsf, corresponding to the last 2.5 m.y., owing to major differences in the cored section in each hole in that interval. In Hole 1211B, the polarity zone correlative to the Brunhes Chron (C1n) is twice as thick as in Hole 1211A, whereas that correlative to C2n is missing from the Hole 1211B section, but not in Hole 1211A. Comparison of magnetic susceptibility measurements between holes (see “Composite Depths,” p. 20) shows that these differences result from gaps between cores and recored intervals in both holes. When depths are computed as meters composite depth, these differences are reconciled (Fig. F11).

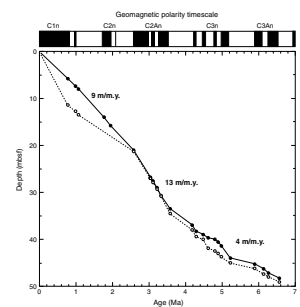
COMPOSITE DEPTHS

Multisensor track (MST) and spectral reflectance (L^*) data collected from Holes 1211A, 1211B, and 1211C were used to determine depth offsets in the composite section. Magnetic susceptibility, gamma ray attenuation (GRA) bulk density, and spectral reflectance measurements were the primary parameters used for core-to-core correlation. GRA bulk density and magnetic susceptibility data were collected at 3-cm intervals and spectral reflectance data were collected at 2.5-cm intervals on all cores (see “MST Measurements,” p. 25, in “Physical Properties” and “Lithostratigraphy,” p. 8, for details about MST and spectral reflectance data).

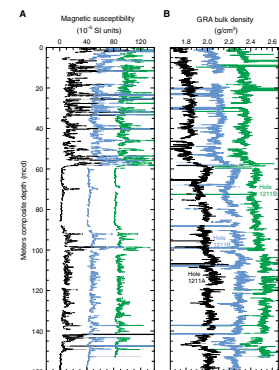
The data used to construct the composite section and determine core overlaps are presented in a composite depth scale in Figure F13. The depth offsets that comprise the composite section for Holes 1211A, 1211B, and 1211C are given in Table T6. Units for the composite depth scale are meters composite depth.

The composite data show that the APC cores from Site 1211 provide a continuous overlap to at least 160 mcd (K/T boundary; ~147.8 mcd in Core 198-1211A-15H). Below the uppermost Maastrichtian, most of the cores from Holes 1211A, 1211B, and 1211C could not be correlated and placed into a composite depth framework because of a low signal amplitude. Expansion of sedimentary features in one hole relative to coeval cores in the other hole indicate distortion of the cored sequence. Because some distortion occurred within individual cores on depth scales

F12. Age-depth curve derived from magnetic stratigraphy, p. 43.



F13. Magnetic susceptibility and GRA bulk density data, p. 44.



T6. Composite depth section, p. 72.

of <9 m, it was not possible to align accurately every feature in the MST and color reflectance records by simply adding a constant to the mbsf core depth.

Following construction of the composite depth section for Site 1211, a single spliced record was assembled for the aligned cores over the upper 160 mcd by using cores from all holes. Intervals having significant disturbance or distortion were avoided. The PETM interval in the composite was taken from Core 198-1211A-13H.

In the uppermost part of the holes, magnetic susceptibility and GRA density patterns are clearly repeated, indicating that several meters of sediment were recovered twice within a single hole (Fig. F14). This caused overlap of data from successive cores in multiple locations on the order of ~3 m. The Site 1211 splice (Table T7) can be used as a guide to sample a single sedimentary sequence between 0 and 160 mcd and can be used to plot other data sets from this site.

SEDIMENTATION AND ACCUMULATION RATES

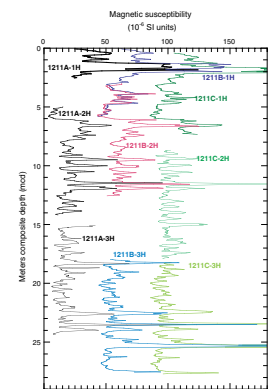
Unconformities and changes in sedimentation rate at Site 1211 are illustrated in a plot of calcareous microfossil datum ages (first and last occurrences) vs. depth (Fig. F15). These rates rely on major calcareous nannofossil and planktonic foraminiferal datums presented in Tables T2 and T3 (see “Biostratigraphy,” p. 13). The Pleistocene–Maastrichtian section cored at Site 1211 is punctuated by unconformities between the upper and middle Miocene and between the upper lower Miocene and upper Oligocene. In addition, an unconformity or condensed interval is present in the middle Eocene section.

An expanded view of the Neogene (Fig. F16) shows that the upper Miocene section accumulated at rates of ~1.8 m/m.y., accelerating to 8.6 m/m.y. in the uppermost Miocene–Pleistocene. Dark-colored, clay-rich sediments in Sections 198-1211A-7H-1 and 198-1211B-6H-6 may represent an unconformity or condensed interval between upper Miocene and lower middle Miocene sediments. The sharp color change in Sections 198-1211A-7H-2 and 198-1211B-6H-7 marks the unconformity separating the upper lower Miocene and the upper Oligocene (Fig. F17).

The Oligocene section accumulated at an average rate of at least 3.4 m/m.y. Sedimentation rates in the Eocene range between 1.5 and 2.2 m/m.y., with the possibility of an unconformity or condensed interval within the middle Eocene section (Fig. F18) (see “Biostratigraphy,” p. 13). Dark-colored sediments in Sections 198-1211A-11H-1 and 198-1211B-10H-4 may reflect this change in sedimentation. The upper Paleocene shows sedimentation rates of ~4.5 m/m.y., whereas much of the middle part of the Paleocene may be somewhat condensed with sedimentation rates ranging between 0.5 and 0.9 m/m.y. By contrast, the lower Danian (lowest Paleocene) is comparatively expanded with rates of 2.5 m/m.y. immediately above the K/T boundary. Shipboard biostratigraphy indicates that the E/O, Paleocene/Eocene (PETM), and K/T boundary intervals are paleontologically complete. Rates for the upper Maastrichtian interval were significantly higher, ranging between 4.5 and 29.5 m/m.y. (Fig. F19).

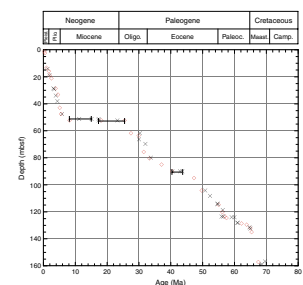
Mass accumulation rates for the bulk sediment, carbonate, and non-carbonate fractions were calculated using dry bulk density (see “Physical Properties,” p. 25) and carbonate concentration (see “Organic Geochemistry,” p. 22) data through 13 linear sedimentation rate segments in the Cretaceous–Neogene section recovered at Site 1211 (Table

F14. Magnetic susceptibility data, 0 to 28 mcd, p. 45.

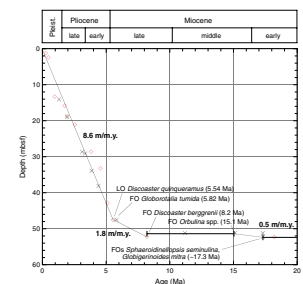


T7. Splice tie points, p. 73.

F15. Age-depth plot of calcareous nannofossil and planktonic foraminiferal datums, p. 46.



F16. Age-depth plot of Neogene calcareous nannofossil and planktonic foraminiferal datums, p. 47.



alkalinity, NH_4^+ , and HPO_4^{2-} reflect the very low organic matter content of the sedimentary section recovered at Site 1211 (see “Carbonate,” p. 22, in “Organic Geochemistry”). The Mn^{2+} and Fe^{2+} pore water profiles exhibit concentration peaks at 8.75 and 18.25 mbsf, respectively (Fig. F23E, F23F). These peak concentration occurrences are consistent with the series of reactions that occur because of a loss of oxygen in sediment pore water, wherein reduction of MnO_2 is followed by the reduction of Fe(III) to Fe(II) (at deeper depths).

Potassium, Calcium, Magnesium, Strontium, and Lithium

Throughout the pore water profile at Site 1211, K^+ , Ca^{2+} , and Mg^{2+} differ little from concentrations in average seawater (Fig. F24A, F24B, F24C). Downcore trends, scarcely distinguishable, are consistent with those resulting from exchange with basaltic basement at depth (Gieskes, 1981), wherein K^+ and Mg^{2+} decrease and Ca^{2+} increases slightly with depth. The convex-upward nature of the upper parts of the Sr^{2+} and Sr/Ca pore water profiles (Fig. F24D) suggests that carbonate dissolution is occurring in the upper ~40–60 m of the sediment column (e.g., Baker et al., 1982). Below this depth, there is little change in either the Sr^{2+} or Sr/Ca profiles, indicating little additional Sr^{2+} input. This lack of variability likely reflects the buffering capacity of the carbonate-dominated Paleogene–Cretaceous sediment, which has not been buried to sufficient depth for the onset of pressure solution. The Li^+ concentrations decrease sharply from 26 μM in the shallowest sample (1.45 mbsf) to a minimum of 18 μM at 27.75 mbsf (Fig. F24E). Below this depth, concentrations gradually increase to 25 μM at the base of the profile (157.75 mbsf).

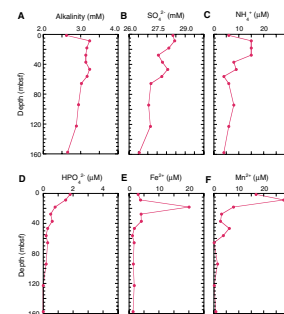
Silica

The morphology of the dissolved silica profile at Site 1211 is generally similar to those observed at Sites 1207–1210, although concentrations in Unit I are lower than in the correlative sections of the other sites (Fig. F25). This is in agreement with lower abundance of both biogenic silica and volcanic ash relative to Sites 1207–1210. Pore water silica concentrations are highest in the Neogene sediments, with an average concentration of $554 \pm 39 \mu\text{M}$ prevailing through the upper ~40 m of the profile. Concentrations decrease gradually to a low of 136 μM at the base of the profile (157.75 mbsf). Elevated concentrations in the upper part of the profile are interpreted to reflect the leaching and weathering of volcanic ash and biogenic silica in the Pliocene–Pleistocene sediments. Lower concentrations occur in the Paleogene–Cretaceous carbonate-dominated sediments, in which biogenic silica is minor and ash is absent. Chert occurs as layers and nodules in the Cretaceous section.

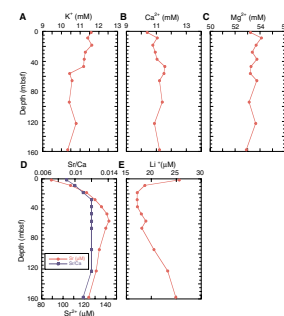
Boron and Barium

Given that the significance of variations in the Ba^{2+} and H_3BO_3 concentrations in pore waters of pelagic sediments is poorly understood, pore water profiles for these parameters at Site 1211 are described largely for purposes of documentation (Table T11). The average boron concentration ($445 \pm 16 \mu\text{M}$) is higher than that of average seawater

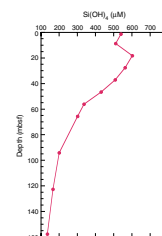
F23. Alkalinity, sulfate, ammonium, phosphate, iron, and manganese profiles, p. 54.



F24. Potassium, calcium, magnesium, strontium, and lithium profiles, p. 55.



F25. Silica profile, p. 56.



(416 μM); concentrations tend to increase downcore. The Ba^{2+} concentrations average $0.5 \pm 0.4 \mu\text{M}$ and show little variability with depth. Concentrations are extremely low but, on average, are higher than those of average seawater, indicating that Ba^{2+} is being added to the system. Possible sources of Ba^{2+} include skeletal debris and minor volcanic ash in the Neogene section, which may be undergoing leaching and/or dissolution.

PHYSICAL PROPERTIES

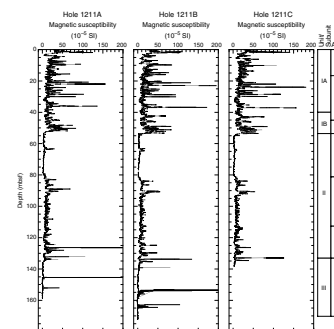
Physical properties at Site 1211 were measured on both whole-round sections and discrete samples from split-core sections. Continuous whole-round measurements were made of magnetic susceptibility, GRA bulk density, and compressional P -wave velocity using the MST for all Site 1211 cores. No natural gamma radiation measurements were made with the MST at Site 1211. Discrete measurements of compressional P -wave velocity were made at a routine frequency of at least one measurement per split-core section in Holes 1211A, 1211B, and 1211C. Index properties were measured on discrete samples from split-core sections at a general frequency of one measurement per section in Hole 1211A.

MST Measurements

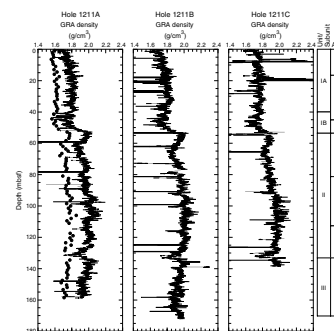
All core sections from Holes 1211A, 1211B, and 1211C were routinely measured on the MST for magnetic susceptibility and GRA bulk density at 3-cm intervals (Figs. F26, F27). MST P -wave velocity was routinely measured at 10-cm intervals on all cores from Holes 1211A, 1211B, and 1211C (Fig. F28). All collected MST data are archived in the Ocean Drilling Program Janus database.

Magnetic susceptibility values (Fig. F26) are generally highest in the uppermost ~ 52 m of the Site 1211 sedimentary column; this interval equates to Pleistocene–Miocene lithologic Unit I (see “Lithologic Unit I,” p. 8., in “Lithostratigraphy”). Peaks in magnetic susceptibility within lithologic Subunits IA and IB may correlate with distinctive ash layers. In the Pleistocene–Miocene section an excellent correlation is also observed between magnetic susceptibility data and color reflectance measurements, primarily the total reflectance value (L^*) and the 550-nm wavelength (see “Lithologic Unit I,” p. 8., in “Lithostratigraphy”). Both magnetic susceptibility and color reflectance data in this interval reveal a pronounced cyclicity, which may be useful in identifying astronomically controlled depositional processes. As already observed at Sites 1209 and 1210, a broad peak in magnetic susceptibility (at ~ 48 – 52 mbsf) characterizes the uppermost Oligocene/lower Miocene unconformity (see “Biostratigraphy,” p. 13). Between ~ 52 and ~ 81 mbsf, throughout the Oligocene segment of lithologic Unit II, magnetic susceptibility values are generally at background levels. Magnetic susceptibilities are higher in the Eocene and Paleocene segments of lithologic Unit II, between ~ 81 and ~ 131 mbsf. A peak in magnetic susceptibility at ~ 90 mbsf correlates with a clay-rich interval within lithologic Unit II (see “Lithologic Unit I,” p. 8, in “Lithostratigraphy”). Within the Eocene and Paleocene intervals of lithologic Unit II there is also a general downhole trend to lower magnetic susceptibility values. As observed at Sites 1209 and 1210, large peaks in magnetic susceptibility values delineate the K/T boundary, which occurs at ~ 133 mbsf in Holes 1211A, 1211B, and 1211C (see “Biostratigraphy,” p. 13). These mag-

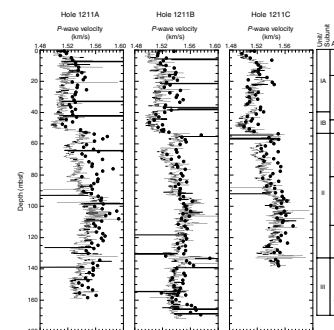
F26. MST magnetic susceptibility, p. 57.



F27. Whole-core MST GRA and discrete bulk density vs. depth, p. 58.



F28. Whole-core MST and discrete P -wave velocity vs. depth, p. 59.



netic susceptibility increases are associated with an increase in clay content and a decrease in carbonate content in this stratigraphic interval (see “[Organic Geochemistry](#),” p. 22). In Cretaceous lithologic Unit III, magnetic susceptibility values are generally close to background, with the exception of some excursions that are related to chert horizons, and do not exhibit any consistent downhole variation.

Site 1211 MST GRA bulk density data (Fig. [F27](#)) do not exhibit a constant downhole increase, as would be expected if increased sediment compaction and dewatering with greater overburden pressure were the only factors controlling this physical property. However, GRA bulk density data do show some distinct variations that relate to lithologic changes at distinct horizons, for example, the uppermost Oligocene/lower Miocene unconformity and the K/T boundary. MST GRA bulk density values exhibit a general downhole increase between the seafloor and ~32 mbsf, within Pleistocene–Pliocene lithologic Subunit IA, before decreasing to lower values through the Pliocene–Miocene components of lithologic Subunits IA and IB, between ~32 and ~50 mbsf. MST GRA bulk density then increases below ~50 mbsf, with a sharp increase at ~53 mbsf occurring at the uppermost Oligocene/lower Miocene unconformity. Cyclical variation in GRA bulk density values, similar to that evident in magnetic susceptibility and color reflectance data (see “[Lithostratigraphy](#),” p. 8), is found within Pleistocene–Miocene lithologic Subunits IA and IB. Between ~53 and 67 mbsf, within the top of the Oligocene segment of lithologic Unit II, MST GRA bulk density decreases. A general trend to higher values with increased burial depth is then evident until ~105 mbsf, through parts of the Oligocene and Eocene components of lithologic Unit II. Within the lower part of lithologic Unit II (Eocene–Paleocene) MST GRA bulk density values decrease with increased burial depth, with a distinct minimum at ~133 mbsf occurring at the Cretaceous/Paleocene boundary (i.e., between lithologic Units II and III). Within Cretaceous lithologic Unit III, MST GRA bulk density values decrease between ~133 and ~165 mbsf, with a small increase in values in the sediments recovered in the basal part of Hole 1211B.

Hole 1211A GRA bulk density values are consistently higher than the discrete wet bulk density measurements (see Fig. [F27](#); Table [T12](#)). These overestimated GRA bulk density values can be explained by the relatively high carbonate content, porosity, and moisture content of sediments; the calibration procedure for the MST GRA sensor is optimized for mixed-lithology sediments. Consequently, the GRA method overestimates the density in carbonate-rich sediments of all lithologic units. This phenomenon is most pronounced in lithologic Unit III because these sediments have the highest carbonate contents (see “[Organic Geochemistry](#),” p. 22).

MST *P*-wave velocities are plotted in Figure [F28](#). Despite some obviously “out of range” values, reliable *P*-wave velocities vary between ~1500 and ~1580 m/s, with the highest velocities generally recorded at greater depths in the sediment column. A linear relationship between increased burial depth and higher MST *P*-wave velocities is not observed at Site 1211. The absence of such a relationship suggests that sediment compaction and dewatering processes are not the only factors influencing *P*-wave velocity values. MST *P*-wave velocities do, however, follow the same downhole trends as the MST GRA bulk density data (Fig. [F27](#)). MST *P*-wave values increase between the seafloor and ~15 mbsf, in the Pleistocene part of lithologic Subunit IA, and then decrease between ~15 and ~48 mbsf, through the Pliocene–Miocene components

[T12](#). Discrete index properties measurements, p. 78.

of lithologic Subunits IA and IB. Between ~48 and ~53 mbsf, in the Miocene part of lithologic Subunit IB, *P*-wave values increase, with an abrupt change from ~1520 to 1540 m/s occurring at ~53 mbsf and corresponding to the uppermost Oligocene/lower Miocene unconformity. From ~53 to ~67 mbsf, *P*-wave velocities again decrease with increasing burial depth (within the Oligocene segment of lithologic Unit II), before exhibiting a general trend to peak values (~1570 m/s) at ~95 mbsf in the Eocene part of lithologic Unit II. In the Eocene–Paleocene of lithologic Unit II, between ~95 and ~131 mbsf, a further trend to decreasing *P*-wave velocities with increased burial depth is observed. At ~131 mbsf an abrupt increase in velocity, from ~1520 to ~1570 m/s, characterizes the Cretaceous/Paleogene boundary and an increase in clay content in this stratigraphic interval. In the upper part of Cretaceous lithologic Unit III, from ~131 to ~155 mbsf, MST *P*-wave velocities decrease, before increasing in the basal portion of Holes 1211A and 1211B.

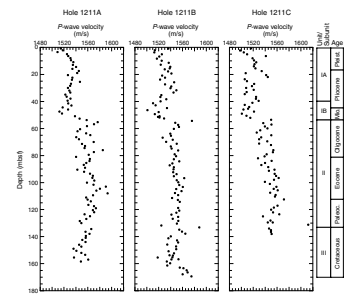
The downhole trends recorded by the reliable MST *P*-wave logger (PWL) values also compare well with the discrete measurements of *P*-wave velocity (Fig. F28, F29; Table T13). However, MST PWL values are generally lower than discrete values; this difference may be due to the assumption in the calibration of the MST PWL that the core liner is full of sediment and that there is no water between the liner and the sediment.

***P*-Wave Velocity**

Discrete measurements of compressional *P*-wave velocity were made on Site 1211 split-core sections using the modified Hamilton frame (PWS3) velocimeter. Data were collected at a routine sampling frequency of one measurement per section (Table T13; Fig. F29). Velocities vary between ~1520 m/s in the soft surface sediments and ~1570 m/s in the more consolidated sediments at Site 1211. Discrete *P*-wave measurements show a general increase in velocity, from ~1520 to ~1540 m/s, between the seafloor and ~20 mbsf in Pleistocene–Pliocene lithologic Subunit IA, before decreasing to ~1510 m/s at ~47 mbsf in Pliocene–Miocene lithologic Subunit IB. Both of these trends are clearly evident in the reliable *P*-wave velocity data obtained with the MST PWL (Fig. F28). Between ~47 and ~55 mbsf, in lithologic Subunit IB and the uppermost part of the Oligocene segment of lithologic Unit II, *P*-wave velocities increase to ~1550 m/s. Velocities then exhibit a general downhole increase through the Oligocene and Eocene segments of lithologic Unit II, to ~1590 (Hole 1211A) or ~1560 (Holes 1211B and 1211C) m/s at ~105 mbsf. In all three holes cored at Site 1211, discrete *P*-wave values decrease through the Eocene and Paleocene parts of lithologic Unit II and the majority of Cretaceous lithologic Unit III. Superimposed on this downhole trend is a peak in discrete *P*-wave values that occurs at ~133 mbsf in Holes 1211B and 1211C and delineates the Cretaceous/Paleogene boundary. At the base of Hole 1211B, *P*-wave velocities between ~162 and ~170 mbsf are higher than those recorded in the upper part of lithologic Unit III.

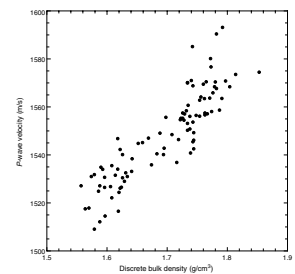
An excellent positive correlation ($R^2 = 0.88$) between Hole 1211A *P*-wave velocity and discrete bulk density (Fig. F30) indicates that these two properties are closely related at Site 1211. The lack of evidence for early diagenetic cementation near the seafloor, as shown by high-percentage porosity in the interval 0–50 mbsf (Fig. F31; Table T12), suggests that increasing *P*-wave velocity and bulk density with depth in the upper ~25 m of Site 1211 is primarily the result of compaction and pore

F29. Discrete *P*-wave velocities, p. 60.

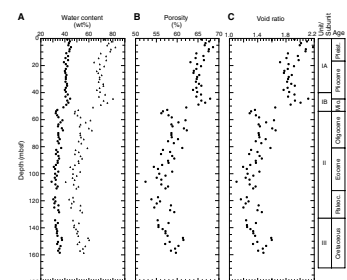


T13. Discrete measurements of *P*-wave velocity, p. 80.

F30. *P*-wave velocities vs. wet bulk density, p. 61.



F31. Water content, porosity, and void ratio vs. depth, p. 62.



fluid expulsion. The lack of any constant increase in either of these two physical properties with greater burial depth further suggests that compaction and pore fluid expulsion are not the only factors influencing the more deeply buried sediments at this locality. It is highly probable that primary sediment composition was an additional important factor that influenced postdepositional changes following sediment burial on the Southern High of Shatsky Rise, as also indicated at Sites 1209 and 1210 (see “[Summary](#),” p. 33, in “Physical Properties” in the “Site 1209” chapter and “[Index Properties](#),” p. 29, in “Physical Properties” in the “Site 1210” chapter).

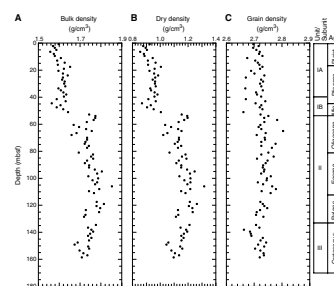
Index Properties

Index properties determined for discrete samples from Hole 1211A are listed in Table [T12](#) and shown in Figures [F31](#) and [F32](#). Index properties reflect progressive sediment compaction and fluid expulsion with depth in the sediment column and also indicate changes in sediment composition as defined by lithologic units and subunits (see “[Lithostratigraphy](#),” p. 8). Bulk and dry density values increase between the seafloor and ~105 mbsf, through Pleistocene–Miocene lithologic Unit I and the Oligocene and Eocene parts of lithologic Unit II. A large stepped increase in both bulk and dry density is further evident at ~53 mbsf, and this change delineates the unconformable (uppermost Oligocene/lower Miocene) boundary between lithologic Units I and II. Below ~105 mbsf, bulk and dry density exhibit a general trend to lower values through the Eocene–Paleocene segments of lithologic Unit II and Cretaceous lithologic Unit III. By comparison, grain density does not exhibit any clear downhole variation, which might explain the relatively good correlation between GRA bulk density and *P*-wave velocity (Fig. [F30](#)). Water content, porosity, and void ratio exhibit a general downhole decrease between the seafloor and ~105 mbsf, through Pleistocene–Miocene lithologic Unit I and the Oligocene and Eocene segments of lithologic Unit II, the corollary to increasing bulk and dry density (Fig. [F32](#)). Below ~105 mbsf, in the Eocene and Paleocene portions of lithologic Unit II and Cretaceous lithologic Unit III, water content, porosity, and void ratio exhibit general trends to higher values with greater burial depth. These trends suggest that overburden on the Cretaceous sediments was not sufficient to cause significant downhole water loss and consequent decrease in porosity.

Summary

As observed at Sites 1209 and 1210, physical properties data at Site 1211 show variation with depth below seafloor that is controlled by progressive compaction and fluid expulsion only in the uppermost part of the sedimentary column (i.e., between 0 and 20 mbsf). In addition, as at Sites 1209 and 1210, a simple relationship between lithology and physical properties is less obvious at Site 1211 than at Sites 1207 and 1208. The absence of these simple relationships may in part be due to the more continuous Late Cretaceous–Holocene sedimentation at Site 1211 and, hence, the absence of major unconformities spanning long periods of geologic time. As observed for Sites 1209 and 1210, the unusual downhole trends in physical properties data cannot be explained by the sediment burial history alone. The physical properties data suggest that there has been less compaction and diagenesis in the sediments below ~105 mbsf relative to those sediments in the overlying

F32. Wet bulk, dry, and grain density vs. depth, p. 63.



stratigraphic interval. This variability may be a reflection of varying microfossil composition within the Site 1211 sediments and the so-called “diagenetic potential” of different sediments (see “**Physical Properties**,” p. 29, in the “Site 1209” chapter).

REFERENCES

- Baker, P.A., Gieskes, J.M., and Elderfield, H., 1982. Diagenesis of carbonates in deep-sea sediments—evidence from Sr²⁺/Ca²⁺ ratios and interstitial dissolved Sr²⁺ data. *J. Sediment. Petrol.*, 52:71–82.
- Berggren, W.A., Kent, D.V., Swisher, C.C., III, and Aubry, M.-P., 1995. A revised Cenozoic geochronology and chronostratigraphy. In Berggren, W.A., Kent, D.V., Aubry, M.-P., and Hardenbol, J. (Eds.), *Geochronology, Time Scales and Global Stratigraphic Correlation*. Spec. Publ.—SEPM (Soc. Sediment. Geol.), 54:129–212.
- Broecker, W.S., and Peng, T.H., 1982. *Tracers in the Sea*: Palisades, New York (Lamont-Doherty Geol. Observ.).
- Bukry, D., 1975. Coccolith and silicoflagellate stratigraphy, northwestern Pacific Ocean, Deep Sea Drilling Project Leg 32. In Larson, R.L., Moberly, R., et al., *Init. Repts. DSDP, 32*: Washington (U.S. Govt. Printing Office), 677–701.
- Cande, S.C., and Kent, D.V., 1995. Revised calibration of the geomagnetic polarity timescale for the Late Cretaceous and Cenozoic. *J. Geophys. Res.*, 100:6093–6095.
- Caron, M., 1975. Late Cretaceous foraminifera from the northwestern Pacific, Leg 32, Deep Sea Drilling Project. In Larson, R.L., Moberly, R., et al., *Init. Repts. DSDP, 32*: Washington (U.S. Govt. Printing Office), 719–724.
- Dickens, G.R., Castillo, M.M., and Walker, J.G.C., 1997. A blast of gas in the latest Paleocene: simulating first-order effects of massive dissociation of oceanic methane hydrate. *Geology*, 25:259–262.
- Dickens, G.R., O’Neil, J.R., Rea, D.K., and Owen, R.M., 1995. Dissociation of oceanic methane hydrate as a cause of the carbon isotope excursion at the end of the Paleocene. *Paleoceanography*, 10:965–971.
- Gieskes, J.M., 1981. Deep-sea drilling interstitial water studies: implications for chemical alteration of the oceanic crust, Layers I and II. In Warme, J.E., Douglas, R.G., and Winterer, E.L. (Eds.), *The Deep Sea Drilling Project: A Decade of Progress*. Spec. Publ.—SEPM (Soc. Sediment. Geol.), 32:149–167.
- Larson, R.L., Moberly, R., et al., 1975. *Init. Repts. DSDP, 32*: Washington (U.S. Govt. Printing Office).
- Luterbacher, H.P., 1975. Early Cretaceous foraminifera from the northwestern Pacific, Leg 32, Deep Sea Drilling Project. In Larson, R.L., Moberly, R., et al., *Init. Repts. DSDP, 32*: Washington (U.S. Govt. Printing Office), 703–718.
- McDuff, R.E., 1985. The chemistry of interstitial waters, Deep Sea Drilling Project Leg 86. In Heath, G.R., Burckle, L.H., et al., *Init. Repts. DSDP, 86*: Washington (U.S. Govt. Printing Office), 675–687.
- Millero, F.J., and Sohn, M.L., 1992. *Chemical Oceanography*: Boca Raton (CRC Press).
- Nakanishi, M., Tamaki, K., and Kobayashi, K., 1989. Mesozoic magnetic anomaly lineations and seafloor spreading history of the Northwestern Pacific. *J. Geophys. Res.*, 94:15437–15462.
- Nyong, E.E., and Olsson, R.K., 1984. A paleoslope model of Campanian to lower Maestrichtian foraminifera in the North American Basin and adjacent continental margin. *Mar. Micropaleontol.*, 8:437–477.
- Oxburgh, R., and Broecker, W.S., 1993. Pacific carbonate dissolution revisited. *Palaeogeogr., Palaeoclimatol., Palaeoecol.*, 103:31–39.
- Perch-Nielsen, K., 1985. Cenozoic calcareous nannofossils. In Bolli, H.M., Saunders, J.B., and Perch-Nielsen, K. (Eds.), *Plankton Stratigraphy*: Cambridge (Cambridge Univ. Press), 427–554.
- Pflum, C.E., Frerichs, W.E., and Sliter, W.V., 1976. *Gulf of Mexico Deep-water Foraminifers*. Spec. Publ.—Cushman Found. Foraminiferal Res., 14.
- Rea, D.K., Basov, I.A., Krissek, L.A., and the Leg 145 Scientific Party, 1995. Scientific results of drilling the North Pacific transect. In Rea, D.K., Basov, I.A., Scholl, D.W., and Allan, J.F. (Eds.), *Proc. ODP, Sci. Results*, 145: College Station, TX (Ocean Drilling Program), 577–596.

- Schrag, D.P., Hampt, G., and Murray, D.W., 1996. Pore fluid constraints on the temperature and oxygen isotopic composition of the glacial ocean. *Science*, 272:1930–1932.
- Sliter, W.V., 1992. Cretaceous planktonic foraminiferal biostratigraphy and paleoceanographic events in the Pacific Ocean with emphasis on indurated sediment. In Ishizaki, K., and Saito, T. (Eds.), *Centenary of Japanese Micropaleontology*: Tokyo (Terra Sci.), 281–299.
- Sliter, W.V., and Brown, G.R., 1993. Shatsky Rise: seismic stratigraphy and sedimentary record of Pacific paleoceanography since the Early Cretaceous. In Natland, J.H., Storms, M.A., et al., *Proc. ODP, Sci. Results*, 132: College Station, TX (Ocean Drilling Program), 3–13.
- van Morkhoven, F.P.C.M., Berggren, W.A., and Edwards, A.S., 1986. Cenozoic cosmopolitan deep-water benthic foraminifera. *Bull. Cent. Rech. Explor.—Prod. Elf-Aquitaine*, 11.
- Woodruff, F., 1985. Changes in Miocene deep-sea benthic foraminiferal distribution in the Pacific Ocean: relationship to paleoceanography. In Kennett, J.P. (Ed.), *The Miocene Ocean: Paleoceanography and Biogeography*. Mem.—Geol. Soc. Am., 163:131–175.
- Zachos, J.C., Lohmann, K.C., Walker, J.C.G., and Wise, S.W., Jr., 1993. Abrupt climate change and transient climates during the Paleogene: a marine perspective. *J. Geol.*, 101:191–213.

Figure F2. Summary diagram of coring results at Site 1211 plotted on the meters composite depth (mcd) scale. The maximum penetration measured with the drill pipe was 169.9 mbsf. MST magnetic susceptibility (brown points) and GRA wet bulk density (dark blue points) were measured every 3.0 cm. The accurate correction factor for the magnetic susceptibility raw instrument values is 0.68×10^{-5} . For details about figure symbols and descriptions see Figure F12, p. 101, in the “Leg 198 Summary” chapter.

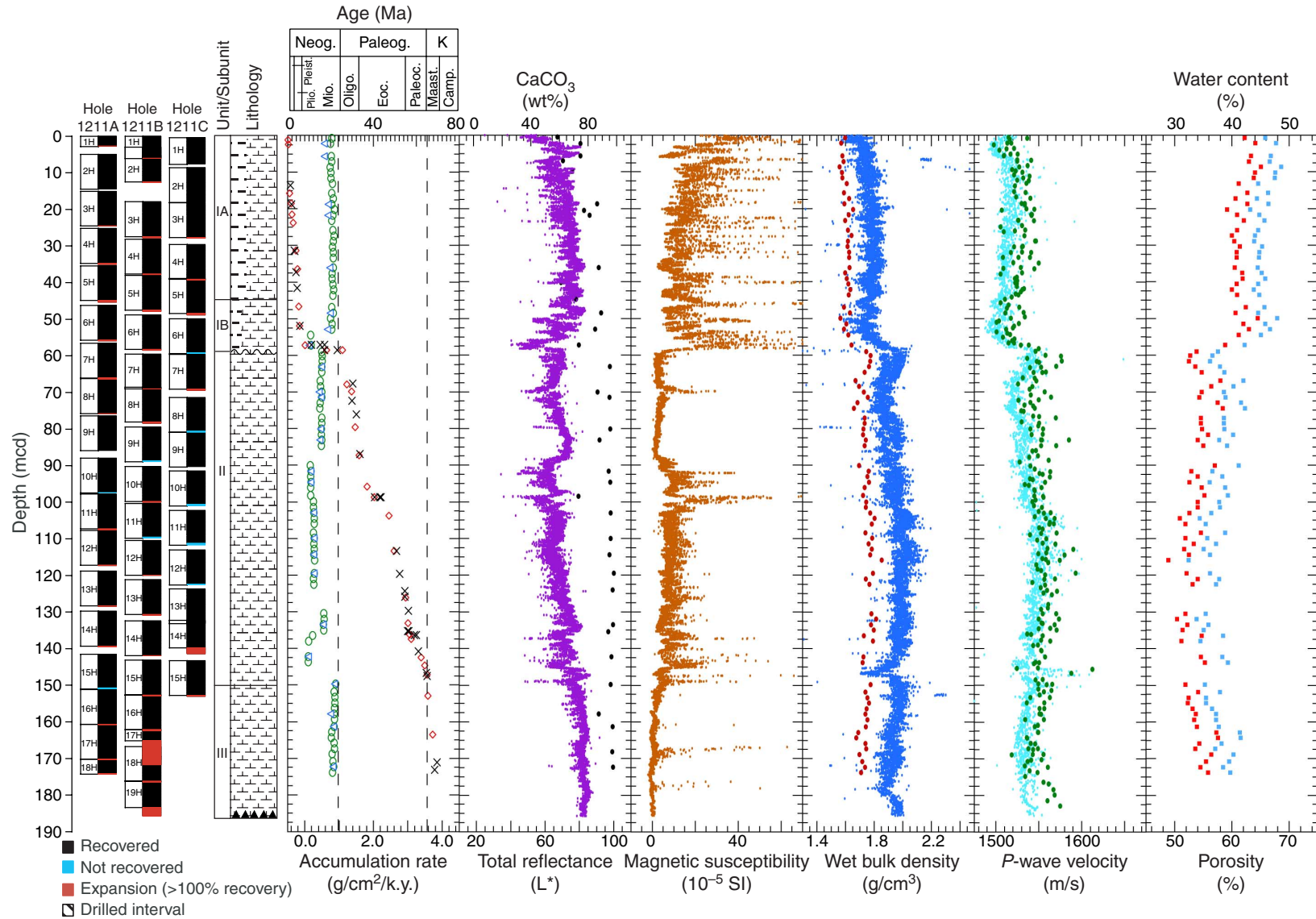


Figure F3. Age-depth curves for Sites 1209, 1210, 1211, and 1212 based on shipboard biostratigraphy. Circles = planktonic foraminiferal datums, squares = nannofossil datums, P. = Pleistocene, Pl. = Pliocene.

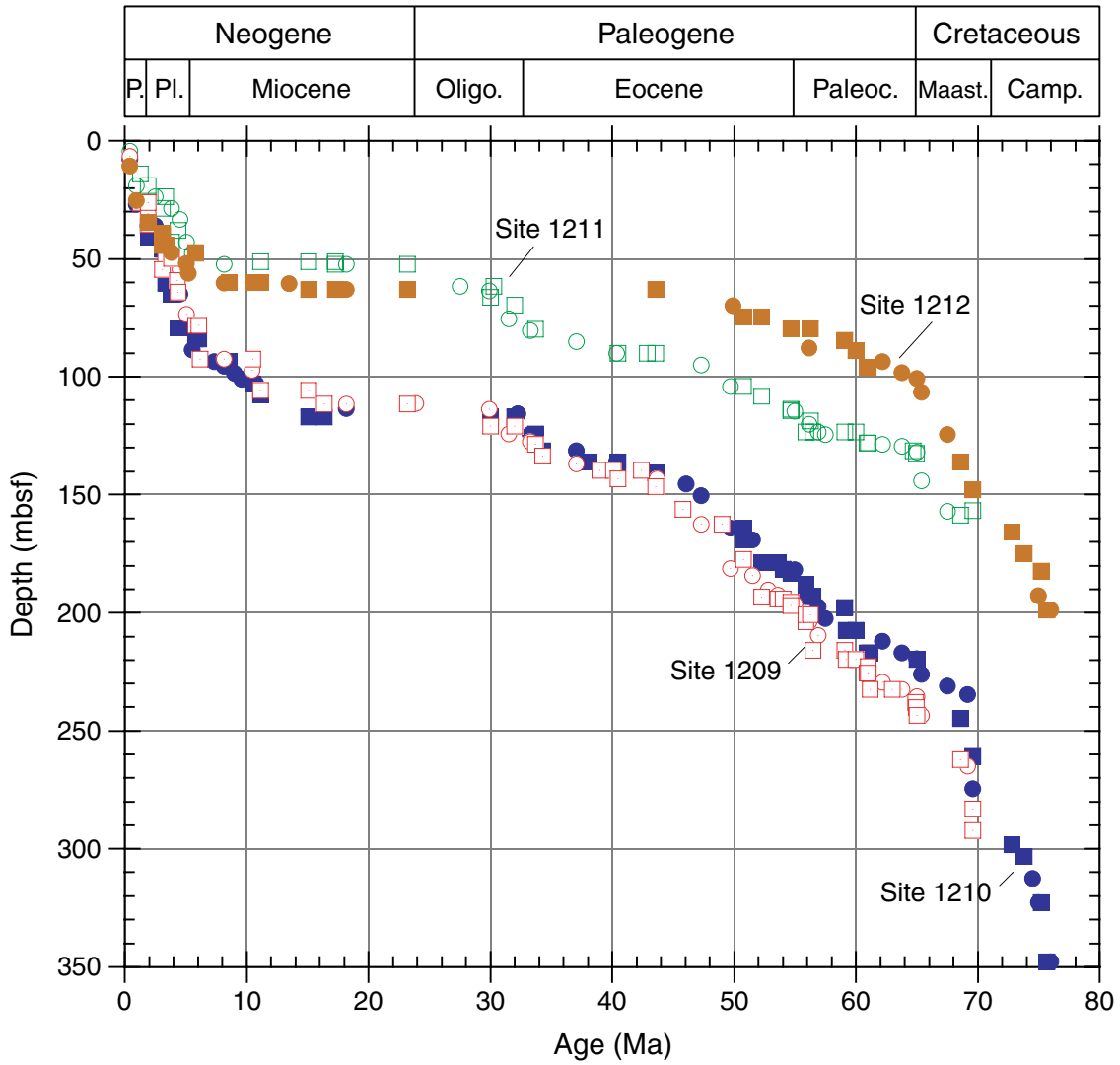


Figure F4. Lithology of the E/O boundary interval in Core 198-1211C-9H. The arrow points to the last observed occurrence of *Hantkenina* sp., the planktonic foraminiferal datum that defines the boundary.

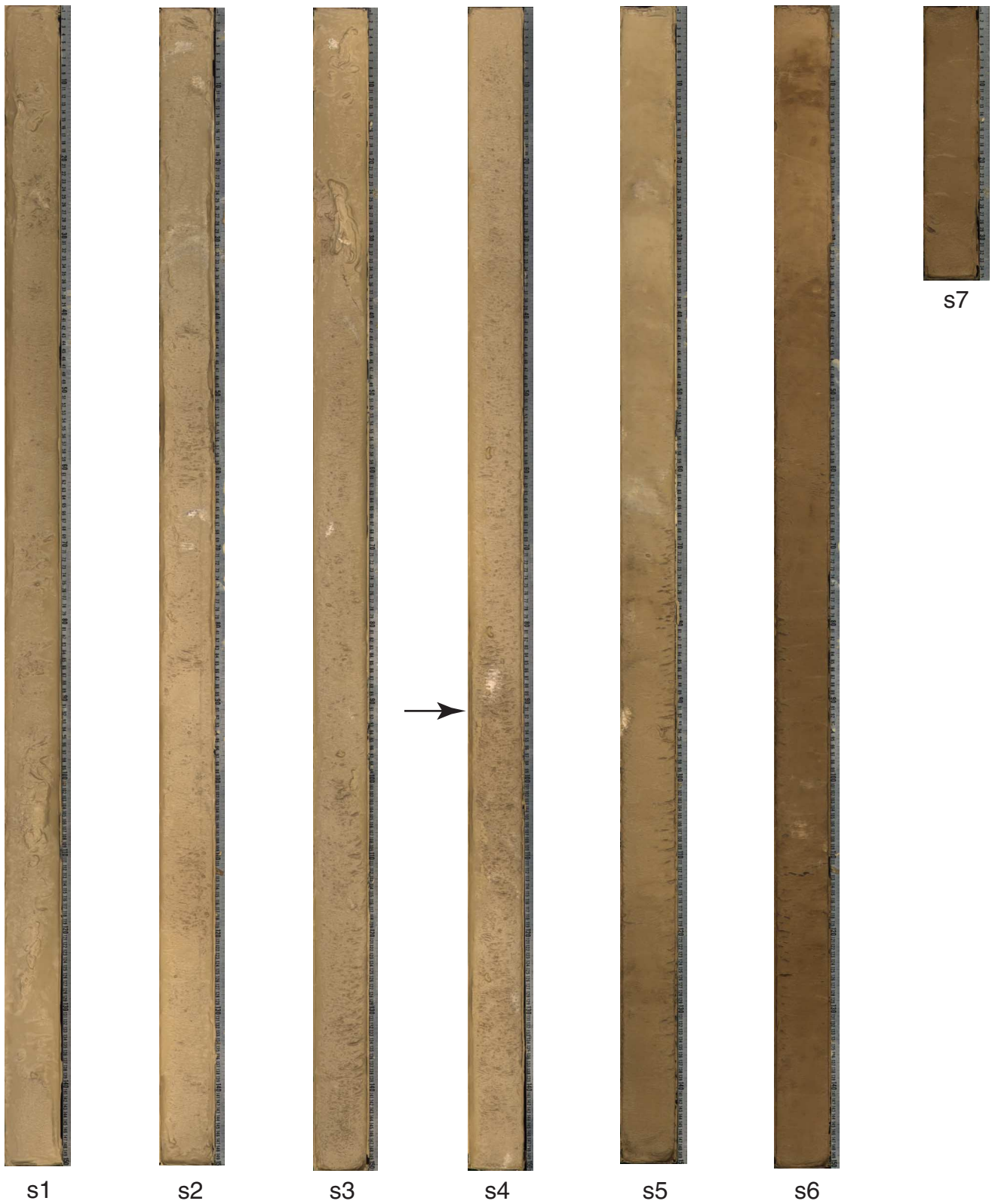


Figure F5. Correlation of PETM sections recovered in Holes 1211A, 1211B, and 1211C.

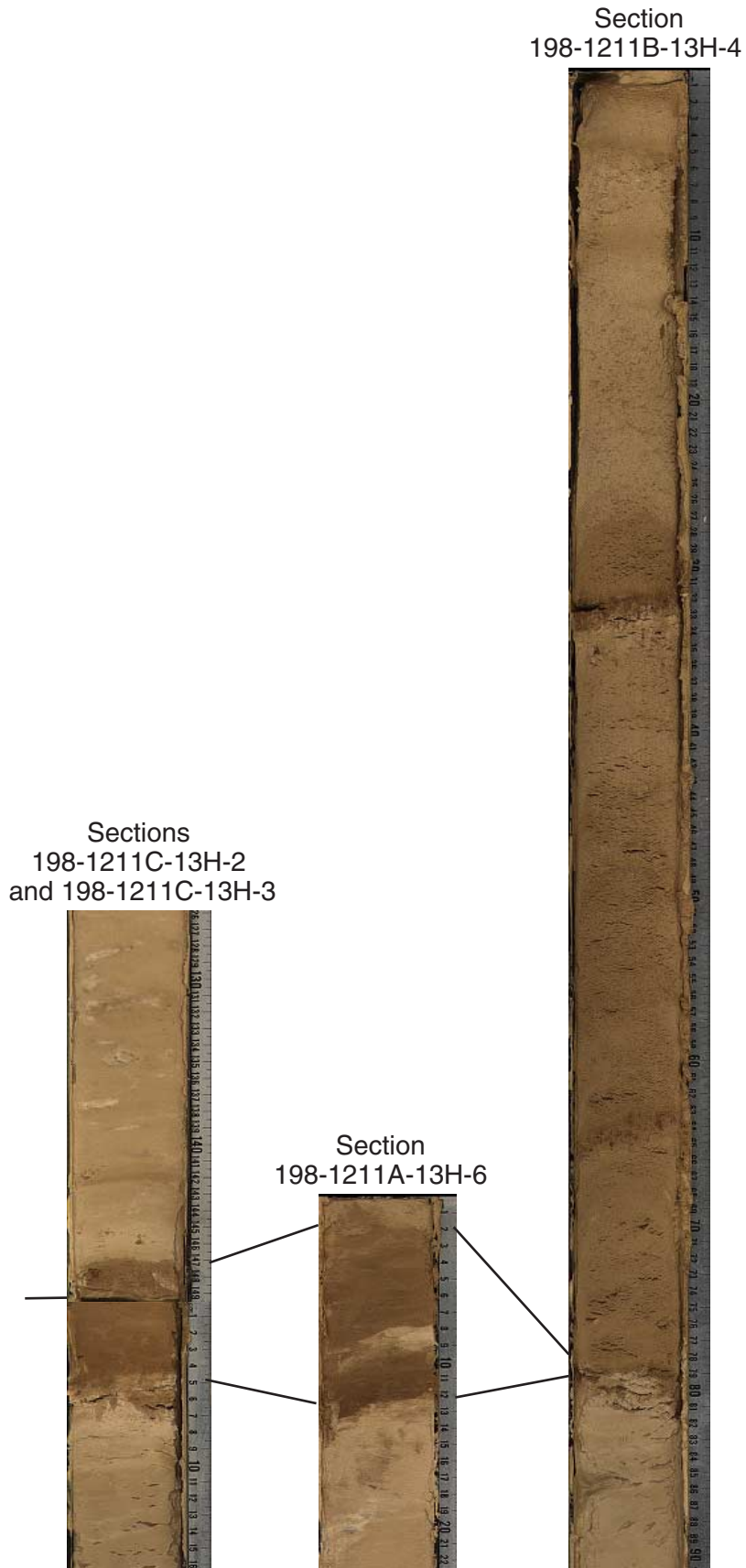


Figure F6. Core recovery, lithology, lithologic units, age with corresponding biostratigraphic zonation, color reflectance (L*), and weight percent carbonate for Hole 1211B. Foram. zn. = foraminiferal zone, nanno. zn. = nannofossil zone.

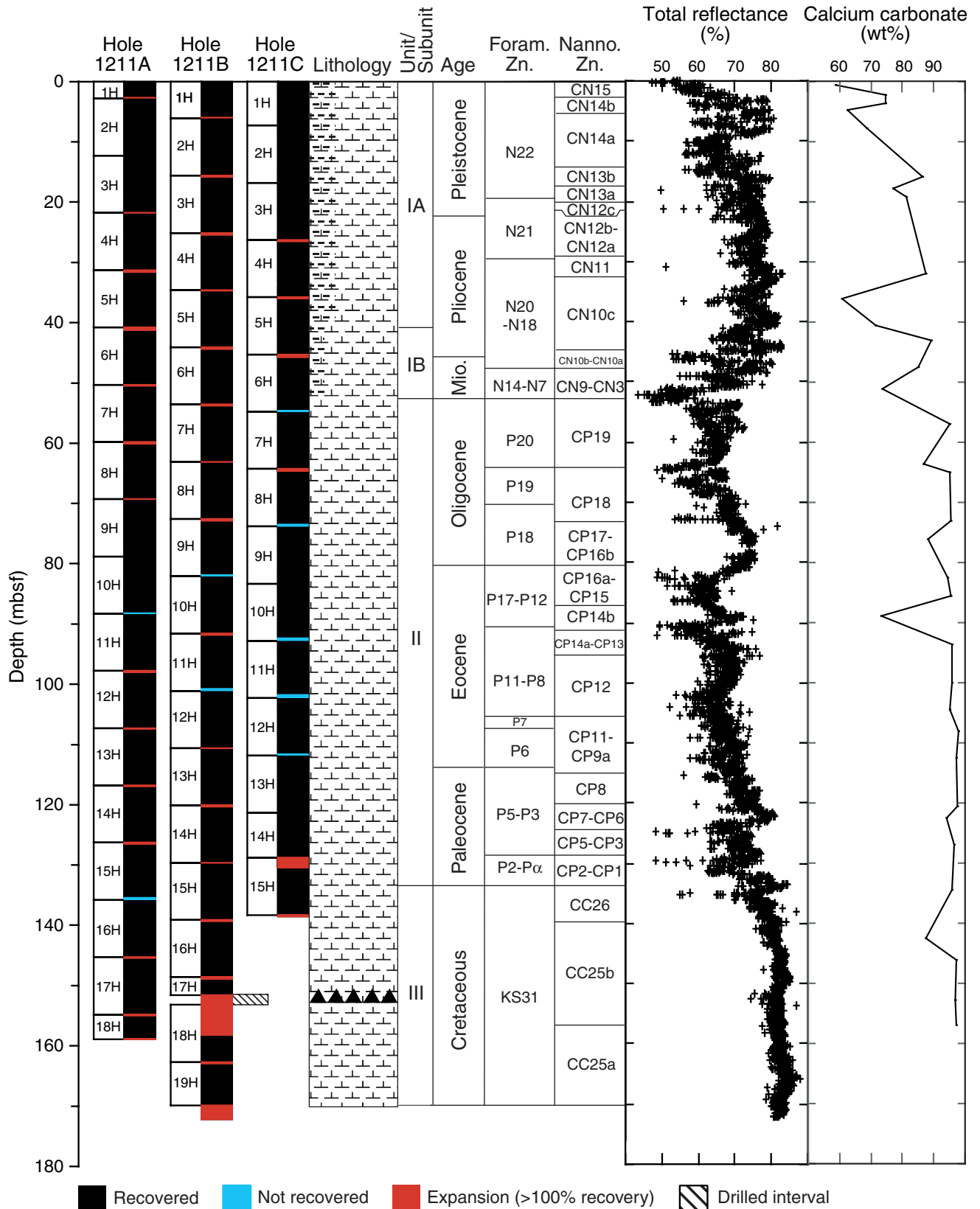


Figure F7. Comparison of color reflectance data of Unit I sediments from Hole 1209A and Hole 1211B demonstrating the diminished amplitude of Site 1211 cyclicity relative to the shallower Site 1209, located farther north on the Southern High.

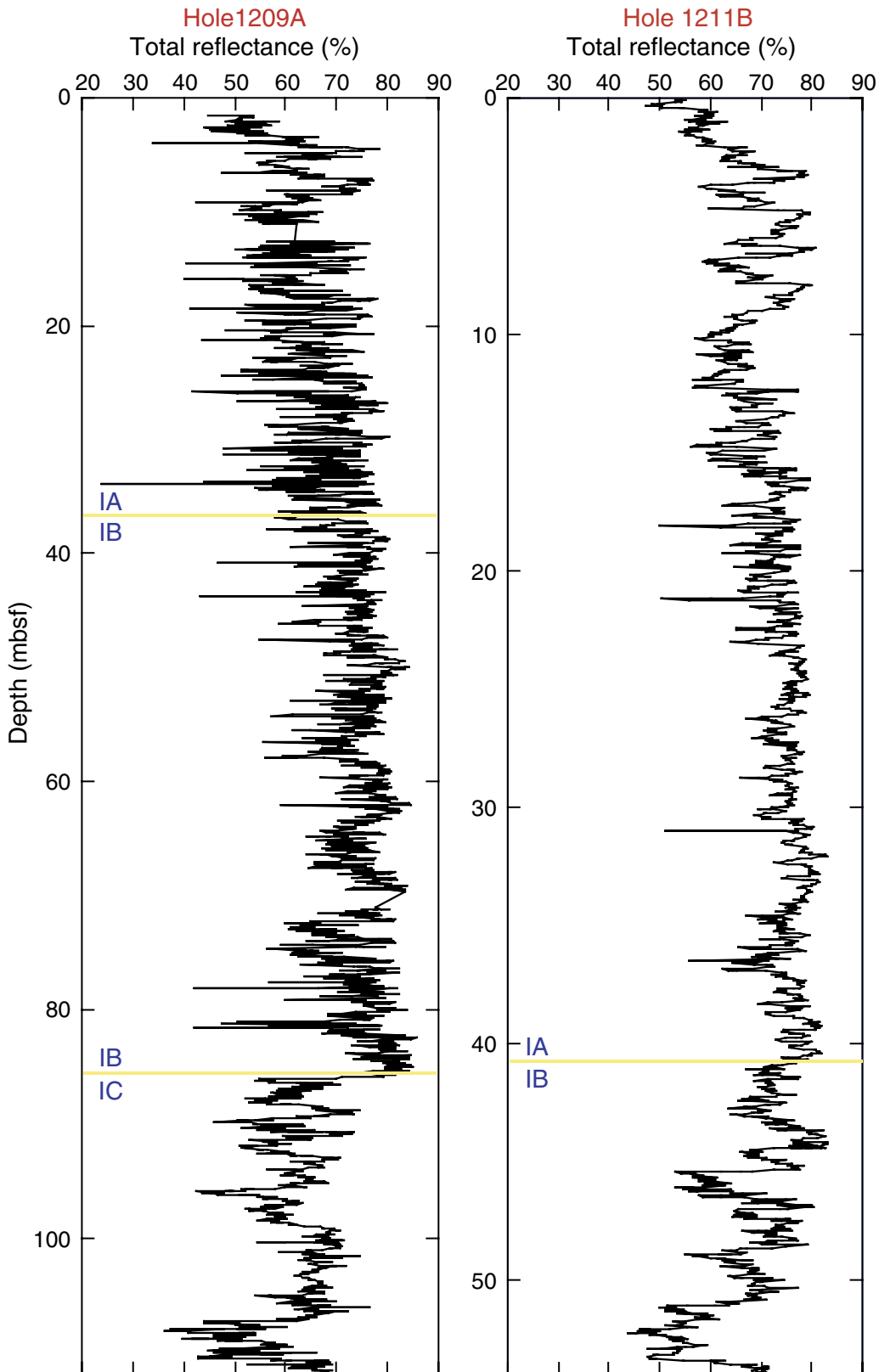


Figure F8. Composite digital photograph, magnetic susceptibility, and color reflectance (L*) for the interval spanning the Unit I/II boundary within Hole 1211B. The accurate correction factor for the magnetic susceptibility raw instrument values is 0.68×10^{-5} .

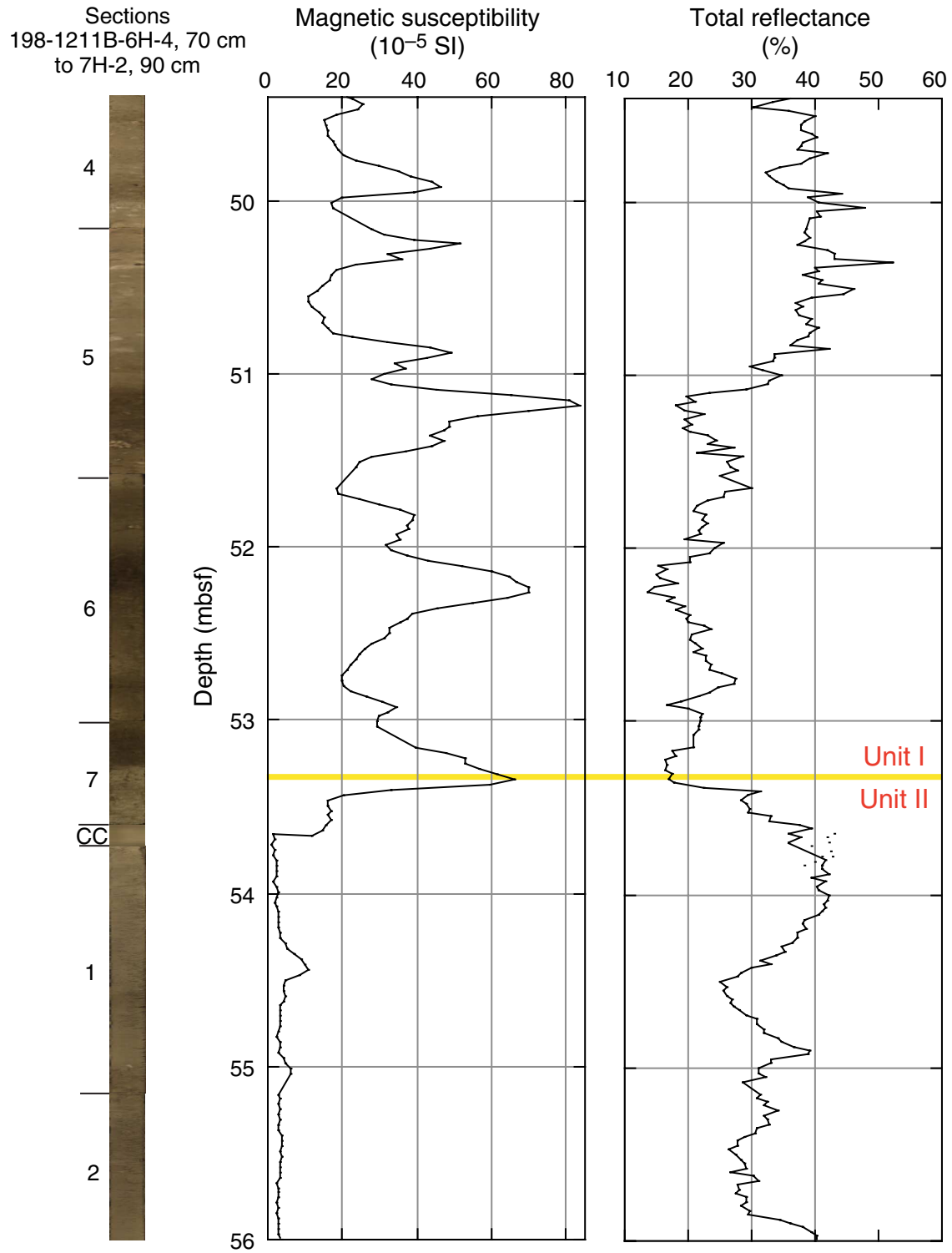


Figure F9. Hole 1211B color reflectance (green) and magnetic susceptibility (red) data for the majority of the interval spanning Unit II and the upper portion of Unit III. The accurate correction factor for the magnetic susceptibility raw instrument values is 0.68×10^{-5} .

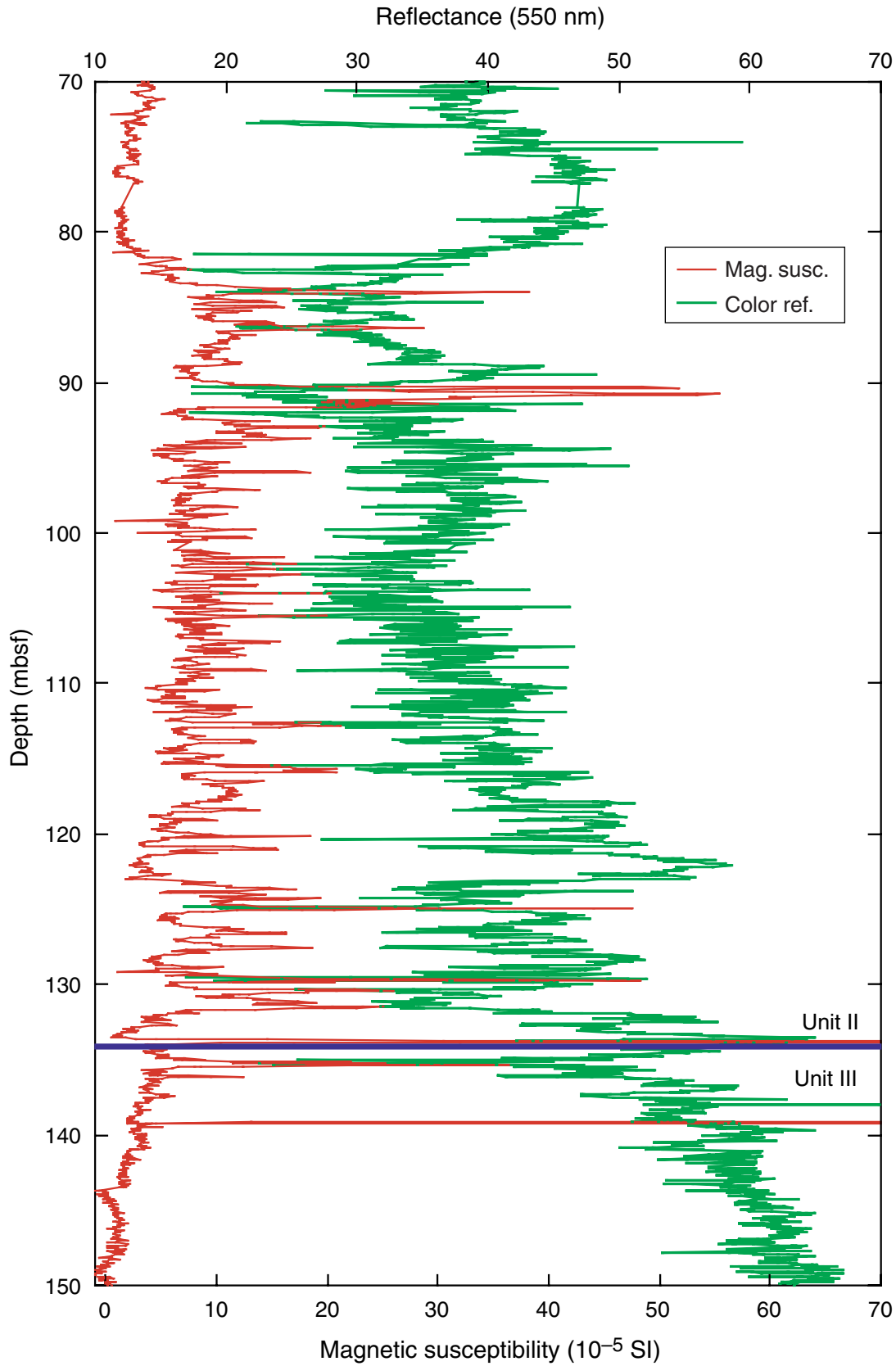


Figure F10. Site 1211 archive-half magnetization intensities after AF demagnetization at peak fields of 20 mT as measured with the shipboard pass-through magnetometer. Open black circles = Hole 1211A, open red circles = Hole 1211B, open green diamonds = Hole 1211C.

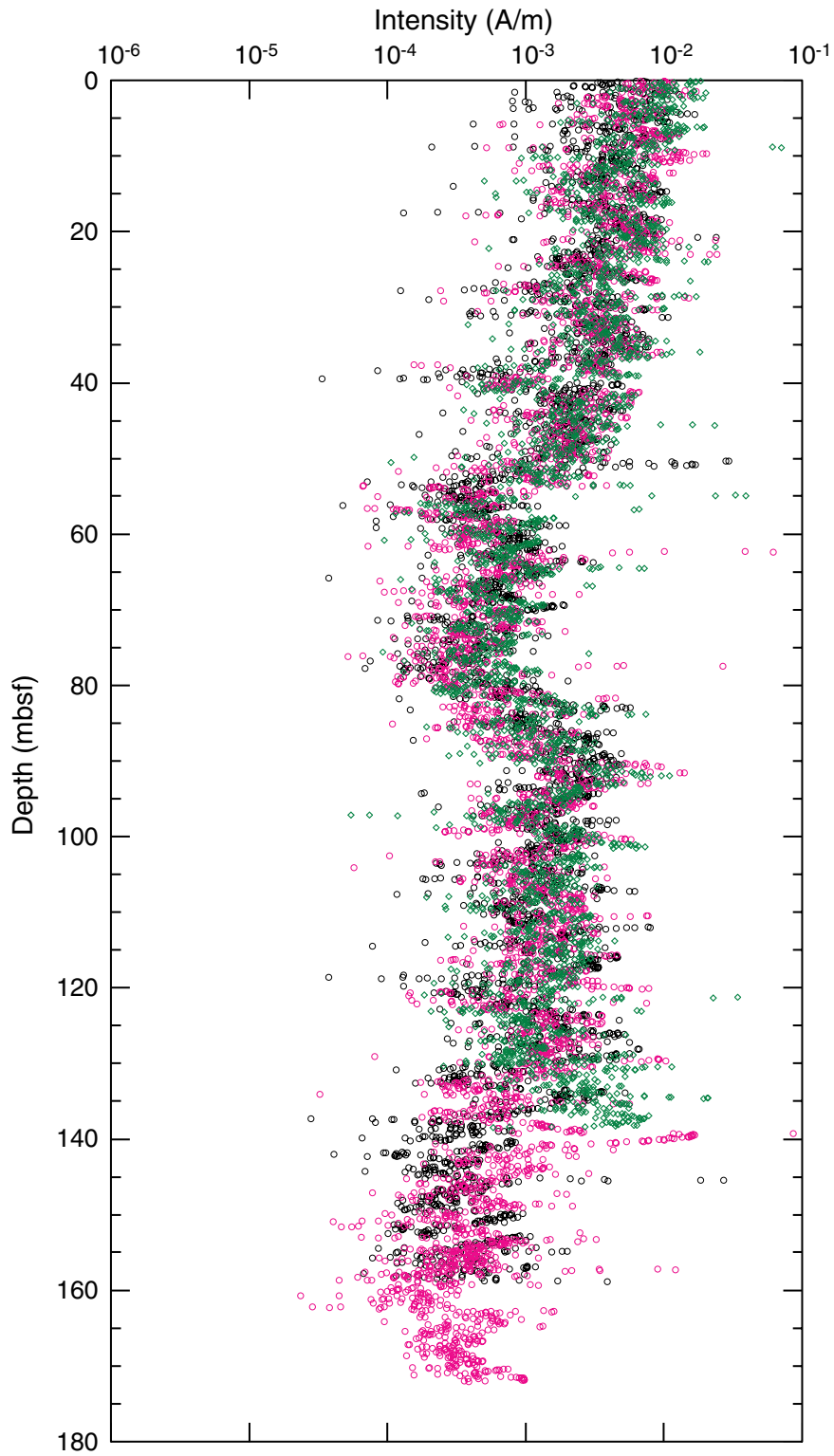


Figure F11. Inclination after AF demagnetization at peak fields of 20 mT as measured with the shipboard pass-through magnetometer for the upper 170 mcd from Holes 1211A (solid black circles), 1211B (solid purple circles), and 1211C (open green circles). The column at center shows interpreted zones of normal (black) and reversed (white) polarity for the 0–50 mcd interval.

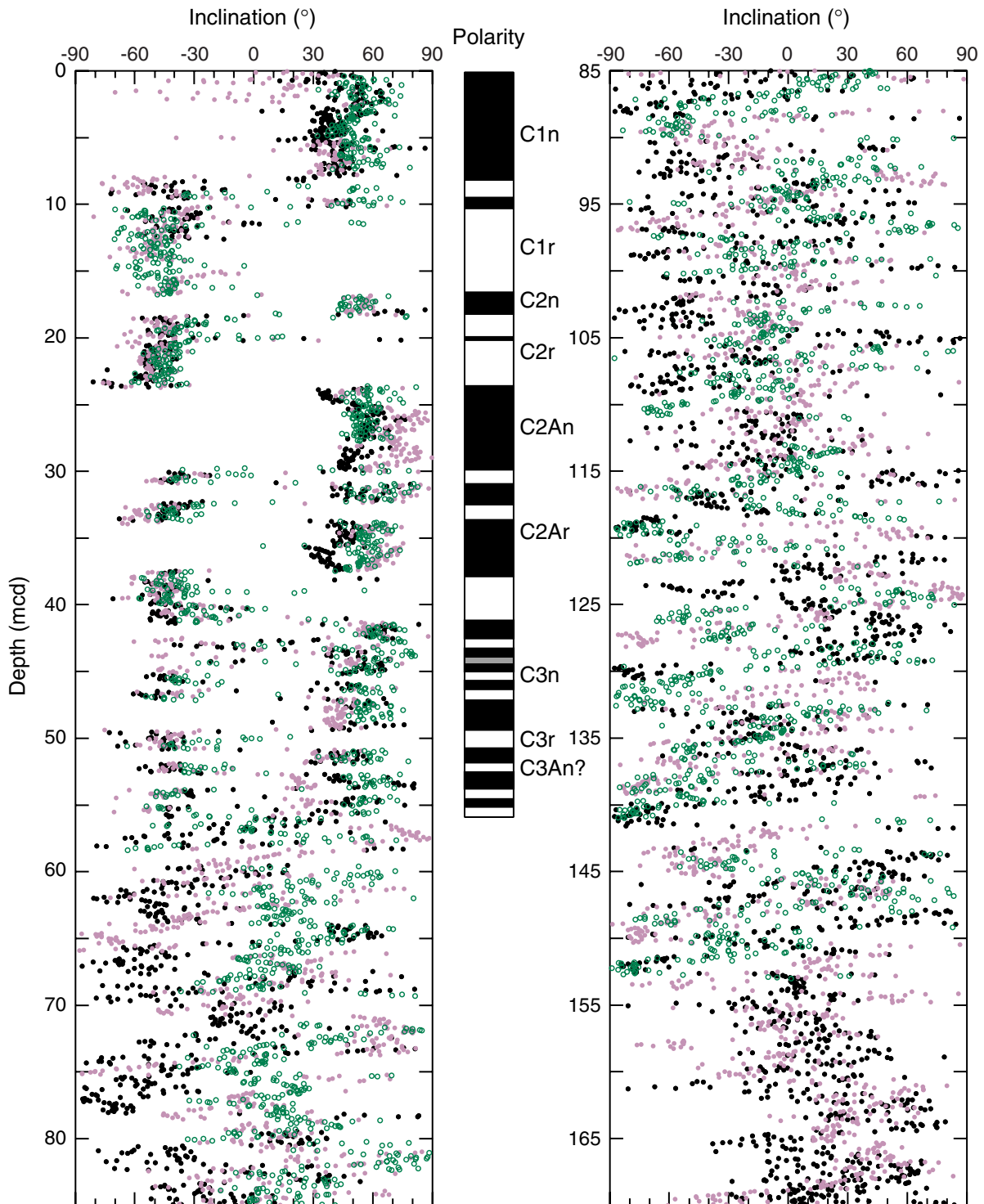


Figure F12. Age-depth curve derived from the Hole 1211A (solid symbols) and Hole 1211B (open symbols) magnetic stratigraphy shown in Figure F11, p. 42, using the geomagnetic polarity timescale of Cande and Kent (1995). Average sedimentation rates are also plotted. Depths are in mbsf (differences between Holes 1211A and 1211B are reconciled when plotted vs. mcd depths).

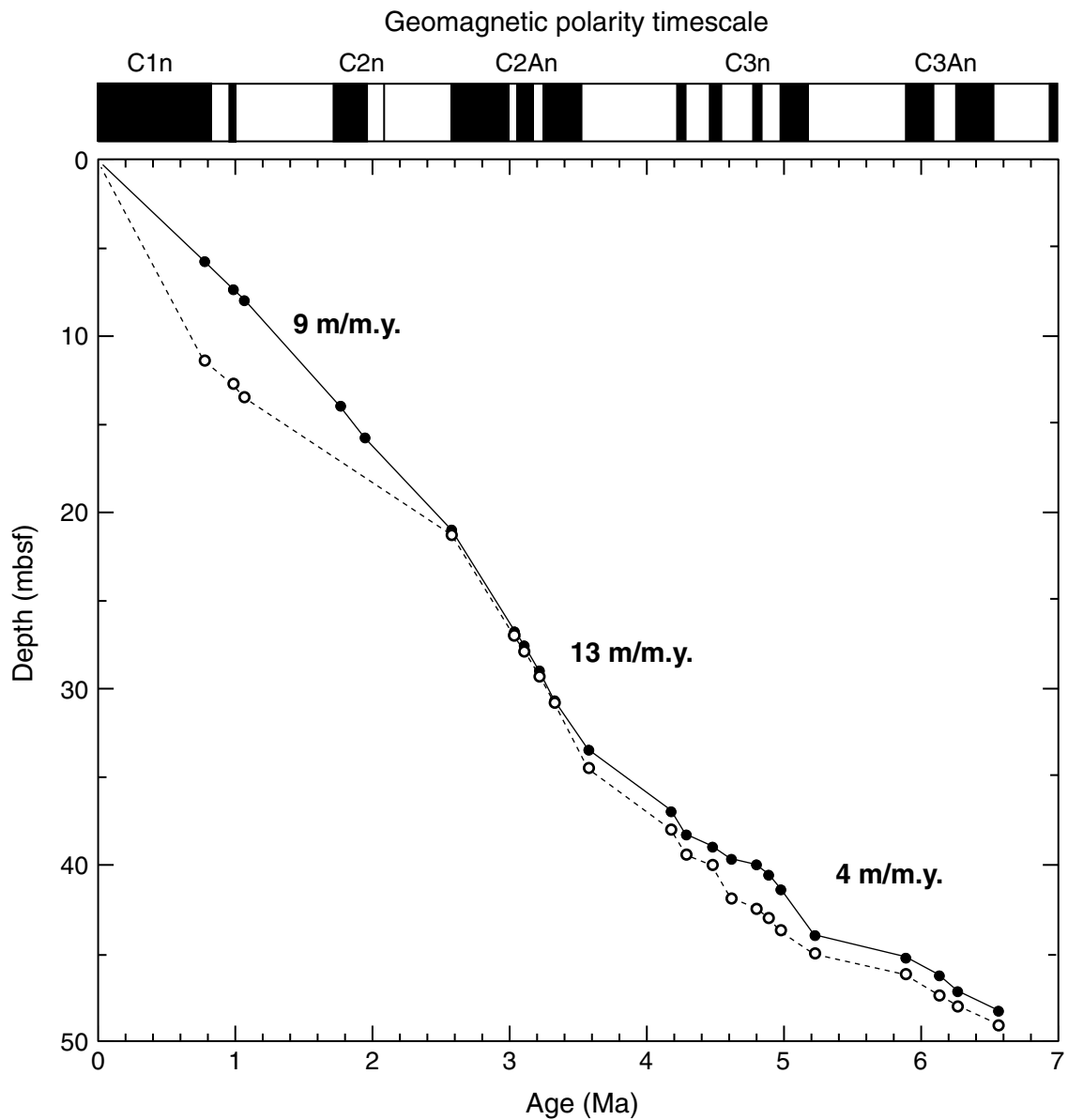


Figure F13. A. Magnetic susceptibility data for 0 to 160 mcd for Site 1211. The accurate correction factor for these raw instrument values is 0.68×10^{-5} . Hole 1211B is offset from Hole 1211A by a constant (40×10^{-6}). Hole 1211C is offset from Hole 1211A by a constant (80×10^{-6}). B. GRA bulk density data for 0 to 160 mcd for Site 1211. Hole 1211B is offset from Hole 1211A by a constant (0.3 g/cm^3). Hole 1211C is offset from Hole 1211A by a constant (0.6 g/cm^3).

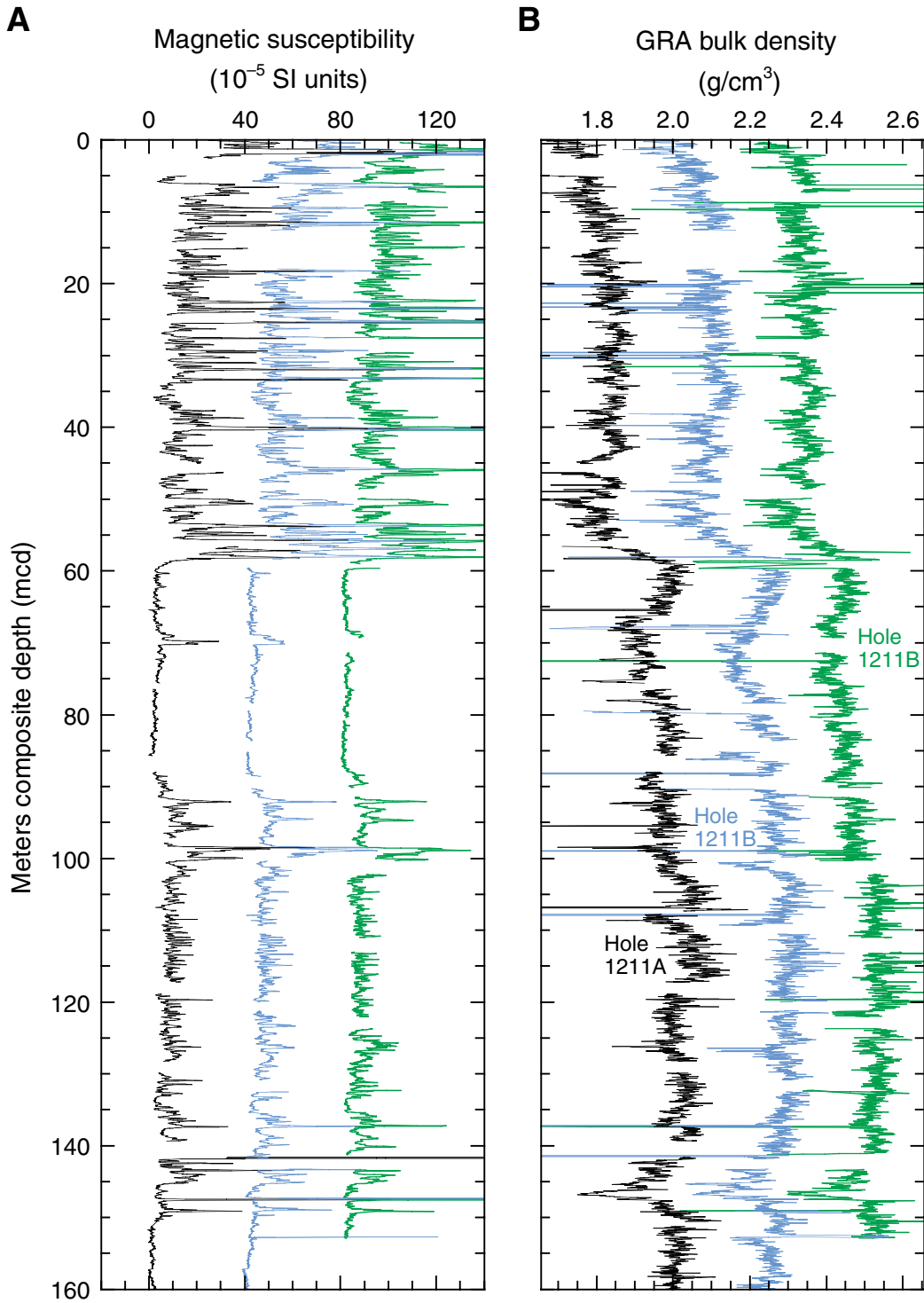


Figure F14. Magnetic susceptibility data for 0 to 28 mcd for Cores 1H through 3H for Holes 1211A, 1211B, and 1211C. This interval includes the uppermost part of the holes demonstrating that Cores 198-1211B-1H and 2H are overlapping each other. These intervals represent recording in the upper portions of the hole. The accurate correction factor for these raw instrument values is 0.68×10^{-6} .

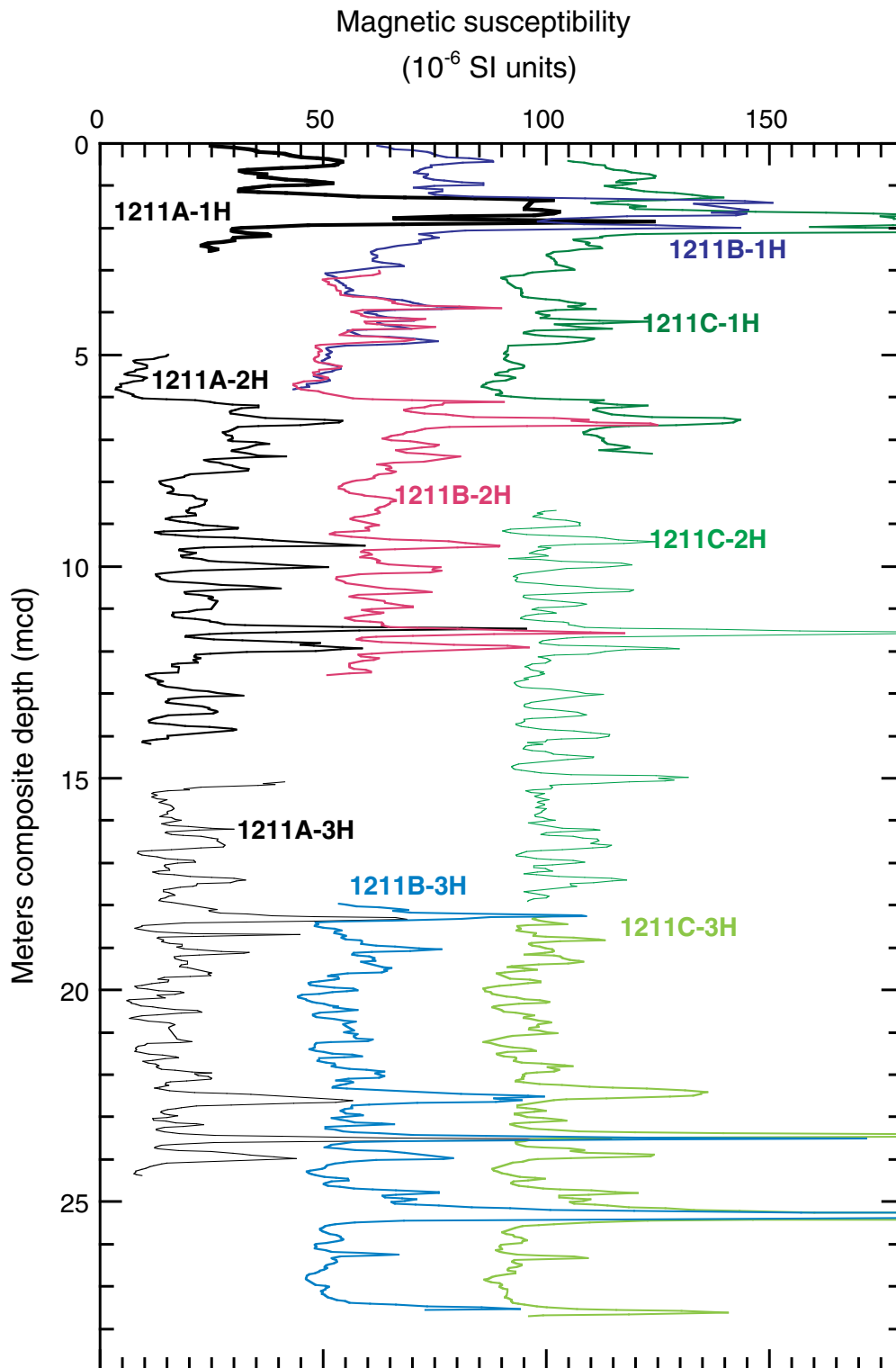


Figure F15. Age-depth plot of calcareous nannofossil (diamonds) and planktonic foraminiferal (crosses) datums at Site 1211. Datum ages and depths are presented in Tables T2, p. 66, and T3, p. 67 (see "Biostratigraphy," p. 13).

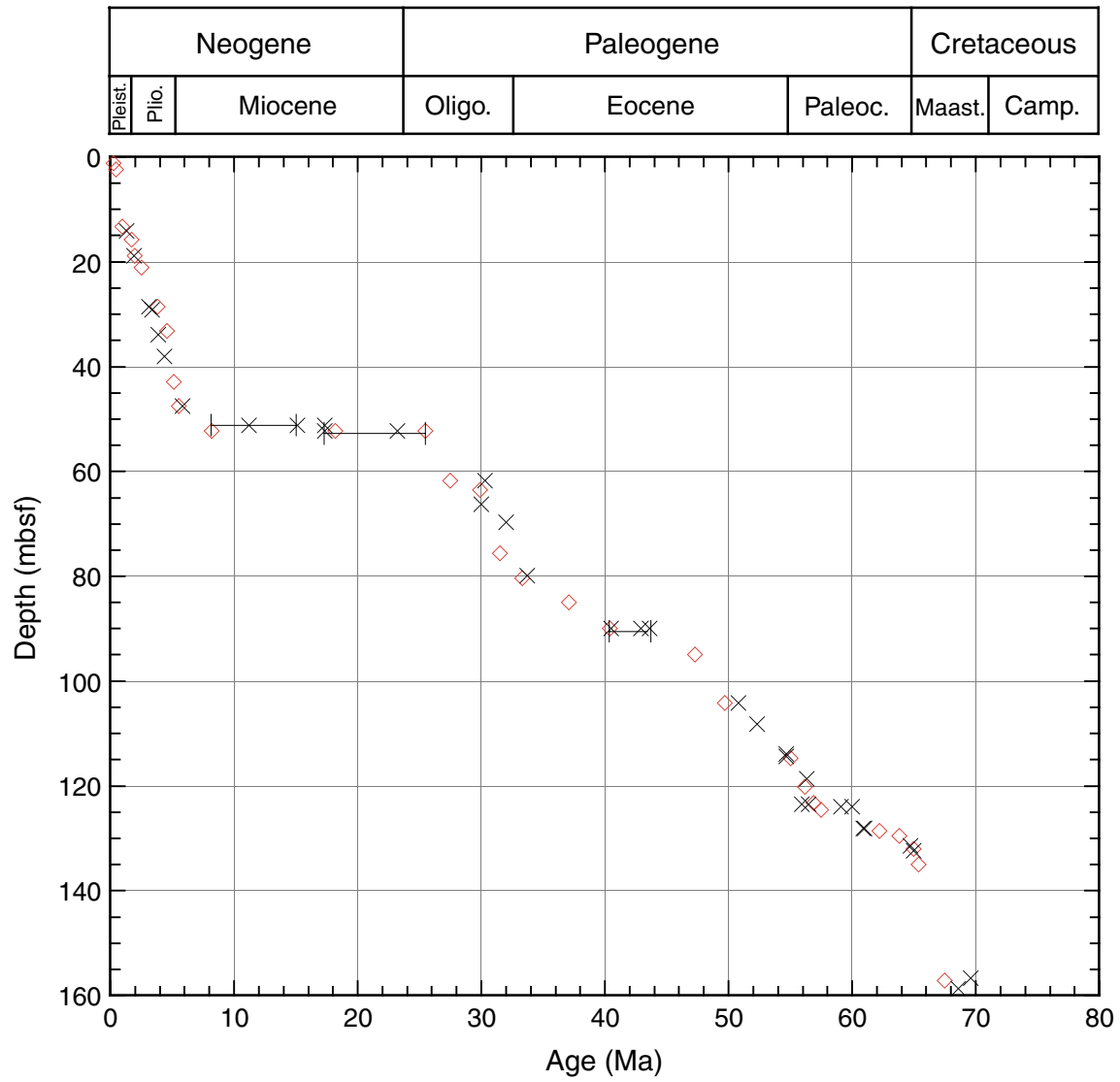


Figure F16. Age-depth plot of Neogene calcareous nannofossil (diamonds) and planktonic foraminiferal (crosses) datums at Site 1211. Datum ages and depths are presented in Tables T2, p. 66, and T3, p. 67. FO = first occurrence, LO = lower occurrence.

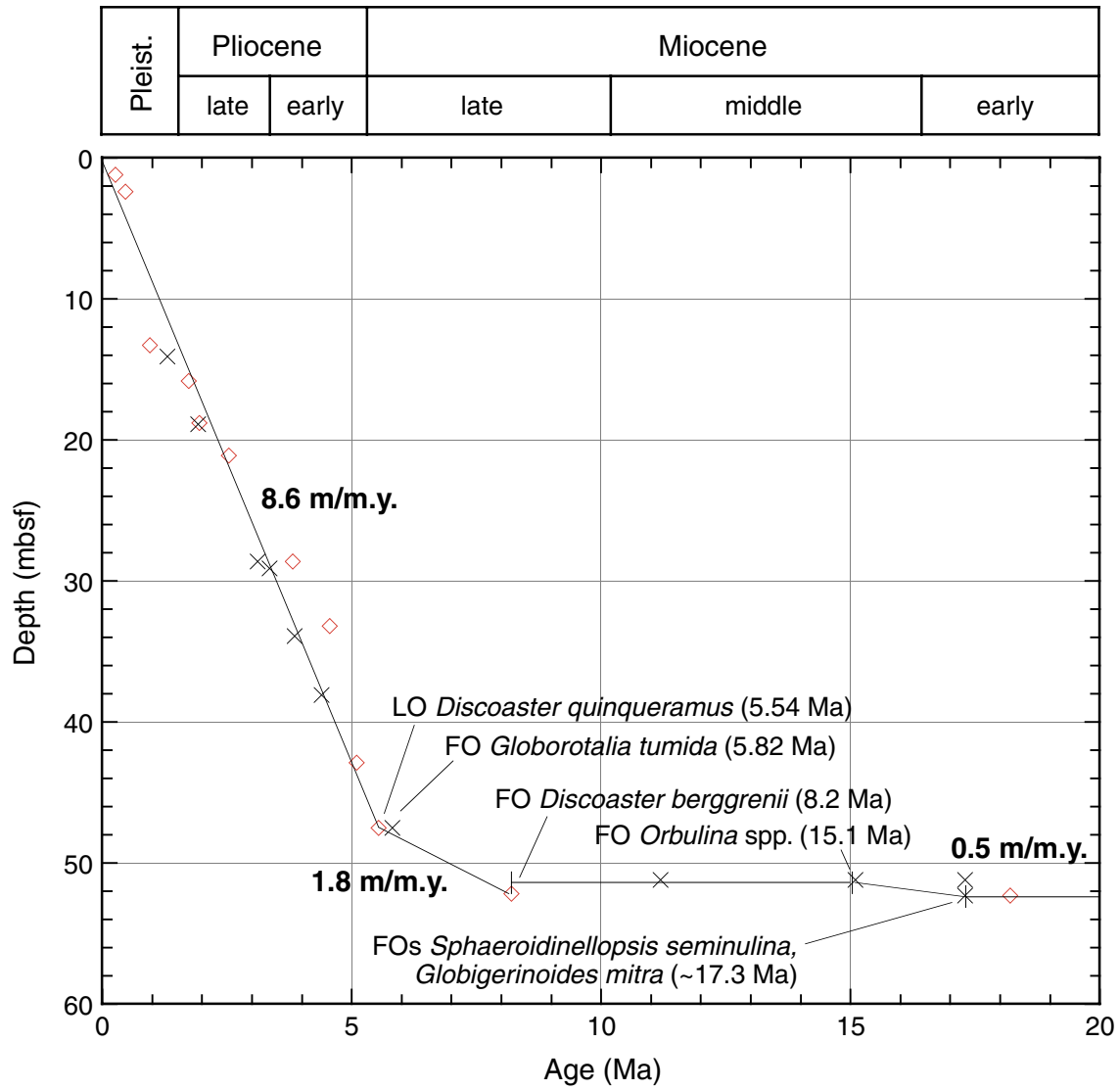


Figure F17. Age-depth plot of middle Miocene–late Eocene calcareous nannofossil (diamonds) and planktonic foraminiferal (crosses) datums at Site 1211. Datum ages and depths are presented in Tables T2, p. 66, and T3, p. 67. FO = first occurrence, LO = last occurrence.

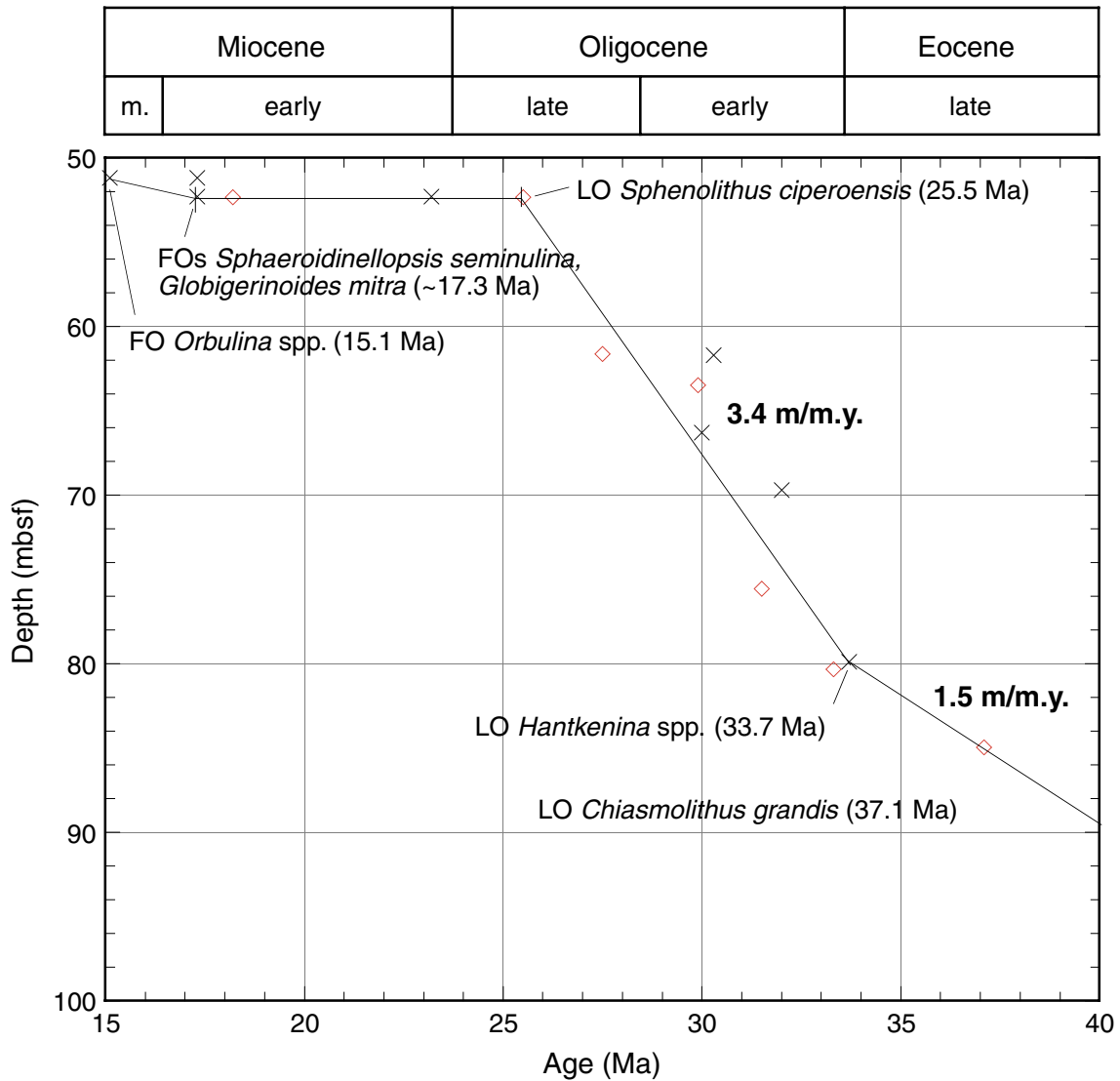


Figure F18. Age-depth plot of early Oligocene–late Paleocene calcareous nannofossil (diamonds) and planktonic foraminiferal (crosses) datums at Site 1211. Datum ages and depths are presented in Tables T2, p. 66, and T3, p. 67. FO = first occurrence, LO = last occurrence.

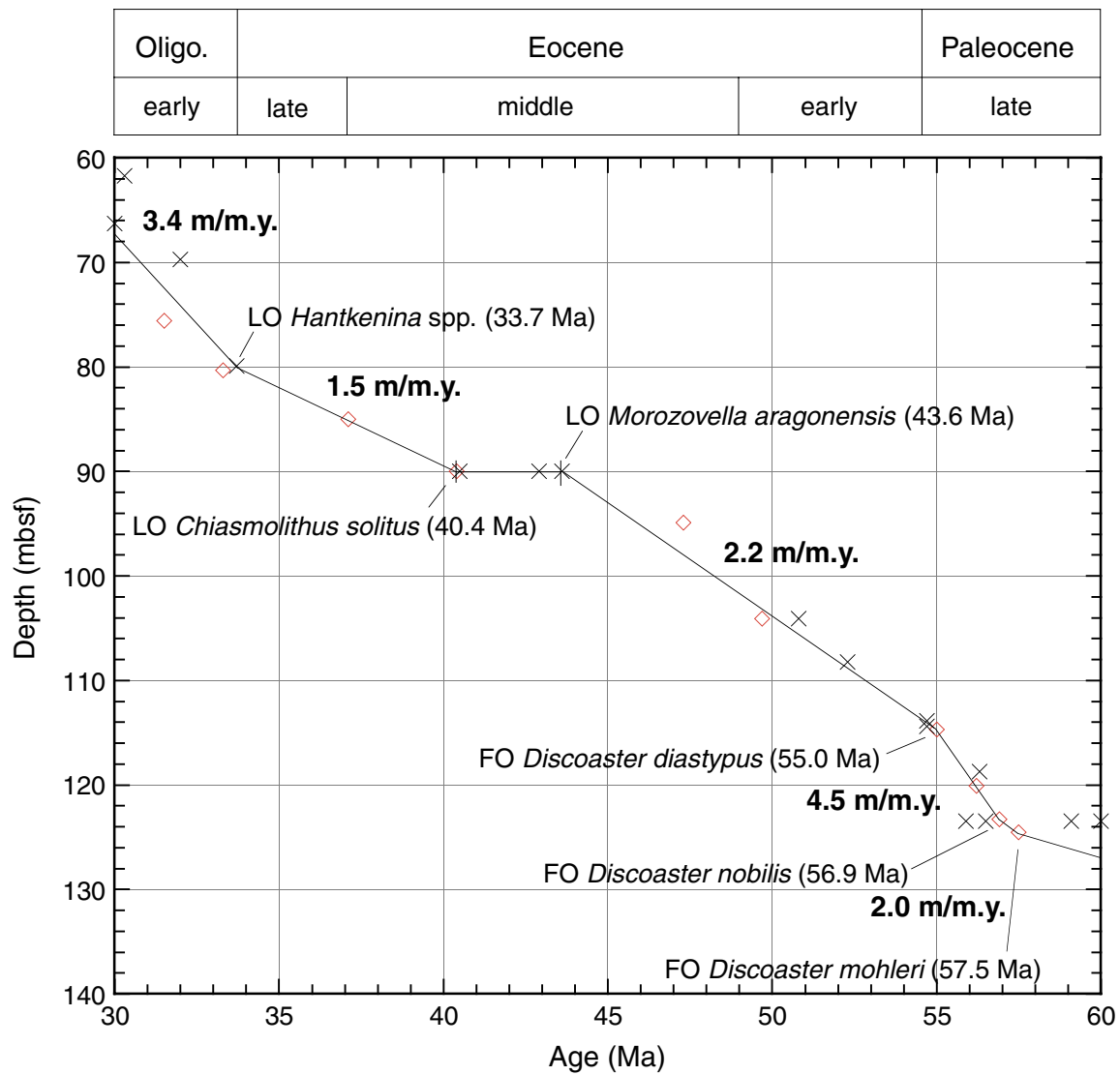


Figure F19. Age-depth plot of early Eocene–Maastrichtian calcareous nannofossil (diamonds) and planktonic foraminiferal (crosses) datums, Site 1211. Datum ages and depths are presented in Tables T2, p. 66, and T3, p. 67.

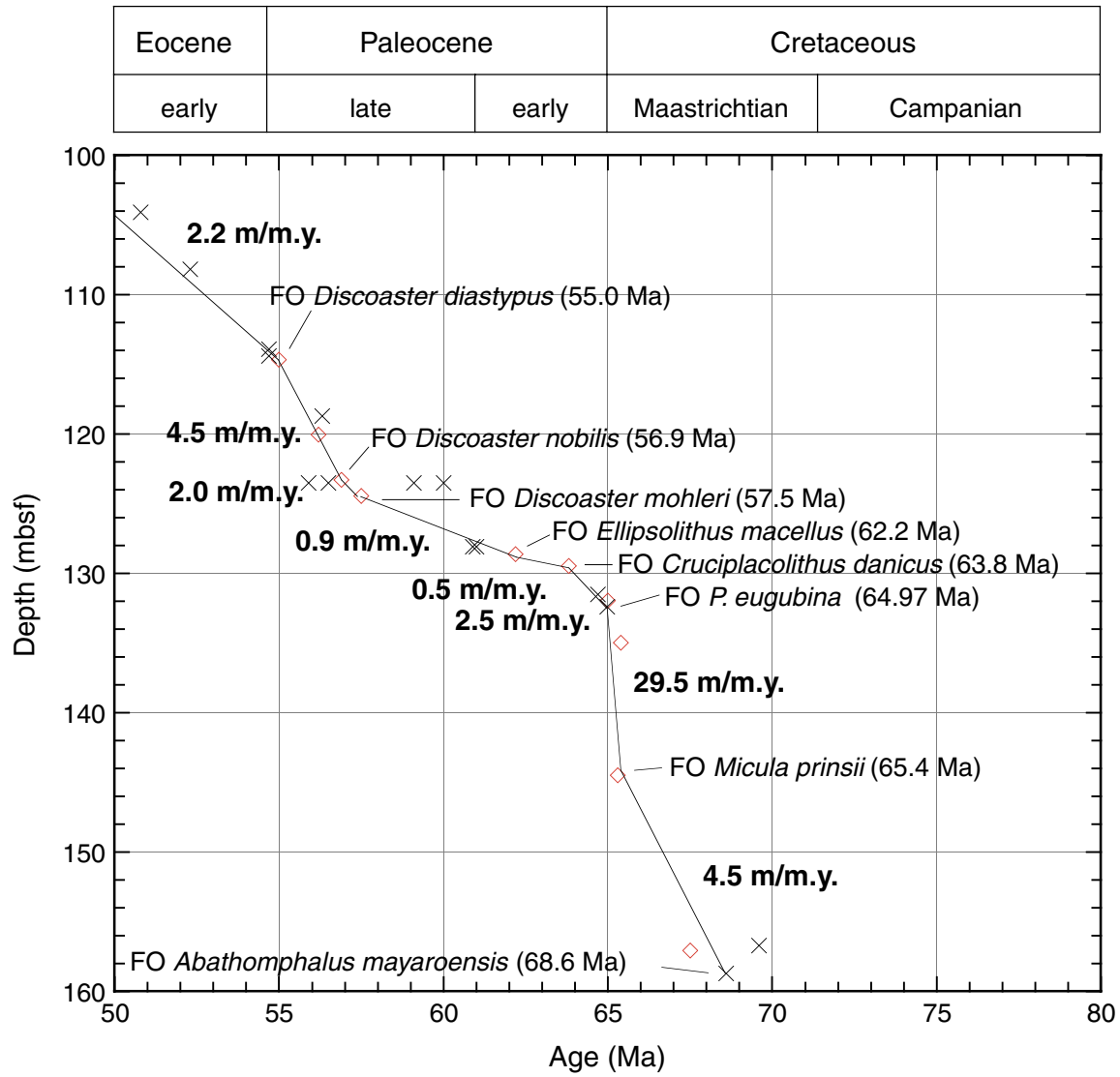


Figure F20. Mass accumulation rates for bulk sediment, carbonate fraction, and noncarbonate fraction vs. (A) depth and (B) age for the Maastrichtian–Pleistocene at Site 1211.

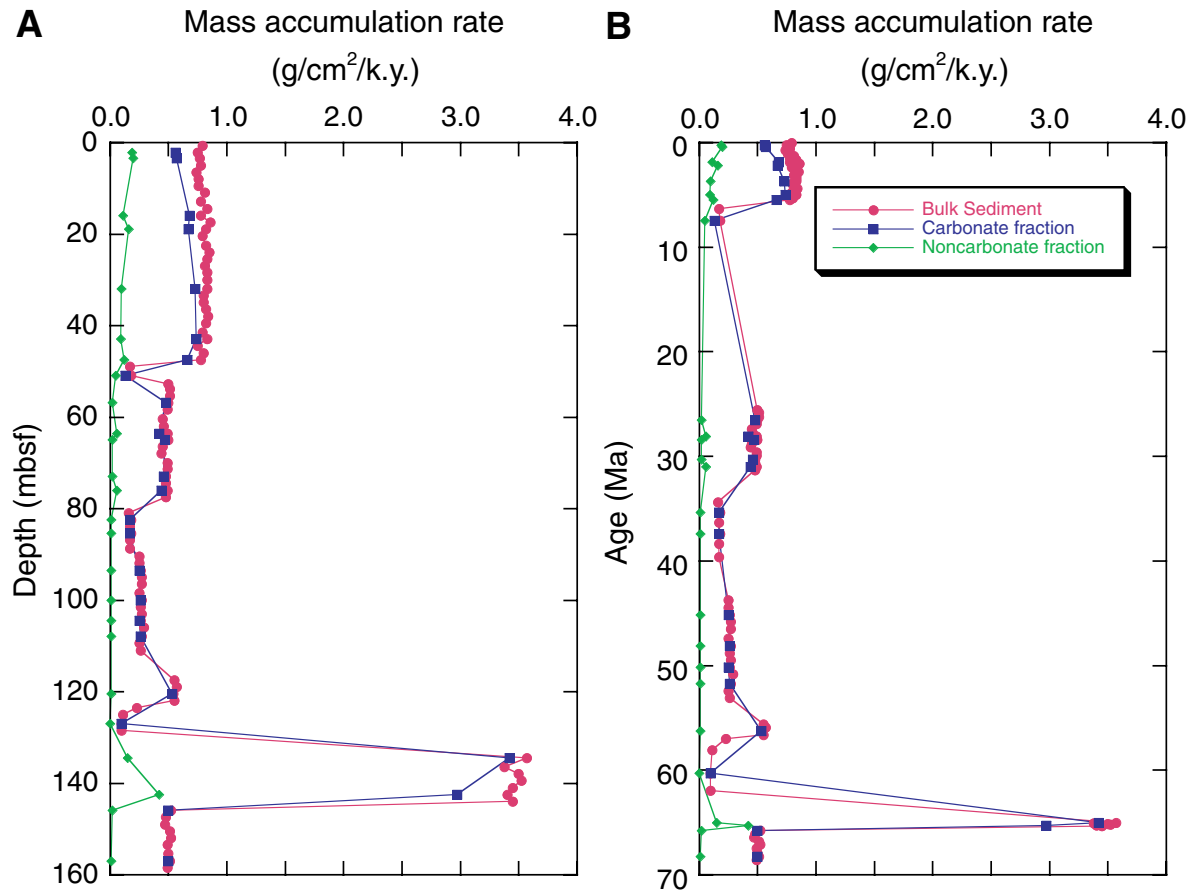


Figure F21. Downhole profiles of carbonate content in Hole 1211A.

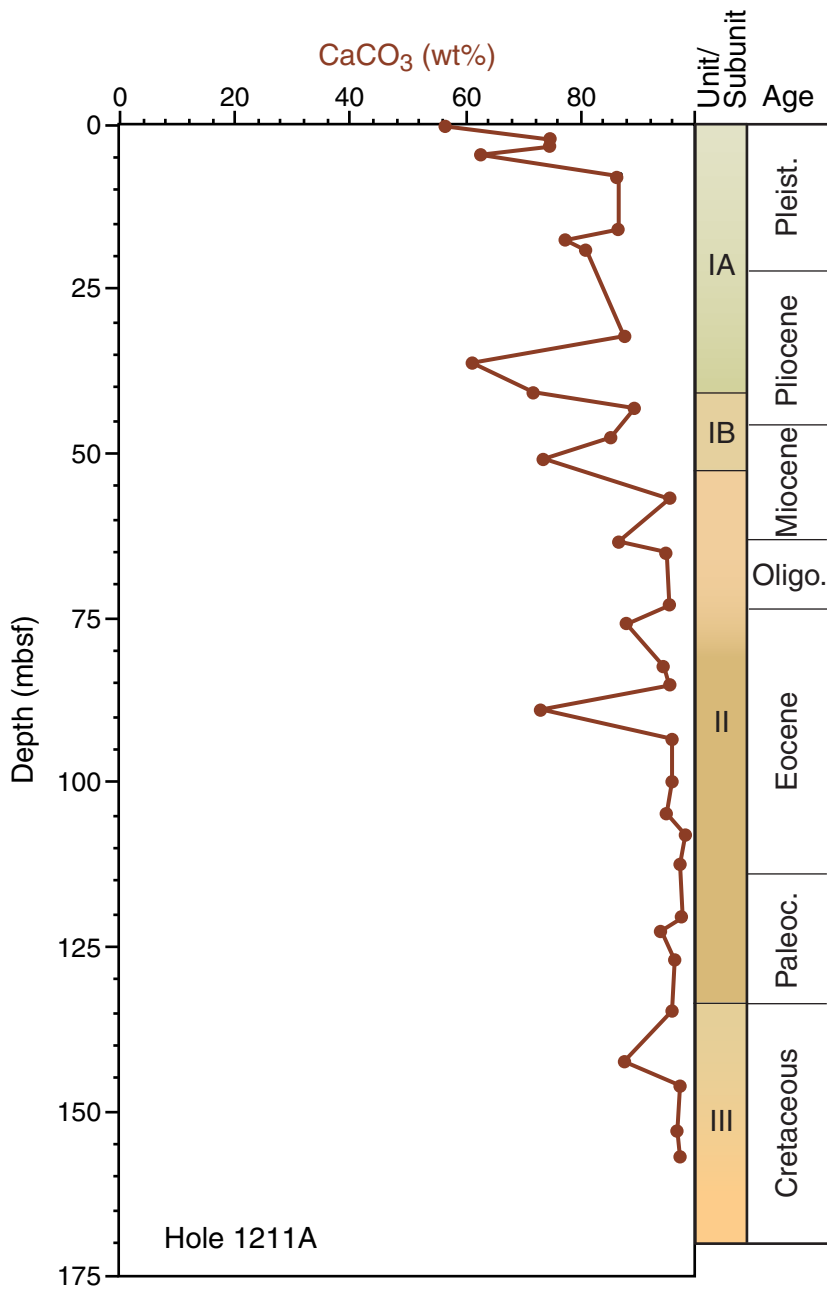


Figure F22. Interstitial water profiles for Na^+ and Cl^- at Site 1211.

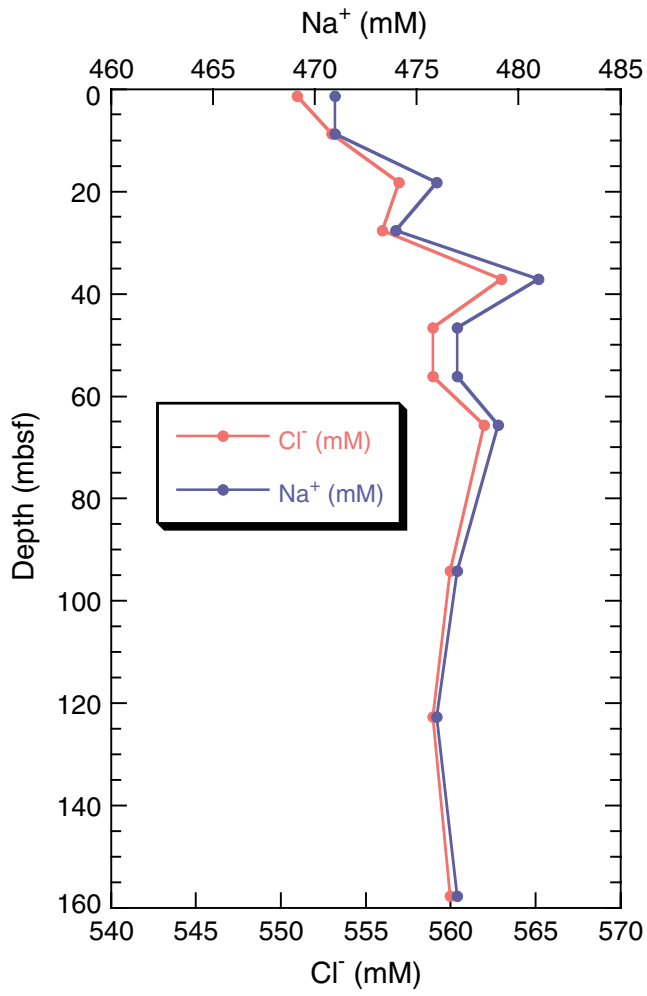


Figure F23. Interstitial water profiles for Site 1211. A. Alkalinity. B. Sulfate. C. Ammonium. D. Phosphate. E. Iron. F. Manganese.

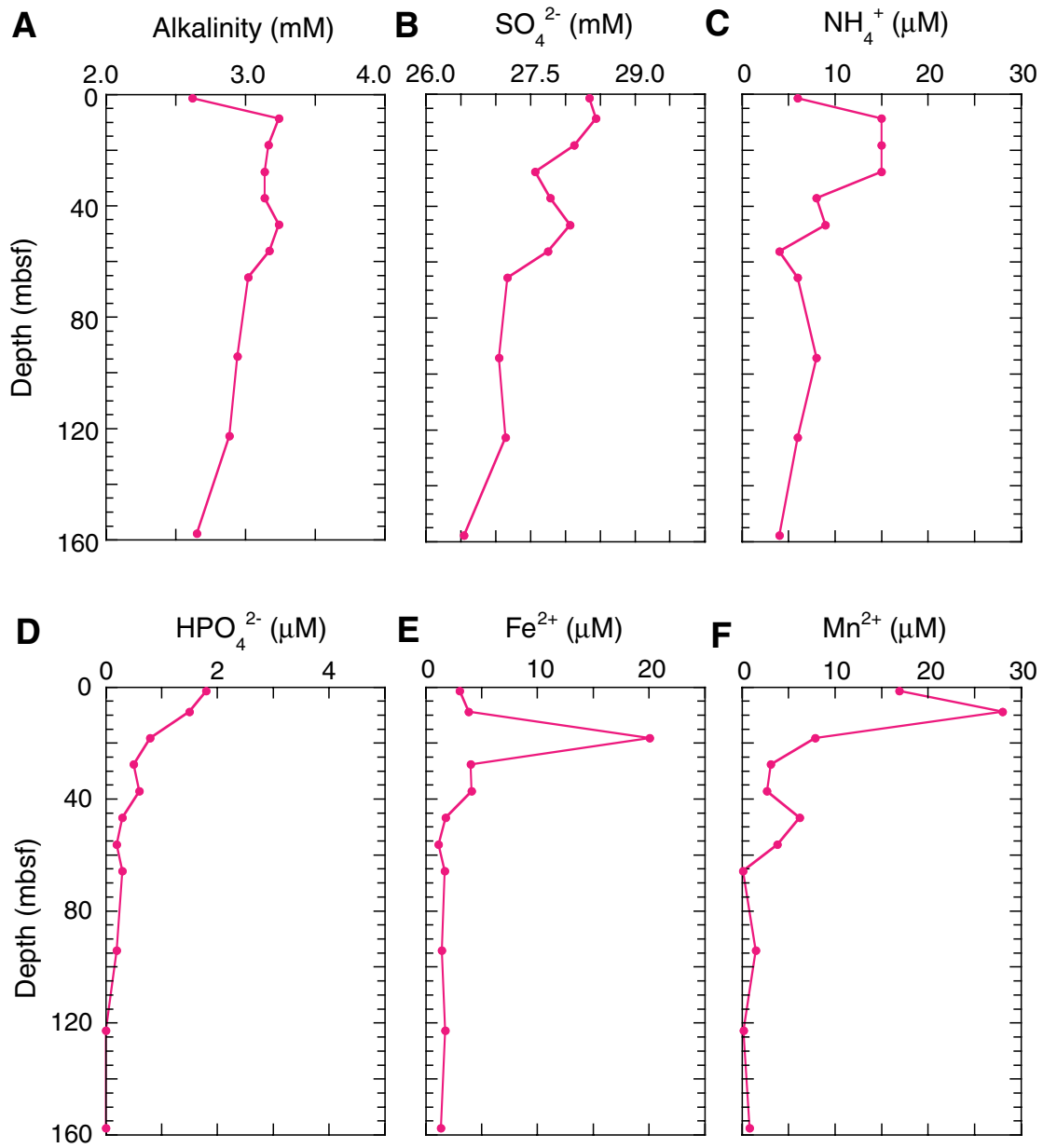


Figure F24. Interstitial water profiles for Site 1211. A. Potassium. B. Calcium. C. Magnesium. D. Sr and Sr/Ca. E. Lithium.

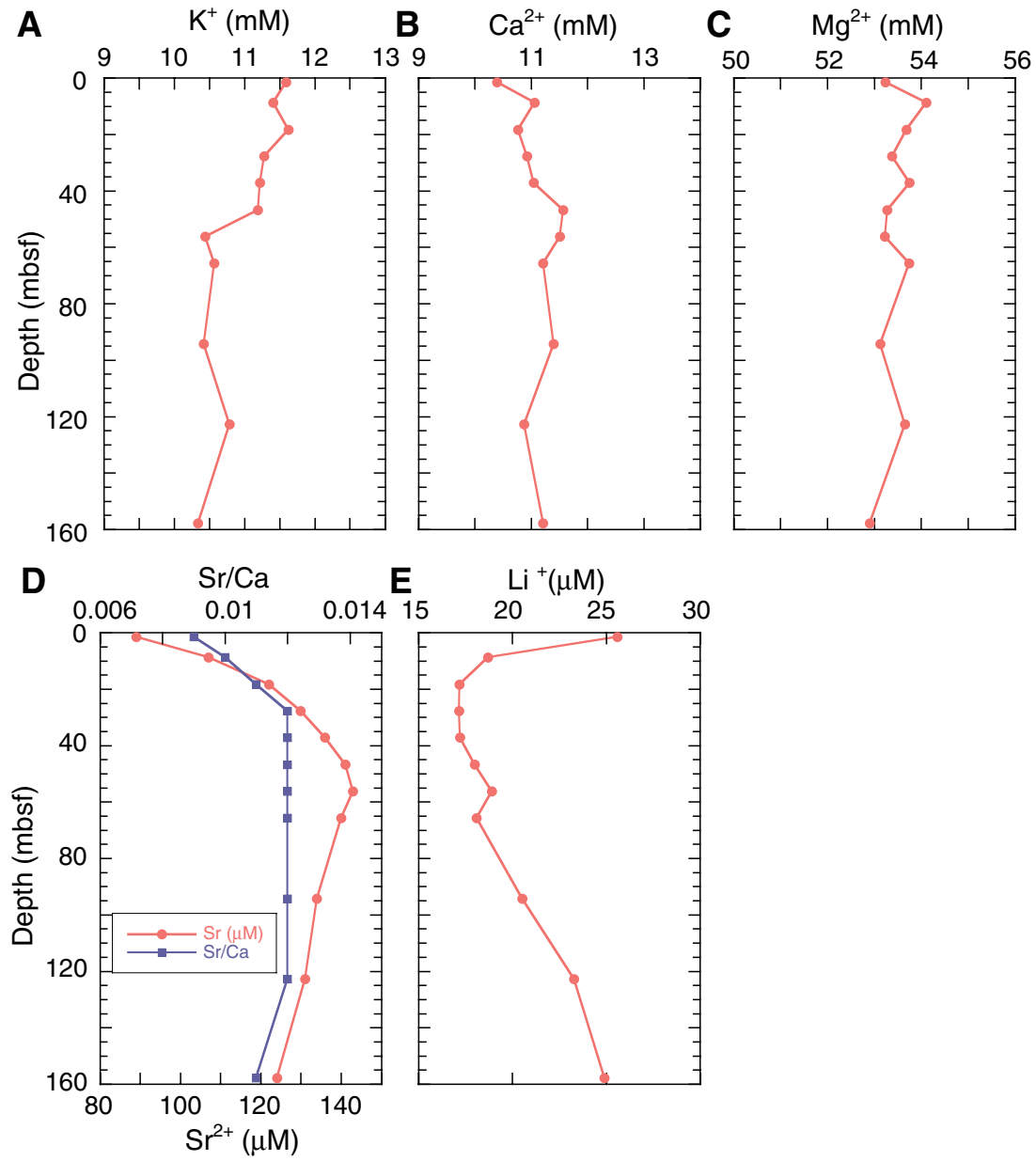


Figure F25. Silica profile for Site 1211.

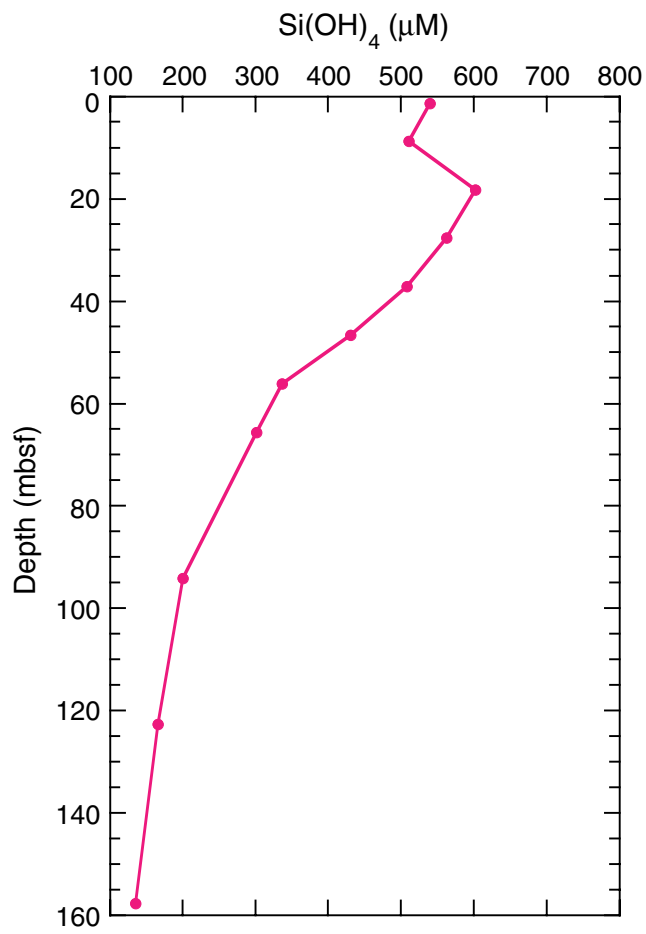


Figure F26. MST magnetic susceptibility measured in whole cores from Holes 1211A, 1211B, and 1211C plotted vs. depth. The accurate correction factor for these raw instrument values is 0.68×10^{-5} .

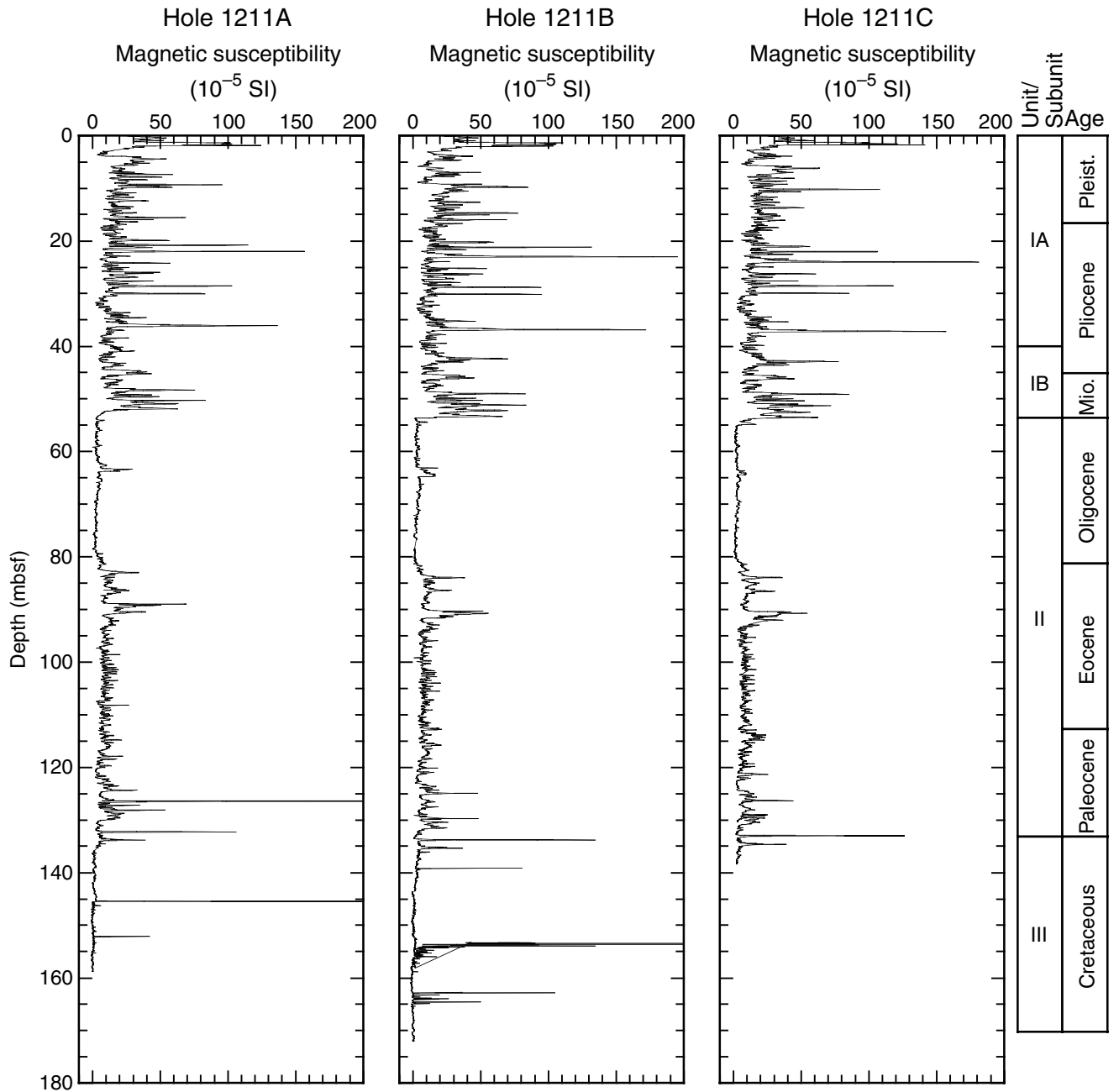


Figure F27. MST GRA bulk density (lines) measured in whole cores from Holes 1211A, 1211B, and 1211C plotted vs. depth. Discrete measurements of wet bulk density (see Table T12, p. 78) (solid circles) are plotted for comparison.

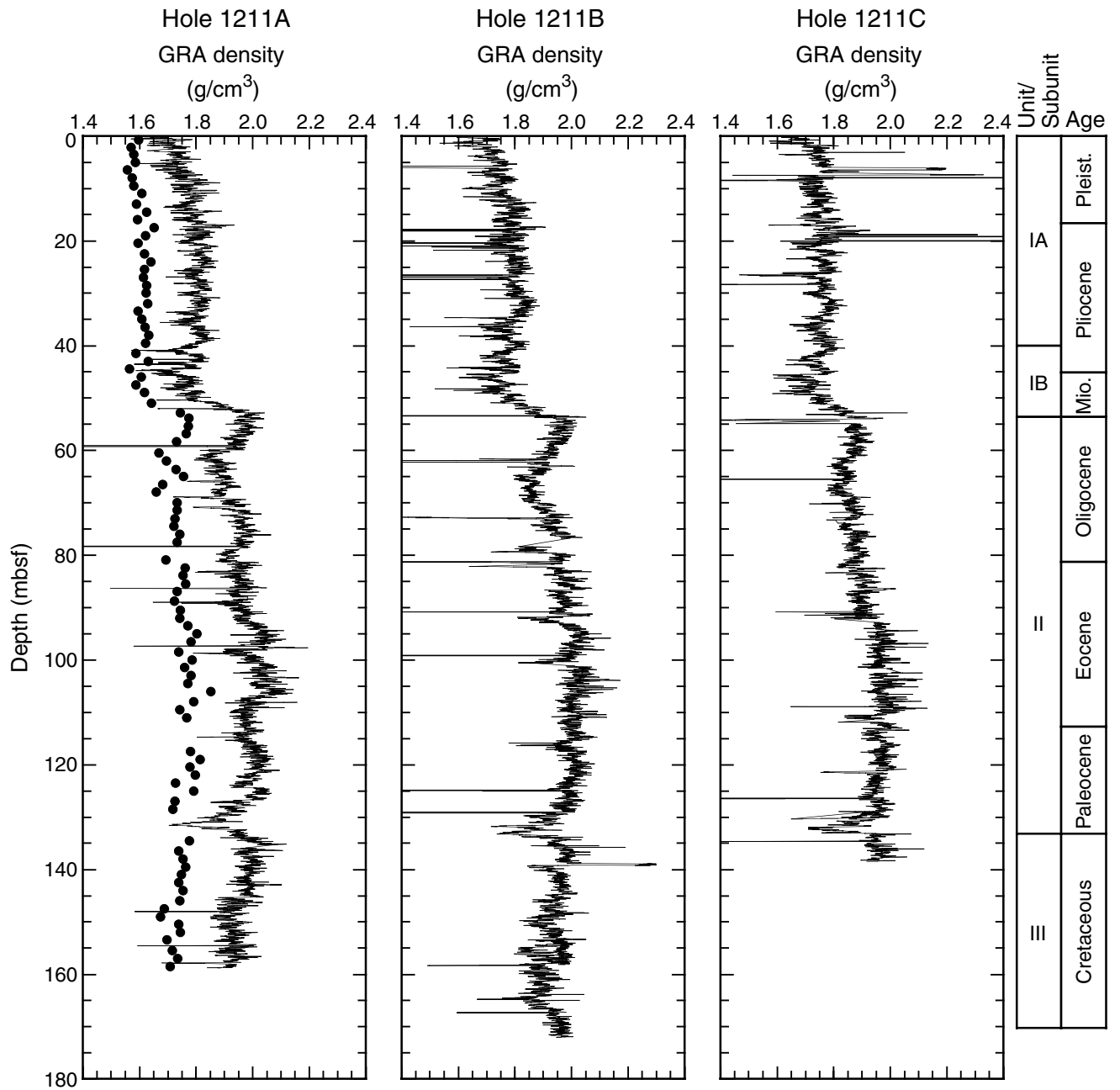


Figure F28. MST *P*-wave velocity (lines) measured in Holes 1211A, 1211B, and 1211C whole cores plotted vs. depth. For comparison, discrete *P*-wave velocity data (solid circles) are also shown.

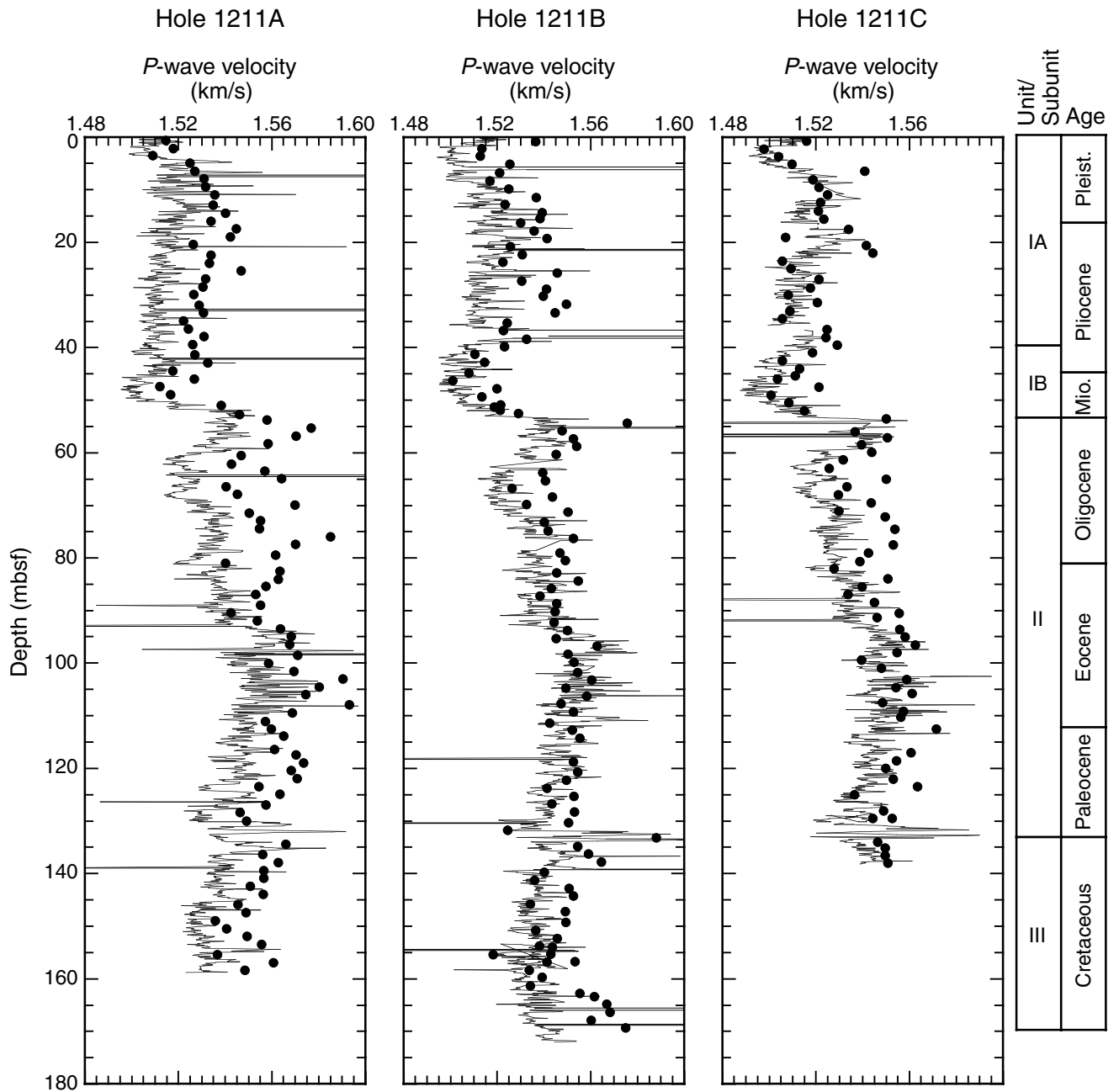


Figure F29. P-wave velocities for discrete samples from Holes 1211A, 1211B, and 1211C (see Table T13, p. 80, for data).

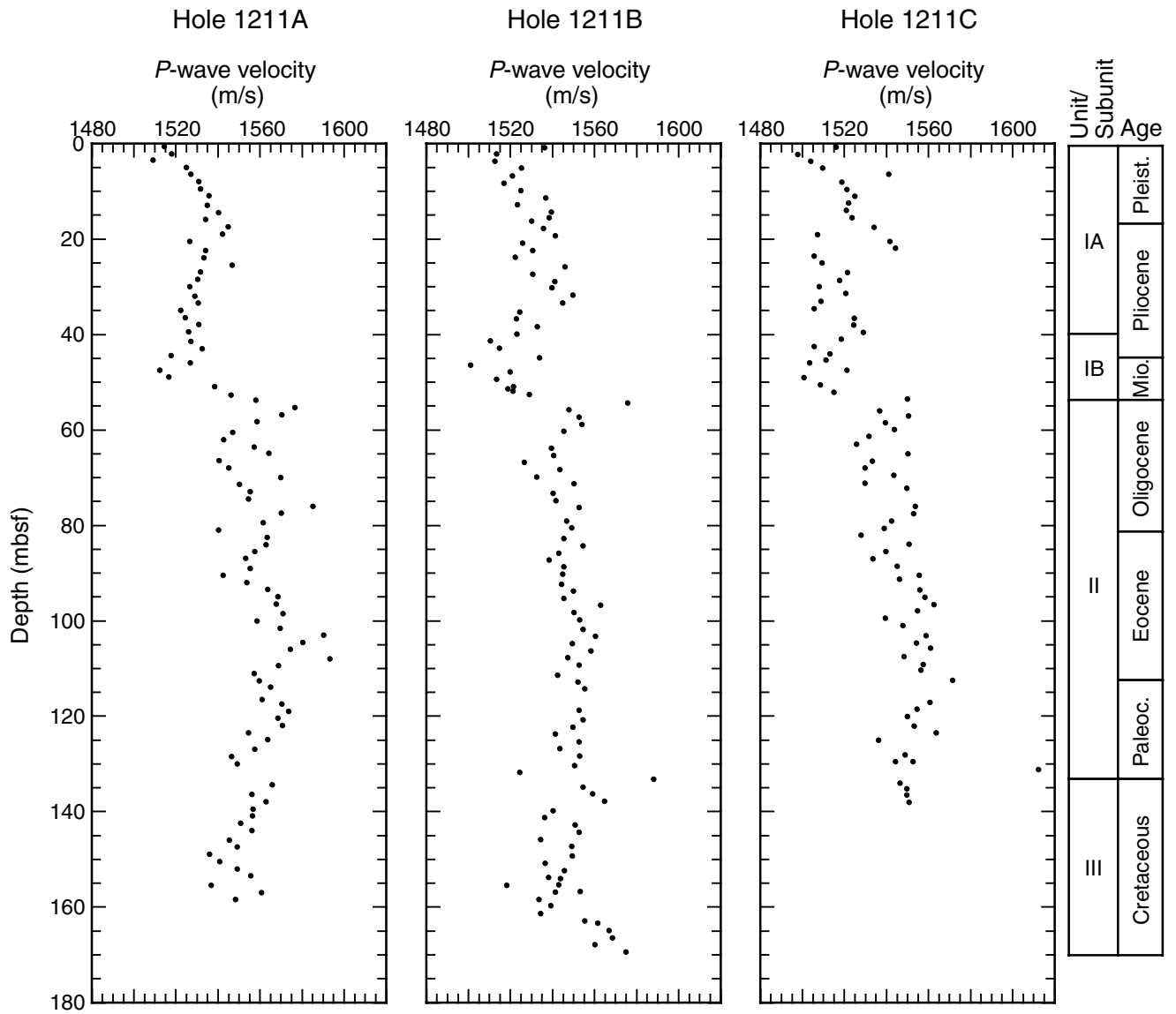


Figure F30. Discrete measurements of *P*-wave velocities plotted vs. discrete wet bulk density measurements at comparable stratigraphic horizons in Hole 1211A.

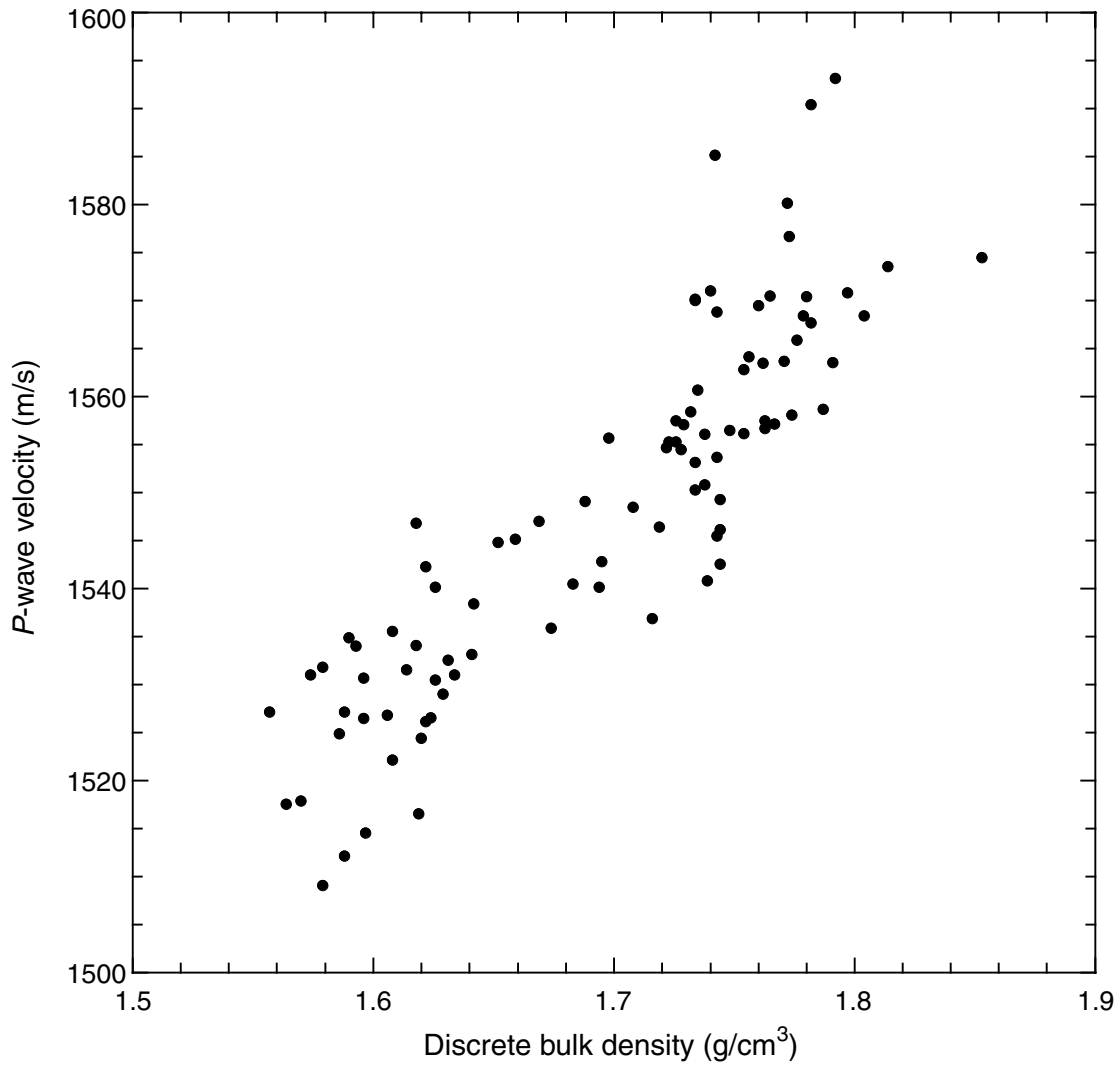


Figure F31. (A) Water content calculated relative to bulk sediment (circles) and solid phase (triangles), (B) porosity, and (C) void ratio determined for discrete samples from Hole 1211A plotted vs. depth.

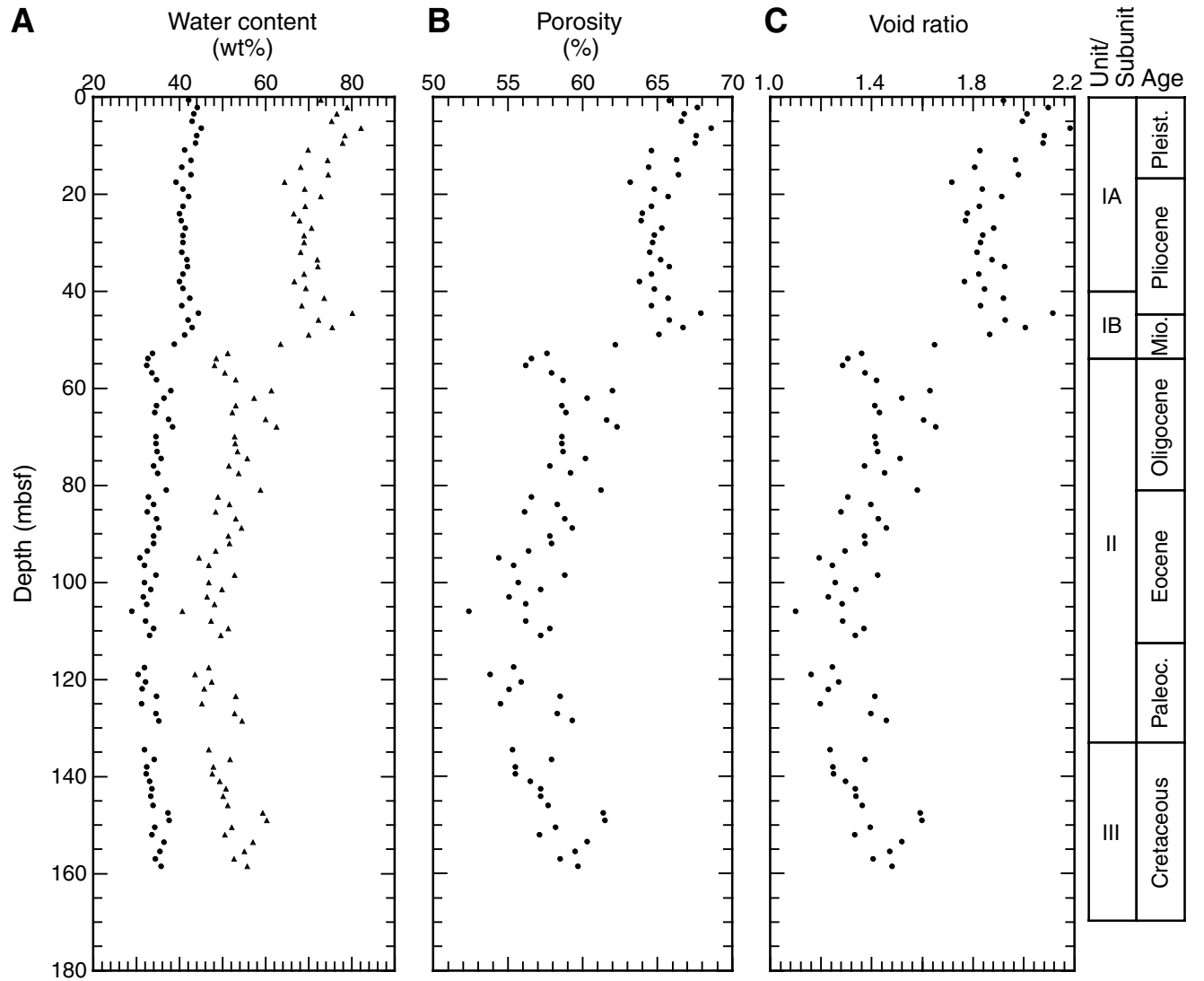


Figure F32. (A) Wet bulk density, (B) dry density, and (C) grain density determined for discrete samples from Hole 1211A plotted vs. depth.

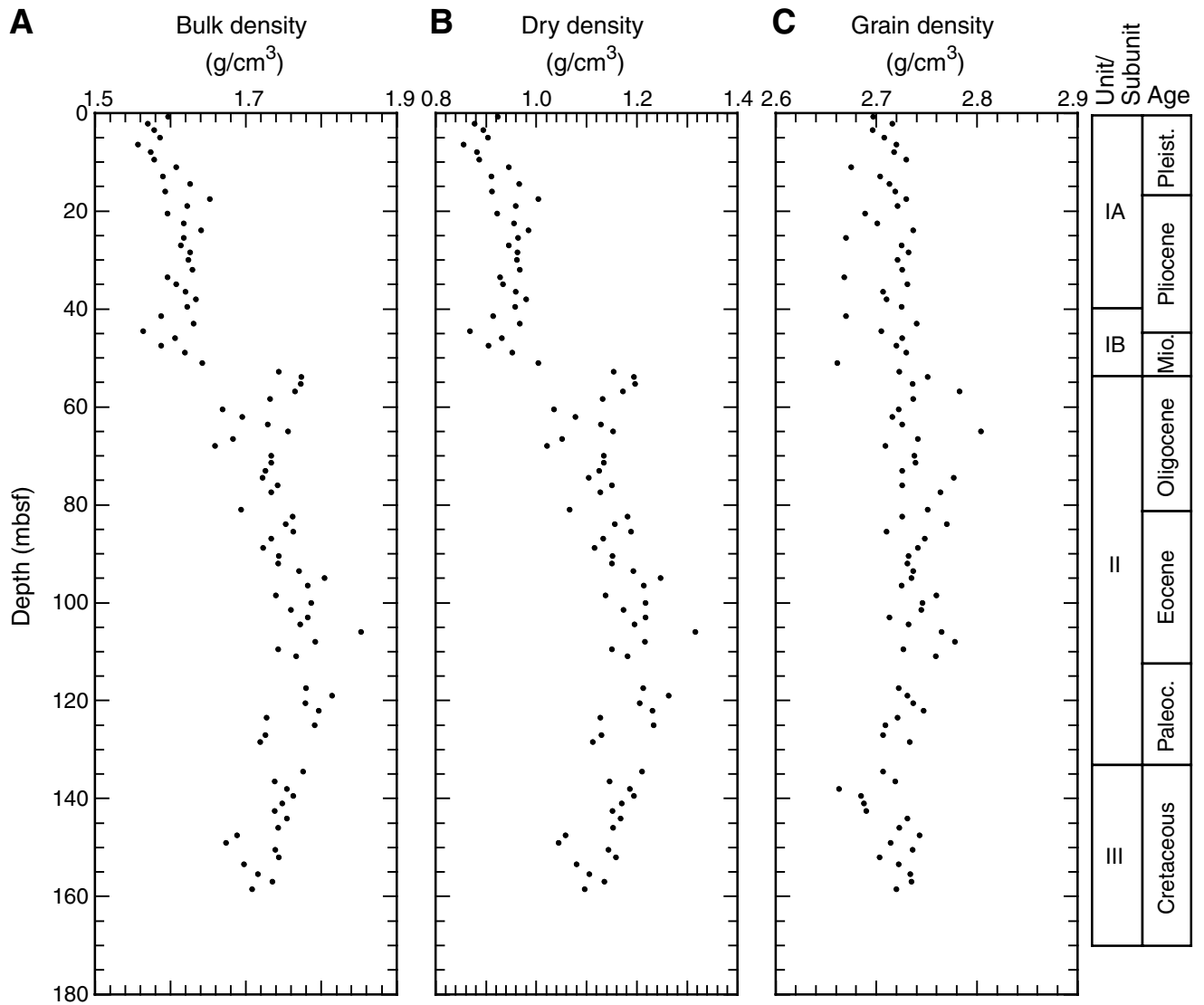


Table T1. Coring summary, Site 1211. (Continued on next page.)

Hole 1211A
 Latitude: 32°0.1300'N
 Longitude: 157°50.9999'E
 Time on site (hr): 83.75 (0230 hr, 27 Sep–0630 hr, 29 Sep 2001 and 1745 hr, 10 Oct–0130 hr, 12 Oct 2001)
 Time on hole (hr): 27.75 (0230 hr, 27 Sep–0615 hr, 28 Sep 2001)
 Seafloor (drill pipe measurement from rig floor, mbrf): 2918.7
 Distance between rig floor and sea level (m): 11.2
 Water depth (drill pipe measurement from sea level, m): 2907.5
 Total depth (drill pipe measurement from rig floor, mbrf): 3077.6
 Total penetration (mbsf): 158.9
 Total length of cored section (m): 158.9
 Total core recovered (m): 162.72
 Core recovery (%): 102.4
 Total number of cores: 18
 Total number of drilled intervals: 0

Hole 1211B
 Latitude: 32°0.1391'N
 Longitude: 157°51.0002'E
 Time on hole (hr): 24.25 (0615 hr, 28 Sep–0630 hr, 29 Sep 2001)
 Seafloor (drill pipe measurement from rig floor, mbrf): 2917.4
 Distance between rig floor and sea level (m): 11.2
 Water depth (drill pipe measurement from sea level, m): 2906.2
 Total depth (drill pipe measurement from rig floor, mbrf): 3087.3
 Total penetration (mbsf): 169.9
 Total length of cored section (m): 168.3
 Total core recovered (m): 181.90
 Core recovery (%): 108.1
 Total number of cores: 19
 Total number of drilled intervals: 1

Hole 1211C
 Latitude: 32°0.1224'N
 Longitude: 157°51.0002'E
 Time on hole (hr): 31.75 (1745 hr, 10 Oct–0130 hr, 12 Oct 2001)
 Seafloor (drill pipe measurement from rig floor, mbrf): 2918.2
 Distance between rig floor and sea level (m): 11.3
 Water depth (drill pipe measurement from sea level, m): 2906.9
 Total depth (drill pipe measurement from rig floor, mbrf): 3056.5
 Total penetration (mbsf): 138.3
 Total length of cored section (m): 138.3
 Total core recovered (m): 140.87
 Core recovery (%): 101.9
 Total number of cores: 15
 Total number of drilled intervals: 0

Core	Date (2001)	Local time (hr)	Depth (mbsf)		Length (m)		Recovery (%)
			Top	Bottom	Cored	Recovered	
198-1211A-							
1H	27 Sep	0930	0.0	2.8	2.8	2.85	101.8
2H	27 Sep	1020	2.8	12.3	9.5	9.55	100.5
3H	27 Sep	1105	12.3	21.8	9.5	9.67	101.8
4H	27 Sep	1155	21.8	31.3	9.5	9.93	104.5
5H	27 Sep	1245	31.3	40.8	9.5	10.08	106.1
6H	27 Sep	1335	40.8	50.3	9.5	9.82	103.4
7H	27 Sep	1420	50.3	59.8	9.5	9.95	104.7
8H	27 Sep	1505	59.8	69.3	9.5	9.61	101.2
9H	27 Sep	1550	69.3	78.8	9.5	9.55	100.5
10H	27 Sep	1635	78.8	88.3	9.5	9.49	99.9
11H	27 Sep	1719	88.3	97.8	9.5	9.85	103.7
12H	27 Sep	2240	97.8	107.3	9.5	9.72	102.3
13H	27 Sep	2340	107.3	116.8	9.5	9.77	102.8
14H	28 Sep	0030	116.8	126.3	9.5	9.83	103.5
15H	28 Sep	0115	126.3	135.8	9.5	9.21	96.9
16H	28 Sep	0225	135.8	145.3	9.5	9.74	102.5
17H	28 Sep	0310	145.3	154.8	9.5	9.84	103.6
18H	28 Sep	0430	154.8	158.9	4.1	4.26	103.9
Cored totals:					158.9	162.72	102.4
198-1211B-							
1H	28 Sep	0715	0.0	6.1	6.1	6.15	100.8
2H	28 Sep	0815	6.1	15.6	9.5	9.89	104.1

Table T1 (continued).

Core	Date (2001)	Local time (hr)	Depth (mbsf)		Length (m)		Recovery (%)	
			Top	Bottom	Cored	Recovered		
3H	28 Sep	0900	15.6	25.1	9.5	9.94	104.6	
4H	28 Sep	0948	25.1	34.6	9.5	9.75	102.6	
5H	28 Sep	1040	34.6	44.1	9.5	9.94	104.6	
6H	28 Sep	1125	44.1	53.6	9.5	9.83	103.5	
7H	28 Sep	1220	53.6	63.1	9.5	9.62	101.3	
8H	28 Sep	1310	63.1	72.6	9.5	9.98	105.1	
9H	28 Sep	1355	72.6	82.1	9.5	9.37	98.6	
10H	28 Sep	1440	82.1	91.6	9.5	9.83	103.5	
11H	28 Sep	1525	91.6	101.1	9.5	9.28	97.7	
12H	28 Sep	1615	101.1	110.6	9.5	9.70	102.1	
13H	28 Sep	1655	110.6	120.1	9.5	9.89	104.1	
14H	28 Sep	1745	120.1	129.6	9.5	9.68	101.9	
15H	28 Sep	1830	129.6	139.1	9.5	9.89	104.1	
16H	28 Sep	1915	139.1	148.6	9.5	9.90	104.2	
17H	28 Sep	2005	148.6	151.6	3.0	9.78	326.0	
*****Drilled from 151.6 to 153.2 mbsf*****								
18H	28 Sep	2225	153.2	162.7	9.5	9.87	103.9	
19H	28 Sep	2330	162.7	169.9	7.2	9.61	133.5	
					Cored totals:	168.3	181.90	108.1
					Drilled total:	1.6		
					Total:	169.9		
198-1211C-								
1H	11 Oct	0605	0.0	7.3	7.3	7.30	100.0	
2H	11 Oct	0705	7.3	16.8	9.5	9.60	101.1	
3H	11 Oct	0750	16.8	26.3	9.5	9.86	103.8	
4H	11 Oct	0840	26.3	35.8	9.5	9.89	104.1	
5H	11 Oct	0926	35.8	45.3	9.5	10.01	105.4	
6H	11 Oct	1015	45.3	54.8	9.5	9.34	98.3	
7H	11 Oct	1105	54.8	64.3	9.5	9.93	104.5	
8H	11 Oct	1200	64.3	73.8	9.5	9.24	97.3	
9H	11 Oct	1250	73.8	83.3	9.5	9.55	100.5	
10H	11 Oct	1345	83.3	92.8	9.5	9.15	96.3	
11H	11 Oct	1435	92.8	102.3	9.5	9.03	95.1	
12H	11 Oct	1518	102.3	111.8	9.5	9.30	97.9	
13H	11 Oct	1610	111.8	121.3	9.5	9.57	100.7	
14H	11 Oct	1705	121.3	128.8	7.5	9.26	123.5	
15H	11 Oct	1750	128.8	138.3	9.5	9.84	103.6	
					Cored totals:	138.3	140.87	101.9

Table T2. Calcareous nannofossil datums, ages, and depths, Site 1211.

Datum	Zone/ Subzone (base)	Core, section, interval (cm)	Depth (mbsf)	Core, section, interval (cm)	Depth (mbsf)	Core, section, interval (cm)	Depth (mbsf)	Age (Ma)
		198-1211A-		198-1211B-		198-1211C-		
LO <i>Pseudoemiliania lacunosa</i>	CN14b	1H-CC	2.80	2H-CC	15.94			0.46
FO <i>Gephyrocapsa parallela</i>	CN14a	2H-CC	12.30			1H-CC	7.25	0.95
LO <i>Discoaster brouweri</i>	CN13					2H-CC	16.85	1.95
LO <i>Discoaster tamalis</i>	CN12b	3H-CC	21.92					
LO <i>Reticulofenestra pseudoumbilicus</i>	CN12a			4H-CC	34.80	3H-CC	26.61	3.82
LO <i>Amaurolithus</i> spp.	CN11	4H-CC	31.68			4H-CC	36.14	4.56
FO <i>Ceratolithus rugosus</i>	CN10c	5H-CC	41.33			5H-CC	45.76	5.1
LO <i>Discoaster quinqueramus</i>	CN10a			5H-CC	44.49			5.54
FO <i>Discoaster berggrenii</i>	CN9	6H-CC	50.57					8.2
LO <i>Discoaster hamatus</i>	CN7							10.476
FO <i>Sphenolithus heteromorphus</i>	CN3	7H-2, 20	52.00					18.2
LO <i>Reticulofenestra bisectus</i>	CN1							23.9
LO <i>Sphenolithus distentus</i>	CP19b	7H-CC	60.05					
FO <i>Sphenolithus ciperoensis</i>	CP19a	8H-3, 30	63.10	7H-CC	63.17	7H-CC	64.63	29.9
FO <i>Sphenolithus distentus</i>	CP18	8H-CC	69.36	8H-CC	73.03	8H-CC	73.49	31.5
TA <i>Ericsonia subdisticha</i>	CP16b	10H-1, 10	78.9					33.3
FO <i>Ismolithus recurvus</i>	CP15b			9H-CC	81.87	9H-CC	83.3	36.0
LO <i>Chiasmolithus grandis</i>	CP15	10H-5, 140	86.20					37.1
LO <i>Chiasmolithus solitus</i>	CP14b	10H-CC	88.24					40.4
FO <i>Reticulofenestra umbilicus</i>	CP14a							43.7
FO <i>Nannotetrina fulgens</i>	CP13			10H-CC	91.83	10H-CC	92.4	47.3
FO <i>Discoaster sublodoensis</i>	CP12	11H-CC	98.05	11H-CC	100.78	11H-CC	101.78	49.7
FO <i>Coccolithus crassus</i>	CP11	12H-CC	107.47	12H-CC	110.75			51.5
FO <i>Discoaster lodoensis</i>	CP10							52.8
FO <i>Tribrachiatulus orthostylus</i>	CP9b					12H-CC	111.55	53.6
FO <i>Discoaster diastypus</i>	CP9a	13H-6, 1	114.66	13H-4, 33	112.13			55.0
FO <i>Tribrachiatulus bramlettei</i>	CP9a							55
FO <i>Discoaster multiradiatus</i>	CP8	14H-1, 114	117.94	13H-CC	120.39			56.2
FO <i>Discoaster nobilis</i>	CP7	14H-4, 90	122.20			13H-CC	121.32	56.9
FO <i>Fasciculithus tympaniformis</i>	CP4	14H-6, 20	124.50					59.7
FO <i>Ellipsolithus macellus</i>	CP3	14H-CC	126.58	14H-CC	129.68	14H-CC	130.51	62.2
FO <i>Chiasmolithus danicus</i>	CP2							63.8
FO <i>Chiasmolithus tenuis</i>	CP1b	15H-2, 130	129.10					
LO Cretaceous taxa	CP1a	15H-4, 115	131.95					65.0
FO <i>Micula prinsii</i>	CC26			15H-CC	139.39			65.4
LO <i>Reinhardtites levis</i>	CC25	17H-CC	155.09			15H-CC	138.59	69.2

Notes: FO = first occurrence, LO = last occurrence, TA = top acme.

Table T3. Planktonic foraminiferal datums, ages, and depths, Site 1211.

Datum	Zone/ Subzone (base)	Core, section, interval (cm)	Depth (mbsf)	Core, section, interval (cm)	Depth (mbsf)	Core, section, interval (cm)	Depth (mbsf)	Age (Ma)
		198-1211A-		198-1211B-		198-1211C-		
LO <i>Globigerinoides obliquus</i>		3H-CC	21.92	2H-CC	15.94	4H-CC	36.14	1.3
FO <i>Truncorotalia truncatulinoides</i>	N22	2H-CC	12.3	2H-CC	15.94	2H-CC	16.85	1.92
LO <i>Globigerinoides extremus</i>		5H-CC	41.33	3H-CC	25.48	1H-CC	7.25	1.98
FO <i>Truncorotalia tosaensis</i>	N21	3H-CC	21.92	2H-CC	15.94	3H-CC	26.61	3.35
LO <i>Dentoglobigerina altispira</i>		4H-CC	31.68	4H-CC	34.8	4H-CC	36.14	3.11
LO <i>Sphaeroidinellopsis seminulina</i>		4H-CC	31.68	4H-CC	34.8	4H-CC	36.14	3.11
LO <i>Globorotalia margaritae</i>				5H-CC	44.49	4H-CC	36.14	3.85
FO <i>Truncorotalia crassaformis</i>		3H-CC	21.92	4H-CC	34.8	4H-CC	36.14	4.31
LO <i>Globoturborotalita nepenthes</i>		5H-CC	41.33	5H-CC	44.49	5H-CC	45.76	4.39
FO <i>Globorotalia tumida</i>	N18	3H-CC	21.92	5H-CC	44.49	5H-CC	45.76	5.82
FO <i>Globorotalia margaritae</i>				5H-CC	44.49	5H-CC	45.76	6.09
LO <i>Paragloborotalia mayeri</i>	N15							10.49
FO <i>Globoturborotalita nepenthes</i>	N14	6H-CC	50.57	5H-CC	44.49	5H-CC	45.76	11.19
FO <i>Orbulina universa</i>	N9	6H-CC	50.57	5H-CC	44.49	5H-CC	45.76	15.1
FO <i>Praeorbulina sicana</i>	N8							16.4
FO <i>Globoquadrina dehiscescens</i>	M1b	6H-CC	50.57					23.2
LO <i>Subbotina angiporoides</i>				8H-CC	73.03	7H-CC	64.63	30.0
LO <i>Pseudohastigerina</i> spp.	P19	11H-CC	98.05			8H-CC	73.49	32.0
LO <i>Hantkenina</i> spp.				9H-CC	81.87	9H-4, 90-91	79.20	33.7
LO <i>Globigerinatheka index</i>		10H-CC	88.24			9H-CC	83.30	34.3
LO <i>Acarinina primitiva</i>		11H-CC	98.05	12H-CC	110.75	10H-CC	92.40	39.0
LO " <i>Orbulinoides</i> " <i>beckmanni</i>	P14							40.1
FO " <i>Orbulinoides</i> " <i>beckmanni</i>	P13							40.5
LO <i>Acarinina bullbrookii</i>		11H-CC	98.05	10H-CC	91.83	10H-CC	92.40	40.5
FO <i>Turborotalia pomeroli</i>								
LO <i>Morozovella aragonensis</i>	P12	11H-CC	98.05	10H-CC	91.83	10H-CC	92.40	43.6
FO <i>Globigerinatheka kugleri</i>	P11							45.8
FO <i>Hantkenina</i> spp.	P10			9H-C	81.87	9H-CC	83.30	49.0
LO <i>Morozovella formosa</i>	P8	12H-CC	107.47	12H-CC	110.75	12H-CC	111.55	50.8
FO <i>Acarinina pentacamerata</i>		11H-CC	98.05	12H-CC	110.75	11H-CC	101.78	50.8
FO <i>Morozovella aragonensis</i>	P7	11H-CC	98.05	11H-CC	100.78	11H-CC	101.78	52.3
LO <i>Morozovella aequa</i>		13H-CC	117.02	13H-CC	120.39			53.6
FO <i>Morozovella formosa</i>	P6b	12H-CC	107.47	12H-CC	110.75	12H-CC	111.55	54.0
LO <i>Morozovella velascoensis</i>	P6a	13H-CC	117.02	13H-CC	120.39	12H-CC	111.55	54.7
FO <i>Morozovella gracilis</i>		12H-CC	107.47					54.7
FO <i>Morozovella subbotinae</i>		13H-CC	117.02	13H-CC	120.39	11H-CC	101.78	55.9
LO <i>Globanomalina pseudomenardii</i>	P5							55.9
LO <i>Acarinina mckannai</i>				13H-CC	120.39	13H-CC	121.32	56.3
FO <i>Acarinina mckannai</i>				13H-CC	120.39	13H-CC	121.32	59.1
FO <i>Globanomalina pseudomenardii</i>	P4a							59.2
FO <i>Morozovella velascoensis</i>		13H-CC	117.02	13H-CC	120.39	14H-CC	130.51	60.0
FO <i>Morozovella conicotruncata</i>		14H-CC	126.58			14H-CC	130.51	60.9
FO <i>Morozovella angulata</i>		14H-CC	126.58			14H-CC	130.51	61.0
FO <i>Igorina pusilla</i>		14H-CC	126.58					61.0
FO <i>Praemurica uncinata</i>	P2			14H-CC	129.68			61.2
FO <i>Praemurica inconstans</i>				14H-CC	129.68			63.0
LO <i>Parvularugoglobigerina eugubina</i>	P1a					15H-3, 80-81	132.60	64.7
FO <i>Parvularugoglobigerina eugubina</i>	P1a					15H-4, 9-10	133.39	64.97
LO <i>Abathomphalus mayaroensis</i>		15H-CC	135.46	15H-CC	139.39	15H-CC	138.59	65.0
FO <i>Abathomphalus mayaroensis</i>	KS31	16H-CC	145.49	17H-CC	158.33			68.6
FO <i>Racemiguembelina fructicosa</i>		17H-CC	155.09	17H-CC	158.33			69.6
FO <i>Contusotruncana contusa</i>		18H-CC	159.01	17H-CC	158.33			69.6

Note: FO = first occurrence, LO = last occurrence.

Table T4 (continued).

Core, section	Depth (mbsf)	Nannofossil zone/subzone	Size fraction (µm)	Preservation	Benthic abundance	Buliminids		Stilostomellids	Uvigerinids	Agglutinated	
						<i>Buliminella grata</i>	<i>Bulimina velascoensis</i> <i>Bulimina jarvisi</i> <i>Bulimina semicostata</i> <i>Bulimina trinitatensis</i> <i>Bulimina impendens</i> <i>Bulimina elongata</i> <i>Quadratobuliminella pyramidalis</i>	<i>Stilostomella</i> spp. <i>Stilostomella gracillima</i> <i>Stilostomella abyssorum</i> <i>Orthomorphina</i> spp. <i>Stilostomella subspinosa</i>	<i>Uvigerina hispidocostata</i> <i>Uvigerina hispida</i> <i>Uvigerina senticosa</i> <i>Uvigerina</i> spp.	<i>Gaudryina pyramidata</i> <i>Tritaxia</i> spp. <i>Marssonella trochoides</i> <i>Spiroplectammima jarvisi</i> <i>Tritaxia gaultina</i> <i>Spiroplectammima spectabilis</i> <i>Vulvulina spinosa</i> <i>Karrerella bradyi</i> <i>Martinottiella</i> sp. <i>Haplophragmoides</i> spp. <i>Eggerella bradyi</i>	
198-1211A-											
1H-CC	2.80	CN14b	>250	VG	C				F C R R		
3H-CC	21.92	CN12b	>250	G	F		T R	R R			R R
5H-CC	41.33	CN11	>250	G	F						
6H-CC	50.57	CN9a	>250	M-G	C						
7H-CC	60.05	CP19b	>125	M	F		R R R R R	C C			
8H-CC	69.36	CP18	>125	M	R		R R R R R	R			
9H-CC	78.80	CP16a(-b)	>125	M	F		R R R R R				
10H-CC	88.24	CP14b	>125	P-M	F	R	R R R R R				
11H-CC	98.05	CP12	>125	M	R		R R R R R				
12H-CC	107.47	CP11	>125	M	F		T R				
13H-CC	117.02	CP8	>125	M	R	A T					
15H-CC	135.46	CC25	>125	M	A						
16H-CC	145.49	CC25	>125	G	A						
18H-CC	159.01	CC24	>125	M	R						

Table T5 (continued).

Core, section	Depth (mbsf)	Nannofossil zone/subzone	Size fraction (µm)	Preservation	Benthic abundance	Buliminids	Stilostomellids	Uvigerinids	Agglutinated	
						<i>Buliminella grata</i> <i>Quadratobuliminella pyramidalis</i> <i>Bulimina semicostata</i> <i>Bulimina jarvisi</i> <i>Bulimina elongata</i> <i>Bulimina impendens</i>	<i>Stilostomella</i> spp. <i>Stilostomella subspinosa</i> <i>Orthomorphina</i> spp. <i>Stilostomella abyssorum</i> <i>Stilostomella gracillima</i>	<i>Rectuvigerina</i> spp. <i>Uvigerina hispida</i> <i>Uvigerina senticosa</i> <i>Uvigerina hispidocostata</i>	<i>Gaudryina pyramidata</i> <i>Marssonella trochooides</i> <i>Tritaxia</i> spp. <i>Spiroplectammima jarvisi</i> <i>Karriella bradyi</i>	<i>Vulvulina spinosa</i> <i>Eggerella bradyi</i> <i>Martinottiella</i> sp.
198-1211B-										
1H-CC	6.10	CN14b	>250	M	F			R		R
3H-CC	25.48	CN12a	>250	VG	F			T		F
5H-CC	44.49	CN10	>250	G	C			T		T
6H-CC	53.88	CP19a	>250	M	F	T				
7H-CC	63.17	CP18	>125	M	R	T			T	F
8H-CC	73.03	CP18	>125	G	F	T	R	F	R	R
9H-CC	81.87	u. CP15	>125	M	C		T	F	R	R
11H-CC	100.78	CP12	>125	M	R		T	F		
12H-CC	110.75	CP11	>125	M	R	T				
13H-CC	120.39	CP8	>125	M	R	F			R	
14H-CC	129.68	CP3	>125	M	R		T		R	R
15H-CC	139.39	CC26	>125	M	T	F			T	
17H-CC	158.33	CC25	>125	M	R	R				
19H-CC	172.21	CC24/25	>125	M	R	T			R	

Table T6. Composite depth section, Site 1211.

Core	Depth (mbsf)	Offset (m)	Depth (mcd)
198-1211A-			
1H	0.0	0.00	0.00
2H	2.8	2.15	4.95
3H	12.3	2.73	15.03
4H	21.8	3.40	25.20
5H	31.3	4.10	35.40
6H	40.8	5.43	46.23
7H	50.3	6.25	56.55
8H	59.8	6.44	66.24
9H	69.3	7.13	76.43
10H	78.8	9.15	87.95
11H	88.3	9.49	97.79
12H	97.8	9.92	107.72
13H	107.3	11.49	118.79
14H	116.8	13.00	129.80
15H	126.3	15.26	141.56
16H	135.8	15.36	151.16
17H	145.3	15.36	160.66
18H	154.8	15.36	170.16
198-1211B-			
1H	0.0	0.00	0.00
2H	6.1	-3.13	2.97
3H	15.6	2.31	17.91
4H	25.1	3.07	28.17
5H	34.6	3.44	38.04
6H	44.1	4.68	48.78
7H	53.6	5.92	59.52
8H	63.1	5.48	68.58
9H	72.6	6.86	79.46
10H	82.1	8.16	90.26
11H	91.6	8.74	100.34
12H	101.1	9.38	110.48
13H	110.6	10.56	121.16
14H	120.1	12.34	132.44
15H	129.6	13.58	143.18
16H	139.1	13.53	152.63
17H	148.6	13.53	162.13
18H	153.2	13.53	166.73
19H	162.7	13.53	176.23
198-1211C-			
1H	0.0	0.36	0.36
2H	7.3	1.31	8.61
3H	16.8	1.38	18.18
4H	26.3	3.31	29.61
5H	35.8	3.11	38.91
6H	45.3	4.59	49.89
7H	54.8	4.81	59.61
8H	64.3	7.10	71.40
9H	73.8	7.07	80.87
10H	83.3	8.19	91.49
11H	92.8	9.43	102.23
12H	102.3	10.76	113.06
13H	111.8	11.88	123.68
14H	121.3	10.96	132.26
15H	128.8	14.50	143.30

Table T7. Splice tie points, Site 1211.

Core, section, interval (cm)	Depth			Core, section, interval (cm)	Depth	
	(mbsf)	(mcd)			(mbsf)	(mcd)
198-				198-		
1211B-1H-4, 78	5.28	5.28	Tie to	1211C-1H-4, 42	4.92	5.28
1211C-1H-5, 45	6.45	6.81	Tie to	1211A-2H-2, 36	4.66	6.81
1211A-2H-7, 12	11.92	14.07	Tie to	1211C-2H-4, 96	12.76	14.07
1211C-2H-7, 6	16.36	17.67	Tie to	1211A-3H-2, 114	14.94	17.67
1211A-3H-6, 111	20.91	23.64	Tie to	1211C-3H-4, 96	22.26	23.64
1211C-3H-7, 48	26.28	27.66	Tie to	1211A-4H-2, 96	24.26	27.66
1211A-4H-6, 66	29.96	33.36	Tie to	1211C-4H-3, 75	30.05	33.36
1211C-4H-7, 18	35.48	38.79	Tie to	1211A-5H-3, 39	34.69	38.79
1211A-5H-6, 144	40.24	44.34	Tie to	1211C-5H-4, 93	41.23	44.34
1211C-5H-6, 144	44.74	47.85	Tie to	1211A-6H-2, 12	42.42	47.85
1211A-6H-6, 129	49.59	55.02	Tie to	1211C-6H-4, 63	50.43	55.02
1211C-6H-6, 81	53.61	58.20	Tie to	1211A-7H-2, 15	51.95	58.20
1211A-7H-7, 57	59.72	65.97	Tie to	1211C-7H-5, 36	61.16	65.97
1211C-7H-7, 57	64.37	69.18	Tie to	1211A-8H-2, 144	62.74	69.18
1211A-8H-7, 21	69.01	75.45	Tie to	1211C-8H-3, 10	68.35	75.45
1211C-8H77, 57	73.12	80.22	Tie to	1211A-9H-3, 78	73.09	80.22
1211A-9H-7, 27	78.57	85.70	Tie to	1211C-9H-4, 33	78.63	85.70
1211C-9H-6, 27	81.57	88.64	Tie to	1211A-10H-1, 69	79.49	88.64
1211A-10H-7, 66	87.96	97.11	Tie to	1211C-10H-4, 111	88.92	97.11
1211C-10H-6, 66	91.46	99.65	Tie to	1211A-11H-2, 36	90.16	99.65
1211A-11H-6, 90	96.70	106.19	Tie to	1211B-11H-4, 135	97.45	106.19
1211B-11H-7, 39	100.29	109.03	Tie to	1211C-11H-5, 79	99.60	109.03
1211C-11H-6, 117	101.47	110.90	Tie to	1211A-12H-3, 18	100.98	110.90
1211A-12H-6, 138	106.68	116.60	Tie to	1211B-12H-5, 12	107.22	116.60
1211B-12H-7, 36	110.46	119.84	Tie to	1211C-12H-5, 78	109.08	119.84
1211C-12H-7, 30	111.10	121.86	Tie to	1211A-13H-3, 6	110.37	121.86
1211A-13H-7, 42	116.57	128.06	Tie to	1211C-13H-3, 138	116.18	128.06
1211C-13H-6, 66	119.96	131.84	Tie to	1211A-14H-2, 54	118.84	131.84
1211A-14H-6, 12	124.42	137.42	Tie to	1211B-14H-4, 48	125.08	137.42
1211B-14H-7, 27	129.37	141.71	Tie to	1211A-15H-1, 15	126.45	141.71
1211A-15H-6, 78	134.58	149.84	Tie to	1211B-15-H-5, 66	136.26	149.84
1211B-15H-7, 63	139.23	152.81				

Table T8. Linear sedimentation rate segments used to calculate mass accumulation rates and average accumulation.

Segment	Depth (mbsf)		Age (Ma)		Age	Average accumulation rate (g/cm ² /k.y.)		
	Top	Bottom	Top	Bottom		Bulk sediment	Carbonate	Noncarbonate
1	0.0	47.5	0.0	5.5	latest Miocene–Pleistocene	0.8	0.7	0.1
2	47.5	51.2	5.5	8.2	late Miocene	0.2	0.1	0.0
3	51.2	52.3	15.1	17.3	late early Miocene–middle Miocene	NA	NA	NA
4	52.3	79.9	25.5	33.7	early Oligocene	0.5	0.5	0.0
5	79.9	90.0	33.7	40.4	middle Eocene–late Eocene	0.2	0.2	0.0
6	90.0	114.7	43.6	55.0	latest Paleocene–middle Eocene	0.3	0.3	0.0
7	114.7	123.3	55.0	56.9	late Paleocene	0.6	0.5	0.0
8	123.3	124.5	56.9	57.5	late Paleocene	0.2	NA	NA
9	124.5	128.6	57.5	62.2	early Paleocene–late Paleocene	0.1	0.1	0.0
10	128.6	129.5	62.2	63.8	early Paleocene	NA	NA	NA
11	129.5	132.4	63.8	65.0	early Paleocene	NA	NA	NA
12	132.4	144.2	65.0	65.4	latest Maastrichtian–earliest Paleocene	3.5	3.2	0.3
13	144.2	158.7	65.4	68.6	late Maastrichtian	0.5	0.5	0.0

Note: NA = no dry bulk density or carbonate concentration data available.

Table T9. Concentrations of CH₄ in headspace gas, Hole 1211A.

Core, section, interval (cm)	Depth (mbsf)	CH ₄ (ppmv)
198-1211A-		
1H-2, 0-5	1.50	1.8
2H-5, 0-5	8.80	1.7
3H-5, 0-5	18.30	1.8
4H-5, 0-5	27.80	1.7
5H-5, 0-5	37.30	1.9
6H-5, 0-5	46.80	1.8
7H-5, 0-5	56.15	1.7
8H-5, 0-5	65.80	1.9
9H-7, 31-36	78.61	1.8
10H-7, 68-73	87.98	1.7
11H-5, 0-5	94.30	1.7
14H-5, 0-5	122.80	1.7

Table T10. Carbonate content, Hole 1211A.

Core, section, interval (cm)	Depth (mbsf)	Total inorganic carbon (wt%)	CaCO ₃ (wt%)
198-1211A-			
1H-1, 50-51	0.50	7.1	58.7
1H-2, 73-74	2.20	9.0	74.8
2H-1, 74-75	3.54	9.0	74.6
2H-2, 55-56	4.85	7.5	62.5
2H-4, 43-44	7.73	8.3	68.8
3H-3, 69-70	15.99	10.4	86.5
3H-4, 94-95	17.74	9.3	77.3
3H-5, 77-78	19.07	9.8	81.2
5H-1, 73-74	32.03	10.5	87.6
5H-4, 29-30	36.09	7.3	61.0
5H-7, 37-38	40.67	8.6	71.6
6H-2, 71-72	43.01	10.7	89.2
6H-5, 71-72	47.51	10.2	85.1
7H-1, 70-71	51.00	8.9	73.7
7H-5, 70-71	56.85	11.4	95.3
8H-3, 78-79	63.58	10.4	86.8
8H-4, 71-72	65.01	11.4	95.1
9H-3, 70-71	73.00	11.5	95.5
9H-5, 70-71	76.00	10.6	88.1
10H-3, 64-65	82.44	11.3	94.4
10H-5, 66-67	85.46	11.5	95.6
11H-1, 71-72	89.01	8.8	73.3
11H-4, 71-72	93.51	11.5	95.9
12H-2, 73-74	100.03	11.5	96.0
12H-5, 72-73	104.52	11.4	95.1
13H-1, 72-73	108.02	11.8	98.1
13H-4, 70-71	112.50	11.7	97.1
14H-3, 71-72	120.51	11.7	97.6
14H-4, 115-116	122.45	11.3	94.2
15H-1, 74-75	127.04	11.6	96.5
15H-6, 72-73	134.52	11.5	95.8
16H-5, 67-68	142.47	10.5	87.5
17H-1, 71-72	146.01	11.7	97.1
17H-5, 146-147	152.76	11.6	96.7
18H-2, 73-74	157.03	11.7	97.4

Table T11. Results of geochemical analyses, Hole 1211A.

Core, section, interval (cm)	Depth (mbsf)	pH	Alkalinity (mM)	Salinity	Cl ⁻ (mM)	SO ₄ ²⁻ (mM)	Na ⁺ (mM)	Mg ²⁺ (mM)	Ca ²⁺ (mM)	K ⁺ (mM)	H ₄ SiO ₄ (μM)	NH ₄ ⁺ (μM)	HPO ₄ ²⁻ (μM)	Sr ²⁺ (μM)	Fe ²⁺ (μM)	Mn ²⁺ (μM)	Li ⁺ (μM)	Ba ²⁺ (μM)	H ₃ BO ₃ (μM)
198-1211-A																			
1H-1, 145-150	1.45	7.53	2.6	34.5	551	28.4	471	53.2	10.4	11.6	540	6	1.8	89	3.1	16.9	25.6	0.9	439
2H-4, 145-150	8.75	7.39	3.2	34.5	553	28.4	471	54.1	11.1	11.4	511	15	1.5	107	3.9	28.0	18.7	0.3	447
3H-4, 145-150	18.25	7.42	3.2	35.0	557	28.1	476	53.7	10.8	11.6	603	15	0.8	122	20.1	7.9	17.2	1.1	447
4H-4, 145-150	27.75	7.40	3.1	35.0	556	27.6	474	53.4	10.9	11.3	563	15	0.5	130	4.0	3.1	17.2	0.3	430
5H-4, 145-150	37.25	7.40	3.1	35.5	563	27.8	481	53.8	11.0	11.2	509	8	0.6	136	4.1	2.7	17.2	0.3	425
6H-4, 145-150	46.75	7.28	3.2	35.0	559	28.1	477	53.3	11.6	11.2	431	9	0.3	141	1.8	6.2	18.0	0.3	435
7H-4, 145-150	56.10	7.45	3.2	35.0	559	27.8	477	53.2	11.5	10.4	337	4	0.2	143	1.2	3.8	18.9	0.3	438
8H-4, 145-150	65.75	7.30	3.0	35.0	562	27.2	479	53.7	11.2	10.6	302	6	0.3	140	1.7	0.1	18.1	0.2	457
11H-4, 145-150	94.25	7.48	2.9	35.0	560	27.1	477	53.1	11.4	10.4	201	8	0.2	134	1.4	1.5	20.5	0.5	446
14H-4, 145-150	122.75	7.49	2.9	35.0	559	27.1	476	53.7	10.9	10.8	166	6	0.0	131	1.8	0.2	23.3	1.5	483
18H-2, 145-150	157.75	7.49	2.7	35.0	560	26.5	477	52.9	11.2	10.3	136	4	0.0	124	1.3	0.8	24.9	0.3	449

Table T12. Discrete index properties measurements, Hole 1211A. (Continued on next page.)

Core, section, interval (cm)	Depth (mbsf)	Water content (wt%)		Density (g/cm ³)			Porosity (%)	Void ratio
		Bulk mass	Dry mass	Bulk	Dry	Grain		
198-1211A-								
1H-1, 70-72	0.70	42.2	72.9	1.60	0.92	2.70	65.8	1.92
1H-2, 70-72	2.20	44.1	79.0	1.57	0.88	2.72	67.7	2.10
2H-1, 70-72	3.50	43.3	76.5	1.58	0.90	2.70	66.8	2.01
2H-2, 70-72	5.00	43.0	75.4	1.59	0.90	2.71	66.6	1.99
2H-3, 70-72	6.50	45.1	82.2	1.56	0.86	2.72	68.6	2.18
2H-4, 70-72	8.00	44.0	78.4	1.57	0.88	2.72	67.6	2.08
2H-5, 70-72	9.50	43.8	77.9	1.58	0.89	2.73	67.5	2.08
2H-6, 70-72	11.00	41.2	69.9	1.61	0.95	2.68	64.6	1.83
3H-1, 70-72	13.00	42.7	74.5	1.59	0.91	2.70	66.3	1.97
3H-2, 70-72	14.50	40.6	68.2	1.63	0.97	2.71	64.4	1.81
3H-3, 70-72	16.00	42.7	74.6	1.59	0.91	2.72	66.4	1.98
3H-4, 70-72	17.50	39.2	64.4	1.65	1.01	2.73	63.2	1.72
3H-5, 70-72	19.00	40.9	69.1	1.62	0.96	2.72	64.8	1.84
3H-6, 70-72	20.50	42.1	72.8	1.60	0.92	2.69	65.7	1.91
4H-1, 70-72	22.50	40.9	69.2	1.62	0.96	2.70	64.6	1.82
4H-2, 70-72	24.00	40.0	66.5	1.64	0.99	2.74	64.0	1.78
4H-3, 70-72	25.50	40.4	67.9	1.62	0.96	2.67	63.9	1.77
4H-4, 70-72	27.00	41.4	70.7	1.61	0.95	2.73	65.3	1.88
4H-5, 70-72	28.50	40.8	68.9	1.63	0.96	2.73	64.8	1.84
4H-6, 70-72	30.00	40.8	68.9	1.62	0.96	2.72	64.7	1.83
5H-1, 70-72	32.00	40.5	68.2	1.63	0.97	2.73	64.5	1.82
5H-2, 70-72	33.50	41.8	72.0	1.60	0.93	2.67	65.2	1.88
5H-3, 70-72	35.00	41.9	72.2	1.61	0.93	2.73	65.8	1.92
5H-4, 70-72	36.50	40.8	69.0	1.62	0.96	2.71	64.6	1.82
5H-5, 70-72	38.00	40.0	66.7	1.63	0.98	2.71	63.8	1.77
5H-6, 70-72	39.50	40.9	69.3	1.62	0.96	2.73	64.8	1.85
6H-1, 70-72	41.50	42.4	73.6	1.59	0.92	2.67	65.7	1.92
6H-2, 70-72	43.00	40.6	68.4	1.63	0.97	2.74	64.6	1.83
6H-3, 70-72	44.50	44.5	80.1	1.56	0.87	2.71	67.9	2.12
6H-4, 70-72	46.00	42.0	72.3	1.61	0.93	2.73	65.8	1.93
6H-5, 70-72	47.50	43.0	75.5	1.59	0.91	2.72	66.7	2.01
6H-6, 70-72	49.00	41.2	70.0	1.62	0.95	2.73	65.1	1.87
7H-1, 70-72	51.00	38.8	63.4	1.64	1.01	2.66	62.2	1.65
7H-2, 98-100	52.78	33.8	51.2	1.74	1.15	2.72	57.6	1.36
7H-3, 70-72	53.85	32.7	48.6	1.77	1.19	2.75	56.6	1.31
7H-4, 70-72	55.35	32.5	48.1	1.77	1.20	2.74	56.2	1.29
7H-5, 70-72	56.85	33.6	50.6	1.77	1.17	2.78	57.9	1.38
7H-6, 70-72	58.35	34.7	53.1	1.73	1.13	2.74	58.7	1.42
8H-1, 70-72	60.50	38.0	61.4	1.67	1.04	2.72	62.0	1.63
8H-2, 78-80	62.08	36.4	57.3	1.70	1.08	2.72	60.3	1.52
8H-3, 80-82	63.60	34.7	53.1	1.73	1.13	2.73	58.6	1.41
8H-4, 70-72	65.00	34.3	52.3	1.76	1.15	2.80	58.9	1.43
8H-5, 70-72	66.50	37.5	60.0	1.68	1.05	2.74	61.6	1.61
8H-6, 70-72	68.00	38.4	62.5	1.66	1.02	2.71	62.3	1.65
9H-1, 70-72	70.00	34.6	52.9	1.73	1.13	2.74	58.6	1.41
9H-2, 60-62	71.40	34.6	53.0	1.73	1.13	2.74	58.6	1.42
9H-3, 70-72	73.00	34.8	53.5	1.73	1.13	2.73	58.7	1.42
9H-4, 70-72	74.50	35.8	55.8	1.72	1.11	2.78	60.2	1.51
9H-5, 70-72	76.00	34.0	51.5	1.74	1.15	2.73	57.8	1.37
9H-6, 70-72	77.50	35.0	53.8	1.73	1.13	2.76	59.2	1.45
10H-2, 64-66	80.94	37.0	58.8	1.69	1.07	2.75	61.2	1.58
10H-3, 65-67	82.45	32.9	49.0	1.76	1.18	2.73	56.6	1.31
10H-4, 60-62	83.90	34.0	51.6	1.75	1.16	2.77	58.3	1.40
10H-5, 68-70	85.48	32.6	48.4	1.76	1.19	2.71	56.1	1.28
10H-6, 60-62	86.90	34.7	53.1	1.73	1.13	2.75	58.8	1.43
11H-1, 50-52	88.80	35.2	54.4	1.72	1.12	2.74	59.3	1.46
11H-2, 70-72	90.50	34.0	51.4	1.74	1.15	2.73	57.8	1.37
11H-3, 70-72	92.00	34.0	51.6	1.74	1.15	2.73	57.9	1.38
11H-4, 70-72	93.50	32.6	48.4	1.77	1.19	2.74	56.4	1.29
11H-5, 70-72	95.00	30.9	44.6	1.80	1.25	2.74	54.4	1.19
11H-6, 70-72	96.50	31.9	46.8	1.78	1.21	2.73	55.4	1.24
12H-1, 70-72	98.50	34.6	52.9	1.74	1.14	2.76	58.8	1.43
12H-2, 70-72	100.00	31.9	46.8	1.79	1.22	2.75	55.7	1.26
12H-3, 70-72	101.50	33.3	49.9	1.76	1.17	2.75	57.2	1.34
12H-4, 70-72	103.00	31.7	46.4	1.78	1.22	2.71	55.1	1.23
12H-5, 70-72	104.50	32.5	48.1	1.77	1.20	2.73	56.2	1.28

Table T12 (continued).

Core, section, interval (cm)	Depth (mbsf)	Water content (wt%)		Density (g/cm ³)			Porosity (%)	Void ratio
		Bulk mass	Dry mass	Bulk	Dry	Grain		
12H-6, 70-72	106.00	28.9	40.7	1.85	1.32	2.77	52.4	1.10
13H-1, 70-72	108.00	32.1	47.3	1.79	1.22	2.78	56.2	1.29
13H-2, 70-72	109.50	34.0	51.4	1.74	1.15	2.73	57.8	1.37
13H-3, 70-72	111.00	33.1	49.6	1.77	1.18	2.76	57.2	1.34
14H-1, 70-72	117.50	31.9	46.8	1.78	1.21	2.72	55.4	1.24
14H-2, 70-72	119.00	30.4	43.6	1.81	1.26	2.73	53.8	1.16
14H-3, 70-72	120.50	32.2	47.5	1.78	1.21	2.74	55.9	1.27
14H-4, 70-72	122.00	31.4	45.8	1.80	1.23	2.75	55.1	1.23
14H-5, 70-72	123.50	34.7	53.1	1.73	1.13	2.72	58.5	1.41
14H-6, 70-72	125.00	31.2	45.2	1.79	1.23	2.71	54.5	1.20
15H-1, 70-72	127.00	34.6	52.8	1.73	1.13	2.71	58.3	1.40
15H-2, 70-72	128.50	35.3	54.6	1.72	1.11	2.73	59.3	1.46
15H-6, 70-72	134.50	31.9	46.8	1.78	1.21	2.71	55.3	1.24
16H-1, 70-72	136.50	34.1	51.7	1.74	1.15	2.72	57.9	1.37
16H-2, 70-72	138.00	32.4	47.9	1.75	1.19	2.66	55.5	1.25
16H-3, 70-72	139.50	32.3	47.6	1.76	1.19	2.69	55.5	1.25
16H-4, 70-72	141.00	33.1	49.4	1.75	1.17	2.69	56.5	1.30
16H-5, 70-72	142.50	33.7	50.8	1.74	1.15	2.69	57.2	1.34
16H-6, 70-72	144.00	33.4	50.2	1.75	1.17	2.73	57.2	1.34
17H-1, 70-72	146.00	33.9	51.2	1.74	1.15	2.72	57.7	1.36
17H-2, 70-72	147.50	37.3	59.4	1.69	1.06	2.74	61.4	1.59
17H-3, 70-72	149.00	37.6	60.3	1.67	1.04	2.71	61.5	1.60
17H-4, 70-72	150.50	34.3	52.2	1.74	1.14	2.74	58.2	1.40
17H-5, 70-72	152.00	33.6	50.5	1.74	1.16	2.70	57.1	1.33
17H-6, 70-72	153.50	36.4	57.1	1.70	1.08	2.72	60.3	1.52
18H-1, 70-72	155.50	35.5	55.1	1.72	1.11	2.73	59.5	1.47
18H-2, 70-72	157.00	34.5	52.7	1.74	1.14	2.74	58.5	1.41
18H-3, 70-72	158.50	35.8	55.7	1.71	1.10	2.72	59.7	1.48

Table T13. Discrete measurements of *P*-wave velocity, Site 1211. (Continued on next page.)

Core, section, interval (cm)	Depth (mbsf)	Velocity (m/s)	Core, section, interval (cm)	Depth (mbsf)	Velocity (m/s)	Core, section, interval (cm)	Depth (mbsf)	Velocity (m/s)
198-1211A-			13H-1, 67	107.96	1593.2	7H-1, 73	54.33	1575.7
1H-1, 63	0.63	1514.6	13H-2, 66	109.46	1568.8	7H-2, 69	55.79	1547.8
1H-2, 66	2.16	1517.9	13H-3, 83	111.13	1557.2	7H-3, 73	57.33	1552.6
2H-1, 66	3.46	1509.1	13H-4, 77	112.57	1559.8	7H-4, 72	58.82	1554.0
2H-2, 66	4.96	1524.9	13H-5, 55	113.85	1565.1	7H-5, 71	60.31	1545.3
2H-3, 66	6.46	1527.2	13H-7, 32	116.47	1561.1	8H-1, 71	63.81	1539.5
2H-4, 66	7.96	1531.0	14H-1, 63	117.43	1570.4	8H-2, 76	65.36	1540.6
2H-5, 66	9.46	1531.8	14H-2, 64	118.94	1573.6	8H-3, 73	66.83	1526.5
2H-6, 65	10.95	1535.6	14H-3, 63	120.43	1568.4	8H-4, 77	68.37	1543.6
3H-1, 66	12.96	1534.9	14H-4, 65	121.95	1570.8	8H-5, 71	69.81	1532.6
3H-2, 66	14.46	1540.2	14H-5, 65	123.45	1554.5	8H-6, 70	71.30	1550.3
3H-3, 66	15.96	1534.0	14H-6, 65	124.94	1563.6	9H-1, 68	73.28	1540.2
3H-4, 66	17.45	1544.8	15H-1, 65	126.95	1557.5	9H-2, 74	74.84	1541.8
3H-5, 66	18.95	1542.3	15H-2, 65	128.45	1546.4	9H-3, 65	76.25	1552.6
3H-6, 67	20.47	1526.5	15H-3, 72	130.02	1549.2	9H-5, 78	79.08	1546.8
4H-1, 65	22.45	1534.1	15H-6, 63	134.43	1565.9	9H-6, 72	80.52	1549.2
4H-2, 66	23.96	1533.2	16H-1, 65	136.45	1556.1	10H-1, 72	82.82	1545.5
4H-3, 65	25.45	1546.8	16H-2, 65	137.95	1562.8	10H-2, 74	84.34	1554.7
4H-4, 66	26.96	1531.6	16H-3, 65	139.45	1556.7	10H-3, 71	85.81	1543.1
4H-5, 67	28.47	1530.5	16H-4, 63	140.93	1556.5	10H-4, 69	87.29	1538.4
4H-6, 66	29.96	1526.6	16H-5, 66	142.46	1550.8	10H-5, 61	88.71	1545.4
5H-1, 64	31.94	1529.0	16H-6, 65	143.95	1556.2	10H-6, 65	90.25	1544.8
5H-2, 64	33.44	1530.7	17H-1, 64	145.94	1545.5	11H-1, 72	92.32	1544.4
5H-3, 66	34.96	1522.2	17H-2, 65	147.45	1549.1	11H-2, 71	93.81	1550.0
5H-4, 65	36.45	1524.4	17H-3, 65	148.95	1535.9	11H-3, 73	95.33	1545.3
5H-5, 65	37.95	1531.0	17H-4, 66	150.46	1540.8	11H-4, 69	96.79	1562.9
5H-6, 65	39.45	1526.2	17H-5, 65	151.95	1549.3	11H-5, 68	98.28	1550.3
6H-1, 65	41.45	1527.2	17H-6, 65	153.45	1555.7	11H-6, 72	99.82	1552.9
6H-2, 65	42.95	1532.6	18H-1, 65	155.45	1536.9	12H-1, 71	101.81	1554.5
6H-3, 65	44.45	1517.6	18H-2, 63	156.93	1560.7	12H-2, 67	103.26	1560.4
6H-4, 67	45.97	1526.8	18H-3, 63	158.43	1548.5	12H-3, 70	104.80	1549.5
6H-5, 65	47.45	1512.2				12H-4, 69	106.29	1558.3
6H-6, 66	48.96	1516.6	198-1211B-			12H-5, 65	107.75	1547.4
7H-1, 67	50.97	1538.4	1H-1, 82	0.82	1536.4	12H-6, 71	109.31	1552.6
7H-2, 93	52.73	1546.2	1H-2, 67	2.17	1513.5	13H-1, 80	111.40	1542.4
7H-3, 66	53.81	1558.1	1H-3, 68	3.68	1512.7	13H-2, 70	112.80	1552.1
7H-4, 66	55.31	1576.7	1H-4, 67	5.17	1525.4	13H-3, 69	114.29	1555.4
7H-5, 66	56.81	1570.5	2H-1, 68	6.78	1521.1	13H-6, 67	118.77	1552.7
7H-6, 64	58.29	1558.4	2H-2, 73	8.33	1517.0	14H-1, 66	120.76	1554.5
8H-1, 75	60.55	1547.0	2H-3, 76	9.86	1525.0	14H-2, 66	122.26	1549.8
8H-2, 83	62.13	1542.8	2H-4, 84	11.44	1536.9	14H-3, 68	123.78	1541.4
8H-3, 73	63.53	1557.1	2H-5, 72	12.82	1523.3	14H-4, 74	125.34	1552.8
8H-4, 65	64.95	1564.2	2H-6, 74	14.34	1539.4	14H-5, 65	126.75	1543.5
8H-5, 65	66.45	1540.5	2H-7, 40	15.50	1538.4	14H-6, 69	128.29	1553.1
8H-6, 65	67.95	1545.2	3H-1, 69	16.29	1530.1	15H-1, 70	130.30	1550.5
9H-1, 67	69.97	1570.0	3H-2, 72	17.82	1535.7	15H-2, 71	131.81	1524.5
9H-2, 64	71.44	1550.3	3H-3, 74	19.34	1541.4	15H-3, 58	133.18	1588.1
9H-3, 66	72.96	1555.3	3H-4, 75	20.85	1525.8	15H-4, 74	134.84	1554.6
9H-4, 66	74.46	1554.7	3H-5, 79	22.39	1530.7	15H-5, 69	136.29	1559.2
9H-5, 67	75.97	1585.2	3H-6, 73	23.83	1522.4	15H-6, 69	137.79	1564.7
9H-6, 67	77.47	1570.2	4H-1, 73	25.83	1545.8	16H-1, 70	139.80	1540.2
10H-1, 73	79.53	1561.6	4H-2, 81	27.41	1530.6	16H-2, 69	141.29	1536.2
10H-2, 72	81.02	1540.2	4H-3, 81	28.91	1541.2	16H-3, 70	142.80	1550.7
10H-3, 75	82.55	1563.5	4H-4, 66	30.25	1539.8	16H-4, 72	144.32	1552.6
10H-4, 77	84.07	1562.9	4H-5, 68	31.78	1549.8	16H-5, 70	145.80	1534.3
10H-5, 66	85.46	1557.5	4H-6, 76	33.36	1544.9	16H-6, 71	147.31	1549.2
10H-6, 62	86.92	1553.2	5H-1, 71	35.31	1524.4	17H-1, 71	149.31	1549.4
11H-1, 73	89.03	1555.3	5H-2, 69	36.79	1522.8	17H-2, 72	150.82	1536.5
11H-2, 65	90.45	1542.6	5H-3, 79	38.39	1532.7	17H-3, 76	152.36	1545.7
11H-3, 66	91.96	1553.7	5H-4, 78	39.88	1523.1	17H-4, 70	153.80	1538.1
11H-4, 67	93.47	1563.7	5H-5, 70	41.30	1510.6	17H-5, 70	155.30	1543.0
11H-5, 66	94.96	1568.4	5H-6, 74	42.84	1514.7	17H-6, 70	156.80	1553.3
11H-6, 65	96.45	1567.7	6H-1, 78	44.88	1533.8	18H-1, 76	153.96	1543.7
12H-1, 71	98.51	1571.0	6H-2, 76	46.36	1501.0	18H-2, 70	155.40	1518.3
12H-2, 78	100.08	1558.7	6H-3, 72	47.82	1520.0	18H-3, 68	156.88	1541.4
12H-3, 76	101.56	1569.5	6H-4, 75	49.35	1513.4	18H-4, 71	158.41	1533.7
12H-4, 75	103.05	1590.4	6H-5, 79	50.89	1521.6	18H-5, 51	159.71	1539.2
12H-5, 75	104.55	1580.2	6H-5, 127	51.37	1518.8	18H-6, 61	161.31	1534.3
12H-6, 67	105.97	1574.5	6H-6, 30	51.90	1521.3	18H-7, 64	162.84	1555.4
			6H-6, 100	52.60	1529.1			

Table T13 (continued).

Core, section, interval (cm)	Depth (mbsf)	Velocity (m/s)	Core, section, interval (cm)	Depth (mbsf)	Velocity (m/s)
19H-1, 71	163.41	1561.6	7H-5, 53	61.33	1531.7
19H-2, 71	164.91	1567.0	7H-6, 70	63.00	1525.7
19H-3, 70	166.40	1568.4	8H-1, 71	65.01	1550.2
19H-4, 72	167.92	1560.3	8H-2, 72	66.52	1533.2
19H-5, 71	169.41	1574.9	8H-3, 71	68.01	1529.7
198-1211C-			8H-4, 72	69.52	1543.6
1H-1, 76	0.76	1516.1	8H-5, 81	71.11	1529.9
1H-2, 79	2.29	1497.9	8H-6, 38	72.18	1549.7
1H-3, 72	3.72	1504.0	9H-2, 76	76.06	1553.7
1H-4, 67	5.17	1509.8	9H-3, 78	77.58	1553.0
1H-5, 50	6.50	1541.0	9H-4, 75	79.05	1542.6
2H-1, 81	8.11	1518.8	9H-5, 87	80.67	1538.9
2H-2, 75	9.55	1521.3	9H-6, 77	82.07	1527.9
2H-3, 70	11.00	1525.0	10H-1, 70	84.00	1550.9
2H-4, 68	12.48	1522.0	10H-2, 72	85.52	1539.7
2H-5, 77	14.06	1521.1	10H-3, 70	87.00	1533.7
2H-6, 76	15.56	1523.5	10H-4, 71	88.51	1545.0
3H-1, 80	17.59	1534.0	10H-5, 120	90.50	1555.7
3H-2, 77	19.07	1507.1	10H-6, 49	91.29	1546.1
3H-3, 76	20.56	1541.7	11H-1, 78	93.58	1556.0
3H-4, 70	22.00	1544.3	11H-2, 75	95.05	1558.2
3H-5, 81	23.61	1505.6	11H-3, 80	96.60	1562.6
3H-6, 69	24.99	1509.4	11H-4, 69	97.99	1554.8
4H-1, 76	27.06	1521.4	11H-5, 66	99.46	1539.6
4H-2, 86	28.66	1517.7	11H-6, 71	101.01	1548.0
4H-3, 69	29.99	1508.2	12H-1, 84	103.14	1558.8
4H-4, 65	31.45	1520.6	12H-2, 88	104.68	1554.2
4H-5, 76	33.06	1508.8	12H-3, 47	105.76	1561.1
4H-6, 75	34.55	1505.6	12H-4, 74	107.54	1548.5
5H-1, 74	36.54	1524.8	12H-5, 85	109.15	1557.5
5H-2, 78	38.08	1524.4	12H-6, 51	110.31	1556.3
5H-3, 73	39.53	1529.1	13H-1, 70	112.50	1571.5
5H-4, 72	41.02	1518.5	13H-4, 77	117.07	1560.8
5H-5, 74	42.53	1505.7	13H-5, 76	118.56	1554.6
5H-6, 73	44.03	1513.1	13H-6, 75	120.05	1549.9
5H-7, 61	45.41	1511.3	14H-1, 75	122.05	1553.2
6H-1, 72	46.02	1503.6	14H-2, 69	123.49	1563.6
6H-2, 71	47.51	1521.3	14H-3, 71	125.01	1536.4
6H-3, 79	49.09	1500.9	14H-5, 74	128.04	1548.9
6H-4, 73	50.53	1508.5	14H-6, 74	129.54	1552.7
6H-5, 76	52.06	1515.0	15H-1, 74	129.54	1544.4
6H-6, 77	53.57	1550.1	15H-2, 85	131.15	1612.4
7H-1, 121	56.01	1536.8	15H-4, 75	134.04	1546.4
7H-2, 86	57.16	1550.5	15H-5, 94	135.14	1549.7
7H-3, 72	58.52	1539.6	15H-6, 84	136.54	1549.6
7H-4, 63	59.93	1543.9	15H-7, 85	138.05	1550.8